

Kafrelsheikh University
Faculty of Agriculture
Agricultural Engineering Department



"Preservation Engineering of Agricultural Production"
Manufacturing a Suitable Evaporative Cooler
for Shelflife Extension of Jew's Mallow

By

Reham Mohamed Ahmed Elmessery

B. Sc. in Agricultural Engineering, Faculty of Agriculture,
Kafrelsheikh University, 2012

Thesis Submitted In Partial Fulfillment of the Requirements

for the degree of

Master of Science

in Agricultural sciences (Agricultural Engineering)

Agricultural Engineering Department,

Faculty of Agriculture, Kafrelsheikh University

Supervision Committee

Professor Dr. Said Elshahat Abdallah

Professor of Agricultural Process Engineering,
Department of Agricultural Engineering,
Faculty of Agriculture, Kafrelsheikh University

Dr. Wael Mohamed Elmessery

Associate Professor of Agricultural Engineering,
Department of Agricultural Engineering,
Faculty of Agriculture,
Kafrelsheikh University

Dr. Mohamed Taha Ebaid

Researcher Head
Agricultural Engineering Research Institute
(AERI)
Agricultural Research Centre (ARC), Dokki, Giza

2022

ACKNOWLEDGEMENTS

First of all, thanks to Allah for the numerous gifts and guidance .

First and foremost, I would like to express my deep gratitude to my major supervisor and director of the dissertation **Professor Dr. Said Elshahat Abdallah**, Professor of Agricultural Process Engineering. Department of Agricultural Engineering. Faculty of Agriculture, Kafrelsheikh University for his expert guidance, sustained interest, constructive suggestions, continuous encouragement and care bestowed throughout the course of this study. Without his support, patience and guidance, this study would not have been completed. It is to him that I owe my deepest gratitude.

The author also wishes to express her most appreciation and deep gratitude to **Dr. Wael Mohamed Elmessery**, Associate Professor of Agricultural Engineering, Department of Agricultural Engineering, Faculty of Agriculture, Kafrelsheikh University, for his supervising, scientific help, continuous encouragement, and revising the manuscript.

The author also wishes to express his most appreciation and deep gratitude to **Dr. Mohamed Taha Ebaid**, Resercher Head, Agricultural Engineering Research Institute, Dokki, Giza for his supervision, scientific help, continuous encouragement.

Finally, I am deeply grateful and thankful to my Mother, Father, Husband, Brothers, Sister and my Sons for their continuous inspiration, encouragement and patience throughout the course of study.

TABLE OF CONTENTS

Item	Title	Page No.
	ACKNOWLEDGEMENTS	I
	LIST OF FIGURES	V
	LIST OF TABLES	XI
	NOMENCLATURE	X
1	INTRODUCTION	1
2	REVIEW OF LITERATURE	3
2.1	Methods of agricultural production storage	4
2.2	Visual and biochemical quality and marketability of leafy vegetables	4
2.3	Factors affecting physiological, biochemical and microbial properties	5
2.4	Evaporative cooling system theory and basic principle	6
2.5	Importance of evaporative cooling process	7
2.6	Importance of storing at low temperature after harvest	11
2.7	Performance evaluation indicators	12
2.8	Factors affecting produce quality under evaporative cooling storage conditions	14
2.9	Methods of evaporative cooling	14
2.9.1	Direct evaporative cooling system (passive types)	15
2.9.2	Direct evaporative cooling system (active types)	18
2.9.3	Indirect evaporative cooling system	19
2.10	Water absorbent materials (cooling pads) for evaporative cooling	21
2.11	Design considerations/choosing the right technology	23
2.12	Physiological mass loss during storage	23
2.13	Factors affecting the performance of a pad-fan evaporative cooling system	24
2.13.1	Weather conditions	25
2.13.2	Pad material	25
2.13.3	Pad thickness and density	27
2.13.4	Pad face air velocity	27
2.14	Humidity rate	28
2.15	Optimum temperatures and relative humidity for storing vegetables and fruits	28
2.16	Developments of image processing fields	31
2.16.1	Visual performance	31

Item	Title	Page No.
2.16.2	Machine vision	36
2.16.3	Machine vision application using 3-D imaging	36
2.16.4	Computer vision system	37
2.16.5	Low-level processes	39
2.17	Imaging devices	40
2.18	Image processing techniques	40
2.18.1	Edge detection	40
2.18.2	Region segmentation	42
2.19	Morphological image processing	44
2.19.1	Morphological image processing based segmentation	45
2.19.2	Gray scale morphological analysis	45
2.20	Illumination correction technique	46
2.21	Histogram features	47
3	MATERIALS AND METHODS	50
3.1	Materials	50
3.1.1	Evaporative cooler manufacturing	50
3.2	Experimental setup	50
3.3	Experimental procedures and measurements	53
3.3.1	Air relative humidity and temperature	53
3.3.2	Instantaneous Jew's Mallow mass	53
3.4	Imageries acquisition procedures	53
3.4.1	Imagery process and analysis techniques	53
3.4.1.1	The output of the CCM-200	55
3.4.1.2	Standard B-H table	55
3.4.1.3	Visualization of leaves color gradient (chlorophyll content)	57
3.4.1.4	Morphological operations	57
3.5	Investigated variables	57
3.6	Instruments and data acquisition of evaporative cooling unit	58
3.6.1	Air temperature and relative humidity measurements	58
3.6.2	Instantaneous Jew's Mallow mass meter	59
3.6.3	Air velocity measurement	59
3.7	Performance evaluation of evaporative cooler	60
3.7.1	Superficial air velocity calculations and regulations	60
3.7.2	Cooling potential of the evaporative cooler	61

Item	Title	Page No.
3.7.3	Saturation efficiency inside evaporative cooler	62
3.7.4	Mass loss of Jew's Mallow analysis.	62
4	RESULTS AND DISCUSSION	63
4.1	evaporative cooler performance	63
4.1.1	Relative humidity inside evaporative cooling system	63
4.1.2	Air temperature inside evaporative cooling system	70
4.1.3	Temperature patterns inside evaporative cooler without cooling system.	72
4.1.4	Instantaneous mass inside evaporative cooling system	75
4.2	The predict air temperature and relative humidity of evaporative cooler	88
4.3	Instantaneous mass reduction of Jew's Mallow	92
4.3.1	Effect of ambient conditions on the instantaneous mass reduction of Jew's Mallow	92
4.4	Wilting percent values of different samples of Jew's Mallow leaves was obtained by CCM-200 and converted to wilting percent according to the standard Table of Horsfall and Barratt (1945)	94
4.5	Chlorophyll Content Index measurements	95
4.6	Morphological system for image processing	97
4.7	RGB histogram for pixel intensity distribution	103
5	SUMMARY AND CONCLUSIONS	109
6	REFERENCES	109
7	APPENDICES	
8	ARABIC SUMMARY	

LIST OF FIGURES

Figure No.	Title	Page No.
1	Evaporative cooling process representation on psychrometric chart	6
2	Evaporative cooler with jute bag as cooling pad	16
3	Evaporative cooler with rice husk as cooling pad	17
4	Evaporative cooler made from bricks	18
5	Evaporative cooler with vortex wind machine	19
6	Indirect active evaporative cooler	21
7	Aspen pad	22
8	Porous ceramic pad	22
9	Pad materials	22
10	Main components of the subjective image quality decision process	35
11	A general paradigm in computer vision	38
12	Edge detection	42
13	Region segmentation	43
14	Solid view of the experimented evaporative cooler	51
15	Engineering drawing of the experimented evaporative cooler	52
16	Opti-Sciences CCM-200	55
17	A digital air temperature and relative humidity meter	58
18	A digital balance of mass meter	59
19	An anemometer of air velocity measurement	60
20	Air relative humidity behavior under superficial air velocity of 0.21m/s, three watering rates of 1, 2, and 4ℓ/h and pad thickness of 7cm	64
21	Air relative humidity behavior under superficial air velocity of 0.17m/s, three watering rates of 1, 2, and 4ℓ/h and pad thickness of 7cm	65
22	Air relative humidity behavior under superficial air velocity of 0.13m/s, three watering rates of 1, 2, and 4ℓ/h and pad thickness of 7cm	65
23	Air relative humidity behavior under the ambient conditions on a typical first summer day	66

Figure No.	Title	Page No.
24	Air relative humidity behavior under superficial air velocity of 0.21m/s, three watering rates of 1, 2, and 4ℓ/h and pad thickness of 10cm	67
25	Air relative humidity behavior under superficial air velocity of 0.17m/s, three watering rates of 1, 2, and 4ℓ/h and pad thickness of 10cm	68
26	Air relative humidity behavior under superficial air velocity of 0.13m/s, three watering rates of 1, 2, and 4ℓ/h and pad thickness of 10cm	68
27	Air relative humidity behavior under the ambient conditions on a typical first summer day	69
28	Air temperature behavior under superficial air velocities of 0.21m/s, three watering rates of 1, 2, and 4ℓ/h and pad thickness of 7cm	70
29	Air temperature behavior under superficial air velocities of 0.17m/s, three watering rates of 1, 2, and 4ℓ/h and pad thickness of 7cm	71
30	Air temperature behavior under superficial air velocities of 0.13m/s, three watering rates of 1, 2, and 4ℓ/h and pad thickness of 7cm	71
31	Air temperature behavior under the ambient conditions on a typical first summer day	72
32	Air temperature behavior under superficial air velocities of 0.21m/s, three watering rates of 1, 2, and 4ℓ/h and pad thickness of 10cm	73
33	Air temperature behavior under superficial air velocities of 0.17m/s, three watering rates of 1, 2, and 4ℓ/h and pad thickness of 10cm	74
34	Air temperature behavior under superficial air velocities of 0.13m/s, three watering rates of 1, 2, and 4ℓ/h and pad thickness of 10cm	74
35	Air temperature behavior under the ambient conditions on a typical first summer day	75
36	Instantaneous mass behavior under the superficial air velocity of 0.21m/s, three watering rates of 1, 2, and 4ℓ/h and pad thickness of 7cm for first processing day	76
37	Instantaneous mass behavior under the superficial air velocity of 0.21m/s, three watering rates of 1, 2, and 4ℓ/h and pad thickness of 7cm for second processing day	76
38	Instantaneous mass behavior under the superficial air	77

Figure No.	Title	Page No.
	velocity of 0.21m/s, three watering rates of 1, 2, and 4ℓ/h and pad thickness of 7cm for third processing day	
39	Instantaneous mass behavior under the ambient conditions for the first, second and third processing day	77
40	Instantaneous mass behavior under the superficial air velocity of 0.17m/s, three watering rates of 1, 2, and 4ℓ/h and pad thickness of 7cm for first processing day	78
41	Instantaneous mass behavior under the superficial air velocity of 0.17m/s, three watering rates of 1, 2, and 4ℓ/h and pad thickness of 7cm for second processing day	78
42	Instantaneous mass behavior under the superficial air velocity of 0.17m/s, three watering rates of 1, 2, and 4ℓ/h and pad thickness of 7cm for third processing day	79
43	Instantaneous mass behavior under the ambient conditions for the first, second and third processing days	79
44	Instantaneous mass behavior under the superficial air velocity of 0.13m/s, three watering rates of 1, 2, and 4ℓ/h and pad thickness of 7cm for first processing day	80
45	Instantaneous mass behavior under the superficial air velocity of 0.13m/s, three watering rates of 1, 2, and 4ℓ/h and pad thickness of 7cm for second processing day	80
46	Instantaneous mass behavior under the superficial air velocity of 0.13m/s, three watering rates of 1, 2, and 4ℓ/h and pad thickness of 7cm for third processing day	81
47	Instantaneous mass behavior under the ambient conditions for the first, second and third processing days	81
48	Instantaneous mass behavior under the superficial air velocity of 0.21m/s, three watering rates of 1, 2, and 4ℓ/h and pad thickness of 10cm for first processing day	82

Figure No.	Title	Page No.
49	Instantaneous mass behavior under the superficial air velocity of 0.21m/s, three watering rates of 1, 2, and 4ℓ/h and pad thickness of 10cm for second processing day	82
50	Instantaneous mass behavior under the superficial air velocity of 0.21m/s, three watering rates of 1, 2, and 4ℓ/h and pad thickness of 10cm for third processing day	83
51	Instantaneous mass behavior under the ambient conditions for the first, second and third processing days	83
52	Instantaneous mass behavior under the superficial air velocity of 0.17m/s, three watering rates of 1, 2, and 4ℓ/h and pad thickness of 10cm for first processing day	84
53	Instantaneous mass behavior under the superficial air velocity of 0.17m/s, three watering rates of 1, 2, and 4ℓ/h and pad thickness of 10cm for second processing day	84
54	Instantaneous mass behavior under the superficial air velocity of 0.17m/s, three watering rates of 1, 2, and 4ℓ/h and pad thickness of 10cm for third processing day	85
55	Instantaneous mass behavior under the ambient conditions for the first, second and third processing days.	85
56	Instantaneous mass behavior under the superficial air velocity of 0.13m/s, three watering rates of 1, 2, and 4ℓ/h and pad thickness of 10cm for first processing day	86
57	Instantaneous mass behavior under the superficial air velocity of 0.13m/s, three watering rates of 1, 2, and 4ℓ/h and pad thickness of 10cm for second processing day	87
58	Instantaneous mass behavior under the superficial air velocity of 0.13m/s, three watering rates of 1, 2, and 4ℓ/h and pad thickness of 10cm for third processing day	87
59	Instantaneous mass behavior under the ambient conditions for the first, second and third processing days	88

Figure No.	Title	Page No.
60	Scatter distribution of the measured versus the predicted relative humidity of the evaporative cooler by Equation 6	90
61	Scatter distribution of the measured versus the predicted air temperature of the evaporative cooler by Equation 7	91
62	Instantaneous mass of Jew's Mallow in the evaporative cooler under: watering rate of 4 l/h and superficial air velocities of 0.21m/s at pad thickness of 10cm	92
63	Instantaneous mass of Jew's Mallow in the evaporative cooler under: watering rate of 4 l/h and superficial air velocities of 0.17 m/s at pad thickness of 10cm	93
64	Instantaneous mass of Jew's Mallow in the evaporative cooler under: watering rate of 4 l/h and superficial air velocities of 0.13 m/s at pad thickness of 10cm.	94
65	General appearance from the first to the fifth experimental day	97
66	Morphological system for image processing	98
67	RGB pixel intensity histogram of leave sample of 0.0% wilting percent	100
68	RGB pixel intensity histogram of leave sample of 1.3% wilting percent	100
69	RGB pixel intensity histogram of leave sample of 3.1% wilting percent	101
70	RGB pixel intensity histogram of leave sample of 3.5% wilting percent	101
71	RGB color-map based on freshness degrees of Jew's Mallow	103

LIST OF TABLES

Table No.	Title	Page No.
1	The measured data and calculated values of the average cooling potential and saturation efficiency at different pad thickness and pad –face air velocities for various configurations of pad	8
2	Percent mass loss of produce after 7 days	24
3	Recommended temperature, relative humidity and storage period of fruits	29
4	The critical relative humidity and temperatures for various fruits and vegetables	29
5	Optimal storage conditions recommended for extended shelve life and maximum eating quality of various produce	30
6	System performance at different affecting factors for some evaporative coolers	31
7	Standard B-H mean and its corresponding value of wilting percent	56
8	Calculated superficial air velocity	61
9	Boundary conditions of the developed model application	89
10	General Appearance measurements of some samples of Jew's Mallow leaves	95
11	Six times daily measurements of CCI for five storing days under laboratory environment conditions	96

NOMENCLATURE

ΔT	Cooling potential (Temperature reduction), °C
T_{db}	Dry- bulb temperature of the ambient air, °C
T_c	Dry- bulb temperature of the cooled air inside the evaporative cooler, °C
SE	Saturation efficiency, %
T_{wb}	Wet-bulb temperature of the ambient air, °C
AV	Superficial air velocity, m/s
WR	Watering rate, ℓ/h
T	Air temperature of evaporative cooler, °C
AT	Ambient air temperature, °C
Q	The airflow rate at suction fan outlet, m ³ /s
A_f	The fan outlet cross sectional area, m ²
V_f	The exhausted air velocity at suction impeller fan outlet, m/s
A_p	The pad surface area, m ²
V_p	The superficial air velocity at suction impeller fan outlet, m/s
AV1	Superficial air velocity of 0.21m/s
AV2	Superficial air velocity of 0.17m/s
AV3	Superficial air velocity of 0.13m/s
WR1	Watering rate of 4ℓ/h
WR2	Watering rate of 2ℓ/h
WR3	Watering rate of 1ℓ/h
ARH1	Ambient relative humidity of first processing day at watering rate of 4ℓ/h, %
ARH2	Ambient relative humidity of first processing day at watering rate of 2ℓ/h, %
ARH3	Ambient relative humidity of first processing day at watering rate of 1ℓ/h, %
AT1	Ambient air temperature of first processing day at superficial air velocity of 0.21m/s, °C
AT2	Ambient air temperature of first processing day at superficial air velocity of 0.17m/s, °C
AT3	Ambient air temperature of first processing day at superficial air velocity of 0.13m/s, °C



Introduction

1. INTRODUCTION

Corchorus olitorius, which is known as "Jew's Mallow", "Bush okra", "Tossa jute", "Krinkrin", or "West African sorrel", "Molokhia, and other local names (**Nyadanu *et al.* , 2017**). It is an important green leafy vegetable in Egypt. Its cultivated area is about 2,112.964 Feddans in Egypt and production is about 912.6 tons with a productivity of 0.472 ton/feddan (**FAO, 2018**). Jew's Mallow has an important place in terms of human health. It is high in minerals like calcium, iron, and phosphorus, as well as vitamins like A and B. Mineral A is essential for the epithelia tissues that cover our bodies and organs, eye health, bone and tooth formation, and the proper functioning of endocrine glands. Vitamin A is also vital for our bodies' reproductive and growth functions, as well as for improving their resistance to illnesses. Leafy vegetables are a good source of minerals, vitamins, fibre, amino acids, and phytochemicals that have antioxidant, antimicrobial, anticancer, and other nutraceutical characteristics.

Jaw's Mallow is considered a leafy vegetable that is highly perishable commodities and presents a lot of difficulties in storage due to their perishable nature. Temperature and humidity play a major role in storage of Jew's Mallow. The single most critical element impacting the rate of deterioration of freshly harvested commodities is temperature; however, correct relative humidity must be maintained during storage. Rapid cooling of food to a safe storage or transit temperature is critical for maintaining quality and extending shelflife by halting physiological and pathological deterioration. Field heat, a considerable portion of the cooling load, is included in the harvested produce and is connected with the product temperature. There are ways to extend the shelflife of food. These methods are used alone or in combination to extend the normal

biological life of foodstuffs and increase sales. They include (a) less damage to product quality, (b) cook-chill combinations that deliver longer high-quality shelflife, (c) new methods of heating that are better controlled and thus deliver milder heat to products, (d) modified atmosphere packaging to retain quality longer and (e) use of antimicrobial systems that are more natural. The process of controlling the quality of mallow leaves during the storage period is very important to obtain a high quality stored product. With the emerge of image processing technologies, this helped the possibility of developing a visual analytical device (nondestructive) that could determine the quality of the stored product in order to reduce the costs of the storage process.

The main objective of this current investigation is controlling fast remove field heat stress appropriately and maintain the Jew's Mallow at good storage environment by manufacturing an accessible compact evaporative cooler that has a potential storage quality monitoring tool.

The specific objectives are as follows:

1. Studying the thermal performance of the manufactured evaporative cooler under different levels of pad watering rates and pad thicknesses,
2. Investigating the influence of superficial air velocities of 0.13, 0.17 and 0.21m/s on the evolution of evaporative cooling process,
3. Developing an empirical equation for the evaporative cooling rate during Jew's Mallow storage, and
4. Extracting an appropriate imagery classifying features for further implementation in machine visions in Jew's Mallow (*Corchorus olitorius*) processing plants in Egypt.



Review of literature

2. REVIEW OF LITERATURE

It is necessary to lower the temperature of the produce by lowering its respiration rates, water loss, ethylene synthesis, and sensitivity to it, as well as limiting microbial development. According to, low relative humidity raises transpiration rates, whereas high relative humidity reduces water evaporation and therefore cooling. When the relative humidity is high, produce retains its nutritional quality, appearance, and flavour while softening and wilting are limited (**Odesola and Onyebuchi, 2009**).

Kassem (1992) reported that many producers in less humid and dry parts of the world favour evaporative cooling systems because of their relative ease of installation in both new and remodelled farm structures (plant and animal structures). It's usually delivered via a misting system or a pad.

Image processing is a classic inverse issue that involves breaking an image picture into meaningful or spatially coherent sections with similar features in order to achieve a concise region-based description of the scene. In many video and computer vision applications, this low-level vision task is often the first (and most important) step. Object recognition or localization, for example, compression, tracking, image retrieval, and understanding are all examples of data compression. In recent years, several novel and creative image processing algorithms have been created, which can be divided into five categories: thresholding, template matching, clustering, edge detection, and region growth (**Krinidis and Pita, 2009**).

2.1. Methods of agricultural production storage

A global goal is to reduce losses in postharvest fruit and vegetable operations (**Clement et al., 2009**).

Packaging is an unavoidable part of ensuring safe handling, and numerous technologies, including cold storage, have been attempted to increase the storage life of fresh spinach (**Mudau et al., 2015**), MAP (**Tudela et al., 2013**), chemical dipping (**Cefola and Pace, 2015**) and irradiation treatments (**Hussain et al., 2016**) which have been proved to maintain freshness and quality throughout the storage term.

2.2. Visual and biochemical quality and marketability of leafy vegetables

Leafy vegetables are commonly considered of as perishable crops because of their rapid loss of moisture content, high rate of respiration, rapid appearance of shrivelling symptoms, and loosening of crispiness, all of which result in high quantitative and qualitative losses in postharvest supply chains. (**Wang et al., 2003 and Kader, 1992**).

A digital refractometer RX 5000 was used to assess the soluble solids concentration (SSC) of spinach juice. Total antioxidants in spinach leaves were calculated by (**Williams et al., 1995**) using the methodology, with the value reported as percent inhibitory activity.

In fruits stored in a cool chamber, the rate of change of physicochemical constituents is slower (**Wasker et al., 1999**).

Chlorophyll content is linked to green color, which is a clear indicator of freshness and quality in leafy vegetables. Unlike fruit vegetables, it quickly loses water and freshness after harvest, resulting in cell wall disintegration as well as sensory and nutritional qualities such as texture and color. Furthermore, physiological factors are intimately linked

to sensory quality, which is one of the most important criterion for product acceptability. Due to their increased water content, active and rapid biological and physiological reactions, and the ease with which they can be bruised after harvest, leaf lettuces are particularly perishable. Despite its popularity and nutritional benefits, consumers may reject or cancel their leaf lettuce purchases if the quality or freshness of the product deteriorates, particularly when the products are consumed fresh (**Esturk *et al.*, 2014**).

Cleaning, physical appearance, and color retention were assessed using a nine-point evaluation scale: 9-excellent, 7-good, 5-fair, 3-bad, and 1-extremely poor (**Medina *et al.*, 2012**).

Weighing the decaying leaves and deducting from the total mass at each removal yielded the fraction of deteriorated leaves in preserved spinach. After three days of storage, 15 leaves from each replicate treatments were selected, and the marketability index was calculated by counting the leaves (**Malik *et al.*, 2021**).

2.3. Factors affecting physiological, biochemical and microbial properties

Using certain treatments, the quality of fresh vegetables at postharvest stages can be preserved and the pace of degradation can be reduced. For example, postharvest parameters such as storage temperature, relative humidity, packaging materials, and packaging method influence the quality of leaf lettuce throughout storage. Leaf lettuce has also been found to have low storage potential after harvest due to high respiration rates. Low temperature inhibits respiration rate and senescence, as well as the growth of spoilage bacteria, which is widely known (**Roura *et al.*, 2000**).

Lettuces are typically handled at room temperature or at a temperature higher than the ideal of 0°C with a humidity of greater than 98 % (Saltveit, 2016).

Furthermore, in Korea and many other countries, the typical market display (shelf) temperature, which is around 10°C, is greater than the residential refrigerator temperature (Jeong *et al.*, 2013 and Mampholo *et al.*, 2013).

2.4. Evaporative cooling system theory and basic principle

Evaporative cooling occurs when a body in contact with a liquid cools as the liquid evaporates into the surrounding air. Because it requires heat to transform a liquid into a vapour, when water evaporates off the body's surface, it becomes significantly cooler (Dadhich *et al.*, 2008).

When water evaporates into air, the wet bulb temperature is compared to the air dry bulb temperature to determine the potential for evaporative cooling. The bigger the temperature differential between the two, the more evaporative cooling occurs. As a result, evaporative cooling creates an effective cooling condition by combining the natural process of water evaporation with an air moving system. The fresh and warm outside air moves through the wet porous pad that cooling the air through water evaporation as shown in **Figure 1** (Watt, 1986).

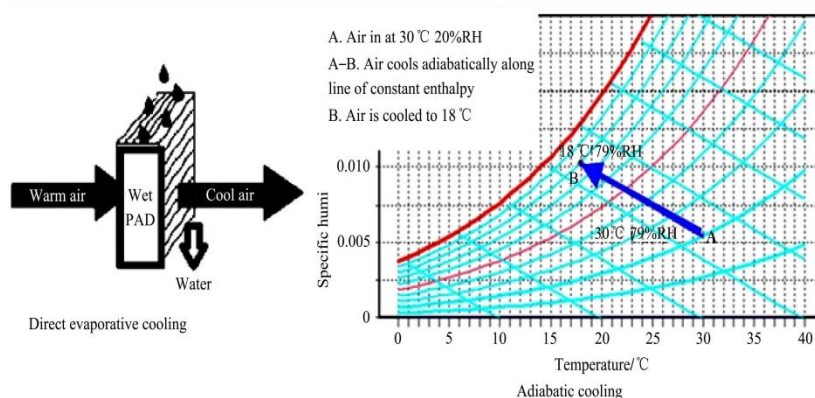


Figure 1. Evaporative cooling process representation on psychrometric chart (Watt, 1986)

Evaporative cooling is an adiabatic heat exchange that happens when ambient air flows across a saturated surface to achieve a low temperature and high humidity, which is perfect for increasing the shelflife of fruits and vegetables (**Das and Chandra, 2001**).

Evaporative cooling is a well-known method of environmental cooling. This is an adiabatic process in which the ambient air cools by transferring its sensible heat to the evaporated water carried by the air. The greatest advantage of the natural environment is taken in the evaporative cooled structure for lowering the temperature of outside ambient air to a very low level (**FAO, 2006**).

The rate of evaporation is influenced by the flow of air and the amount of surface area. When water evaporates from a surface, the humidity of the air near the water surface tends to rise. If this humid air persists, the rate of evaporation will begin to slow as the humidity level rises. The rate of evaporation, on the other hand, will either remain constant or increase if humid air and the water surface are repeatedly shifted away and replaced by drier air. The cooling surface, which determines the efficiency of the evaporative cooling structure, is the heart of the evaporative cooling system (**Jha and Kudos, 2006**).

2.5. Importance of evaporative cooling process

Basiouny and Abdallah (2013) demonstrated that the multihorizontal pad design produced the highest average cooled air temperature within the wind tunnel, with a pad thickness of 15cm and a pad-face air velocity of 1m/s. By expanding pad thickness from 3 to 15cm and using a multi-horizontal pad design with a 1m/s pad face air velocity, the mean cooling potential was raised from 7.46 to 11.78 °C (+57.91 %). For all pad configurations, the needed airflow rate was increased by increasing pad thickness and pad-face air velocity. Because of the fast

variations in airflow resistance, it has achieved its maximum levels when using the multi-horizontal pad design and the static pressure drop across the pad was raised from 31.39 to 70.63 Pa (+125 %) as listed in **Table 1**.

Table 1. The measured data and calculated values of the average cooling potential and saturation efficiency at different pad thickness and pad –face air velocities for various configurations of pad **Basiouny and Abdallah (2013)**

Pad thickness, cm	Pad-face air velocity, m/s	Vertical pad						Horizontal pad					
		T _{ab} , °C	SD of T _{ab} , °C	RH, %	T _e , °C	ΔT, °C	SE, %	T _{db} , °C	SD of T _{ab} , °C	RH, %	T _e , °C	ΔT, °C	SE, %
15	0.75	34.99	3.31	47.83	29.17	5.82	59.71	35.79	3.51	46.70	29.01	6.78	66.59
	1.00	34.97	3.24	48.39	27.80	7.16	76.76	34.35	3.35	47.60	27.32	7.58	79.80
	1.25	34.75	3.32	48.13	28.35	6.40	66.77	33.50	3.50	48.20	28.19	7.22	74.39
11	0.75	34.18	2.90	52.71	29.04	5.14	60.49	34.44	3.24	50.90	28.57	5.87	64.19
	1.00	34.35	2.67	52.35	28.64	5.71	68.45	34.76	3.47	49.70	27.71	7.06	78.36
	1.25	33.79	2.82	54.04	28.57	5.22	63.05	34.65	3.55	50.60	28.23	6.42	69.42
7	0.75	34.61	3.21	50.90	30.81	3.82	42.40	34.36	3.43	50.30	30.31	4.05	44.69
	1.00	34.47	3.39	49.67	29.54	5.42	59.08	34.71	3.15	49.70	28.82	5.88	65.46
	1.25	34.42	3.42	43.88	30.14	4.70	43.10	34.05	3.03	51.70	28.88	5.17	58.91
3	0.75	33.75	2.48	48.30	30.86	2.89	31.00	34.40	2.88	51.10	30.70	3.70	41.71
	1.00	33.64	2.82	46.30	28.93	4.71	48.93	34.16	3.33	52.40	28.64	5.52	65.97
	1.25	34.21	2.84	47.20	30.14	4.08	40.50	33.67	2.85	52.30	29.23	4.44	51.12

Pad thickness, cm	Pad-face air velocity, m/s	Multi-horizontal pad					
		T _{ab} , °C	SD of T _{ab} , °C	RH, %	T _e , °C	ΔT, °C	SE, %
15	0.75	34.18	3.37	50.00	27.03	7.15	78.85
	1.00	34.73	3.33	49.70	26.56	8.18	89.59
	1.25	34.58	3.66	49.80	27.09	7.48	81.43
11	0.75	35.53	3.46	46.20	28.54	6.99	67.97
	1.00	34.90	3.38	49.10	27.57	7.57	82.57
	1.25	34.60	2.90	48.90	27.67	6.99	74.71
7	0.75	32.88	2.36	54.10	28.60	4.28	52.97
	1.00	33.70	2.73	52.50	27.28	6.42	78.09
	1.25	33.47	1.92	51.60	27.77	5.70	67.86
3	0.75	34.22	3.41	49.90	30.21	4.01	44.29
	1.00	34.40	2.58	50.10	28.37	6.03	67.38
	1.25	33.30	2.65	53.40	28.40	4.90	58.50

the pad, Pa;
 ρ : density of water, 1000 kg/m³;
 g : acceleration of gravity, 9.81 m/s² and
 h : head of water, m.
 Single exponential regression equations were developed to describe the relationship between pad thickness and static pressure drop at different pad-face air velocities for each configuration of pad.

Horticultural items stored in the cool chamber have proved to have less physiological mass loss, better color, firmer texture, and a shelflife of 1–2 weeks in other regions of the country. Cool chambers are helpful for preserving fruit acceptability for extended periods of time while also minimising mass loss during storage (**Bhatnagar et al., 1990**).

It's also used to chill fruits and vegetables before shipping and storing them in cold storage (**Maini and Anand, 1992**).

Evaporative cooling storage is crucial for horticulture commodity marketing and distribution, as well as balancing daily supply and demand changes. In addition, using the best postharvest handling procedures throughout storage, transit, and distribution to market will help reduce losses. For harvested fruits and vegetables, evaporative cooling technology is available to establish and maintain appropriate temperature, relative humidity, and atmospheric composition throughout storage (**Chakraverty *et al.*, 2003**).

Anyanwu (2004) carried out the design, construction, and performance testing of a porous evaporative cooler for the preservation of fruits and vegetables. A cuboid-shaped porous clay container nested inside another clay container makes up the experimental cooler, which has a total storage volume of 0.014 m³. The area between them is filled with coconut fibre. Water is pumped into the gap from a reservoir connected to the chiller at the top through a flexible conduit, keeping the coconut fibre moist at all times. According to the results of the transient performance testing, the cooler storage chamber temperature drops below the ambient air temperature ranged from 0.1 to 12°C. During the test periods, ambient air temperatures ranged from 22 to 38 °C. The findings also show that the cooler outperforms open-air preservation of vegetables shortly after harvest during daytime operations. As a result, the evaporative cooler could be useful for preserving vegetables and fruits in the short term following harvest.

The shelflife of a product is determined by the species, variety, and pre-harvest conditions, particularly quality and ripeness. Fruits and vegetables, which are alive at the time of storage, distribution, and sale,

are divided into three categories: (1) foods that are alive at the time of storage, distribution, and sale, such as fruits and vegetables, (2) foods that are no longer alive but have been processed in some way, such as meat and fish products, and (3) goods that benefit from controlled temperature. Nonliving foods are more difficult to preserve because they are prone to spoilage. The key to extend the storage life and maintain marketable quality is proper temperature and relative humidity regulation. Fruit and vegetables kept in the cool chamber were found to have a shelflife of 90 days, up from 3 days at room temperature (**Chowdhury, 2005**).

Singh and Satapathy (2006) assessed the evaporative coolers performance. It was put to the test for two years, with the shelflife of bitter gourd, capsicum, tomato, cauliflower, pineapple, and peach being evaluated in both an evaporative cooler and a regular room. The mean maximum temperature within the evaporative cooler was roughly 5°C and 6°C lower than the ambient temperature throughout the summer and winter seasons, respectively. Throughout the year, the relative humidity (RH) within the evaporative cooler varied between 80 and 94 %, whereas it varied between 70 and 83 % in normal room conditions. During the summer and winter months, the RH within the evaporative cooler was about 13.34 % and 12.34 % higher, respectively. When stored in an evaporative cooler, the shelflife of bitter gourd, capsicum, and cauliflower was found to be improved by 5 days, whilst the shelflife of tomato, peach, and pineapple was found to be increased by 6 and 9 days, respectively, when compared to normal room conditions.

Dadhich et al., (2008) used baked bricks and riverbed sand to construct an evaporative cool chamber. The interior temperature was found to be 10–15°C lower than the outside temperature, the inside humidity was 30–40% higher than the outside humidity, and the mass

loss of fruits and vegetables stored within the chamber was less than that of those stored outside the chamber. In the chamber, fruits and vegetables can last up to 3 to 5 days longer than they would outside.

Evaporative cooling is one of the pre-cooling technologies used to quickly cool agricultural products to a safe storage or transit temperature. It improves shelflife by reducing the deteriorative changes caused by pathological and physiological agents. Field heat is a large element of the cooling load since the harvested product contains a significant quantity of heat. After harvesting, precooling is the process of rapidly removing heat from the product. Unless the product is promptly and correctly chilled, it will lose its quality in no time, depending on the temperature (**Rashwan, 2016**).

Cooling the environment can be accomplished in a variety of ways. Among these, evaporative cooling is a well-known system. The temperature decreases significantly and the humidity rises to a level that is ideal for short-term perishable storage on the farm in this cooling system (**Jha and Kudos, 2006**).

2.6. Importance of storing at low temperature after harvest

One of the most pressing difficulties in a tropical region is the storage of fresh horticultural produce after harvest. Fruits and vegetables have a short shelflife and are prone to spoilage due to their high moisture content. Furthermore, they are living organisms that continue to transpire, breathe, and mature even after harvest. Fresh horticulture product metabolism continues after harvest, deterioration rate increases as ripening, senescence, and unfavourable environmental variables increase. As a result, storing these items in their fresh state necessitates careful regulation of space temperature and humidity to keep chemical, biochemical, and physiological changes to a minimum (**Chandra *et al.*, 1999**).

Soon after harvesting, storing fruits and vegetables at a low temperature lowers the rate of respiration, resulting in less heat, thermal degradation, and microbiological deterioration, as well as extending the quality and freshness of the material (**Chopra *et al.*, 2003**).

Horticultural goods require proper storage for marketing and distribution. Storage also helps to keep supply and demand in check on a daily demand (**Chakraverty *et al.*, 2003**).

2.7. Performance evaluation indicators

Peterson (1993) made a comparison. To manage fruits held in room temperatures (28°C–33°C, 45–65 % RH) during the summer in Mysore, tomatoes were matured under evaporative cooling (EC) storage conditions (20°C–25°C, 92–95 % RH). On the 15th day, EC ripened tomatoes had a maximum ripening index (RI) of 100 % a ratio of redness to yellowishness (a/b) of 2.48, and a hue angle (°) of 22.1°, whereas control tomatoes had a RI of 83.3 %, a/b ratio of 1.59, and a hue angle of 32.9°. Lycopene levels in EC-ripened fruits are twice as high as in control fruits. EC maintained apples had decreased rupture and shear forces. Control fruits lost moisture at a rate of 6.5 times that of the experimental fruits, as great as for EC stored tomatoes.

Mehta and Kaul (1997) reported that Physiological losses in tubers of three potato cultivars remained under 10% following 12 weeks of storage under evaporative cooling. Sugar content rose by just 52.4–242.1 % in tubers stored in evaporatively cooled storage, compared to 90.5–484.2 % in tubers stored in refrigerated storage until 14 weeks. Potatoes stored in evaporatively cooled storage had fewer physiological losses and lower reducing sugar concentration, making them more suitable for processing into chips and french fries.

Mordi and Olorunda (2003) developed an evaporative cooler structure for fresh tomato storage with an average temperature drop of 8.2 °C from ambient of 33 °C and a RH increase of 36.6 % over ambient of 60.4 % The visual quality features and marketability of the evaporative cooler samples were higher than those stored in ambient settings. Fresh tomatoes without packing had a storage life of 11 days in an evaporative cooler, compared to 4 days under ambient conditions.

Bhardwaj and Sen (2003) treated Fresh mandarin fruits from Nagpur Santra with 0, 10, and 20% neem leaf extract and stored at ambient temperature (14.7–31.2°C, 19.4–55.1% relative humidity) and in an evaporative cooler (11.1–22.0°C, 89.9– 95.0% RH). The results showed that employing an evaporative cooler containing 20% neem leaf extract reduced physiological mass loss (PLW, 17.88%), rotting (18.07%), juice content loss (11.08%), organoleptic taste score (6.08), and diameter reduction significantly (11.54%). Under the same conditions, the TSS (11.61° Brix) and total sugar (7.15%) were steadily increased, but the rate of rise was slower. In an evaporative cooler with 20% leaf extract, the maximum retention of acidity (0.400 %) and ascorbic acid (27.17 mg/100 ml juice) was recorded on the 42nd day of storage. Fresh fruits may be preserved for up to 42 days with the same treatment, compared to only 20 days in ambient conditions (control).

Jha (2008) designed and tested a 5 tonne capacity Evaporative Cooled Storage Structure (ECSS) for fruits and vegetables grown in hot and arid locations on a pilot scale. In 2005 and 2006, the performance of ECSS was examined by preserving potatoes (4.5 tonnes), Kinnow (4.5 tonnes), and tomatoes (0.5 tonnes) at CIPHET, Ludhiana, in terms of temperature drop in ECSS and mass loss of kept materials.

The higher the rate of evaporation, the larger the surface area from which water can evaporate (**Odesola and Onyebuchi, 2009**).

2.8. Factors affecting produce quality under evaporative cooling storage conditions:

(Wassner and Ravetta, 2005) reported that rate of leaf appearance was greatly impacted by temperature, and the leaf stem ratio was higher in preserved leafy vegetables stored at low temperatures.

The transpiration rate, or the rate at which water is lost from produce, is determined by the moisture content of the air, which is often expressed as relative humidity. When relative humidity is high, produce preserves its saleable mass, appearance, nutritional content, and flavour, but wilting, softening, and juiciness are reduced. When the relative humidity is low, the air can only hold a fraction of the total amount of water vapour it can hold, and it can also absorb additional moisture. When the relative humidity is low, the rate of transpiration increases. However, when the relative humidity is high, water evaporation is slow (Odesola and Onyebuchi, 2009).

2.9. Methods of evaporative cooling

The two types of evaporative cooling systems are direct and indirect evaporative cooling systems (Otterbein, 1996).

The air passes directly through the humidifier into the cooling chamber in a direct evaporative cooling system, however in an indirect evaporative cooling system, the air is precooled with mostly heat exchangers before passing through the cooling pad or vice versa, depending on the purpose (Jain, 2007).

In direct evaporative cooling, the process is adiabatic, and cooling is impossible since total saturation of the air is not achievable (Xuan *et al.*, 2012).

Direct evaporative cooling systems' performance and application have been constrained as a result of this. Active and passive evaporative cooling systems are the two most common forms of direct evaporative cooling systems. The ambient air is driven through the wet pad into the system by a set of suction impeller fans or blowers in active evaporative cooling systems. This system can withstand high static pressure and is occasionally used in conjunction with a heat exchanger (indirect evaporative cooling). To pump cold air into the system, passive evaporative cooling systems rely on natural air circulation (direct evaporative cooling). In windy situations with a lot of air moving around and a low pressure head, passive systems are extremely useful. This is the first form of evaporative cooling, often known as zero-energy cooling (Ndukwu *et al.*, 2013).

2.9.1 Direct evaporative cooling system (passive types)

Neil (2008) reported that direct evaporative cooling is a cooling method that has been around for a long time. The incoming air is simply passed through a wet porous humidifier in this manner. Here, two things are accomplished: (i) the inlet temperature is lowered, and (ii) the inlet air humidity is increased. The cold storage of agricultural produce necessitates these two conditions.

Wescor (2011) reported the heat transmission mechanism in direct evaporative cooling is assumed to be adiabatic, and hence follows the psychometric chart's constant enthalpy line. In this scenario, Lowering the input temperature is more difficult than increasing the incoming air's relative humidity. However, because the contact time may be insufficient and the pad may not be entirely saturated, 100% efficiency is not possible. Researchers are grappling with the lack of long-lasting construction materials for evaporative cooling systems, as well as the

high cost of suction impeller fans and blowers.

FAO (1995) reported the straw packinghouse was used to keep the goods cool. The packinghouse is constructed of natural materials that can be dampened with water. The wetting of the roof and walls on a regular basis generates the ideal conditions for evaporative cooling. Because the degree of cooling is limited to 1 to 2°C above the wet bulb temperature, these coolers are best suited to lower humidity conditions.

Acedo (1997) presented two basic evaporative coolers for cooling and storing vegetables that were created in the Philippines. **Figure 2** is standing atop a galvanized iron water pan with another water pan on top of it. Jute sacks are used to cover the sides and top, which are maintained wet by dipping the top and bottom edges into water pans. In **Figure 2**, the inner sidewalls are composed of fine mesh (0.32cm) wire, while the outer walls are built of planar galvanised sheet with fine perforations (spaced 5cm).

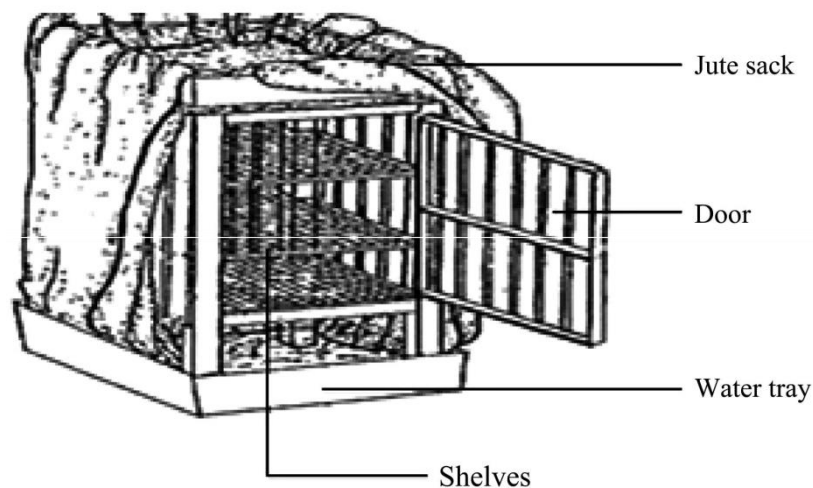


Figure 2.Evaporative cooler with jute bag as cooling pad (**Acedo, 1997**)

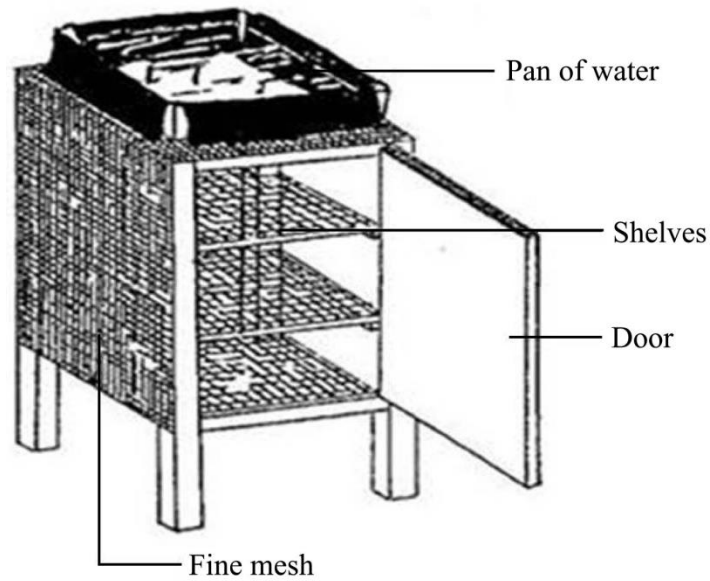


Figure 3. Evaporative cooler with rice husk as cooling pad (Acedo, 1997)

Rice husk fills the 1.5cm gap between the inner and outer walls, which is kept moist by contact with a cloth dropping into the water pan on top of the cooler. The vegetables kept in these coolers has a three-week shelflife. By washing with chlorinated water before cooling, decay can be avoided.

Roy (1994) proposed a low-cost cooling chamber made of bricks water-soaked sand fills the area between the walls as shown in **Figure 4**. Fruits and vegetables are placed in the chamber, which is then covered with a moist rush pad. Due to the large amount of resources necessary to build it, this cold storage chamber may only be useful for processing high-value products. This chamber is used to keep an internal temperature of 15-18°C and a relative humidity of around 95% during India's hot summer months.

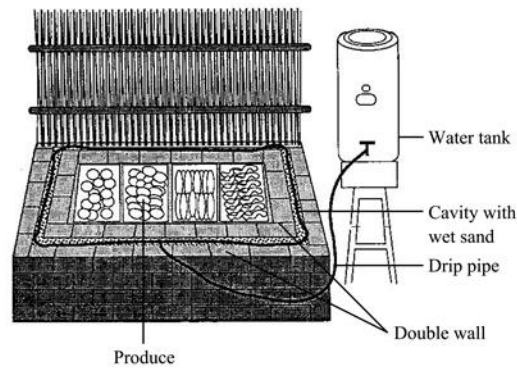


Figure 4. Evaporative cooler made from bricks (Roy, 1994)

2.9.2. Direct evaporative cooling system (active types)

Mogaji and Fapetu (2011) reported that to drive the air towards the cooling pad, a mechanical approach might be used. This can be accomplished by using a suction impeller fan or blower, or any other means that draws air towards the pad. However, this usually comes at a higher price.

Acedo (1997) presented an active evaporative cooler for preservation of fruit and vegetable, **Figure 5**. The direct evaporative cooling system is how the evaporative cooler works. A vortex wind machine is installed in the cooler, and chicken wire was utilized to build two thin boxes on opposing sides of the cooler to retain moist chunks of charcoal or straw. The wind spins the turbine, pulling wet, cool air through the load of vegetables inside the cooler, while water is dropped onto the charcoal or straw. The indoor temperature was decreased to 3-5°C below the ambient air temperature, with a relative humidity is about 85%.

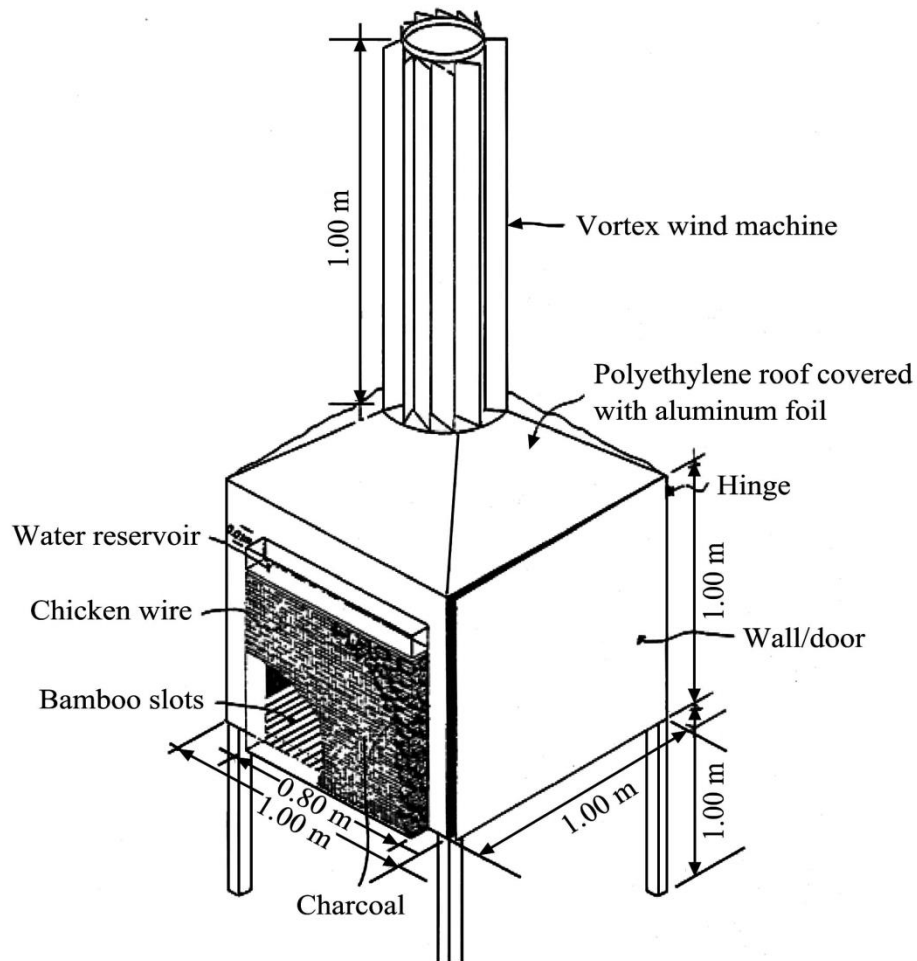


Figure 5. Evaporative cooler with vortex wind machine (Acedo, 1997)

2.9.3. Indirect evaporative cooling system

Abdalla (2009) reported that The draught air is handled twice or more by the equipment designers in indirect evaporative cooling. Before sending the primary air to the next level of cooling, they use a pre-cooler.

Zhao *et al.*, (2008) told that both dry and wet surface indirect evaporative coolers are available. They're divided into groups based on how heat and mass are exchanged in heat exchangers. Before entering the indirect heat exchanger, the secondary air is cooled by direct evaporative cooling. In a normal air-to-air heat exchange, this evaporatively cooled secondary air is subsequently used to cool main air via heat transfer.

This technology will be ideal for cooling residential homes because it removes moisture from the air. A wet surface heat exchanger is used for non-adiabatic evaporation in the wet surface type (**Ghassem *et al.*, (2009).**

Many of the works are for cooling homes, greenhouses, metallurgical production processes, vehicle engines, and tractor cabins (**Xuan *et al.*, 2012).**

Jain (2007) showed an active evaporative chiller that is indirect as shown in **Figure 6**. To improve evaporative cooling effectiveness for greater humidity and low temperature air conditioning for fruit and vegetable storage, a two-stage evaporative cooler was developed in India. It is based on the wet surface type and comprises of a plate type heat exchanger and two evaporative chambers. External air is cleaned before entering the heat exchanger by passing through the cooling pad. The humidifying pad is retained vertically across the airflow. The first cooling pad humidifies the heat exchanger's sensibly cooled fresh air. It is permissible for the storeroom to receive conditioned air. The air from the storage chamber passes through the second cooling pad, is humidified, and then flows vertically upward through the heat exchangers to act as coolant-air (second stream). The second stream cools the air from the first stream before exhausting it to storage. The cooler reduced the temperature by 18 to 16°C. Over the straight evaporative cooler, the two-stage cooler had a cooling efficiency of 1.1-1.2. It produced a room with a relative humidity of roughly 50% to 75%, which is quite low for fresh storage, and this could be due to some moisture was removed during the main cooling of the draught air.

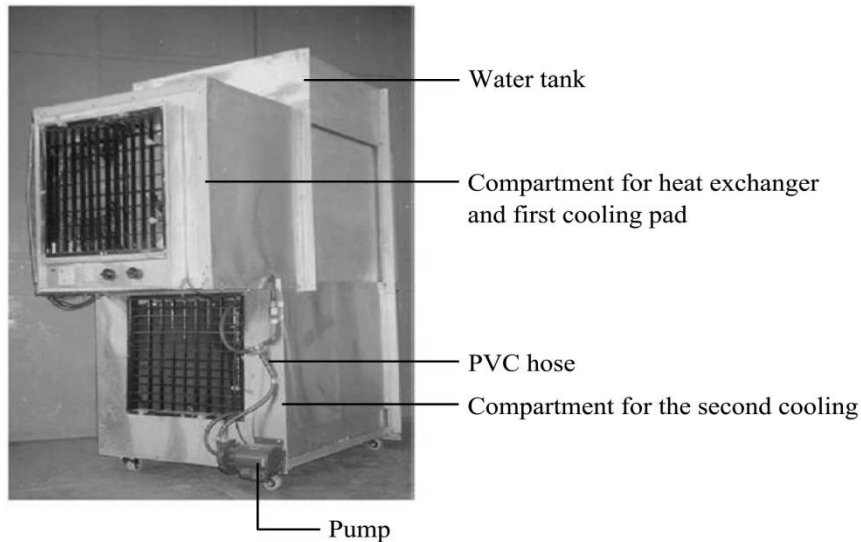


Figure 6. Indirect active evaporative cooler (**Jain, 2007**)

2.10. Water absorbent materials (cooling pads) for evaporative cooling

Evaporative cooling systems use water as the working fluid, and a variety of materials have been used to produce a wet surface for air-water contact in the designs. The ability to store water while allowing air to get through is the most important feature of these materials (**Xuan *et al.*, 2012**).

Various types of cooling surfaces, such as bare bricks and wood shavings-based silicon pads (**Dilip and Gopal, 2002**).

Under various climates, a variety of organic and inorganic materials have been studied for evaporative cooling. Metal pads, cellulose pads, hessian pads, Aspen, PVC pads, porous ceramic pads, wood shaved, jute, rice straw; excelsior of pine, fir, cotton wool, charcoal, and latex foam are just a few examples. Luffa, cedar, red wood, spruce, plain and etched glass fibres, copper, bronze, galvanised screening, vermiculite, perlite, palm leaf, palm fruit fibre, expanded paper, woven plastic (**Al-Sulaiman, 2002**). Some of these materials are shown in **Figures** from **7** to **9**.

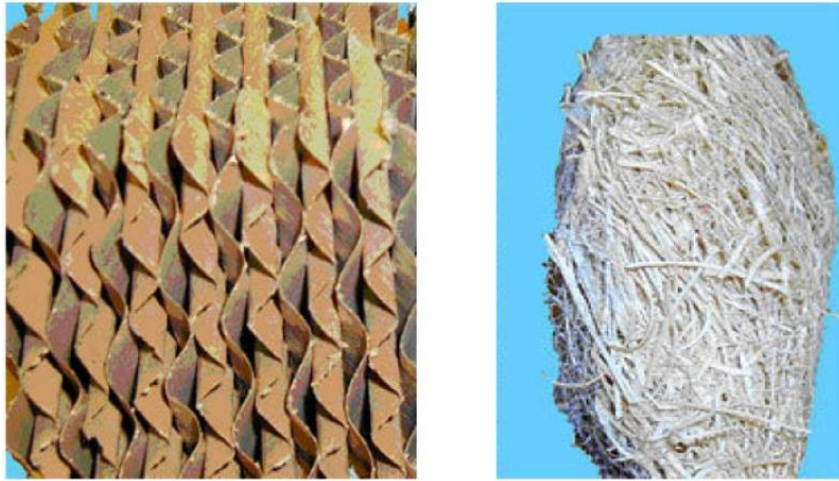


Figure 7. Aspen pad (Al-Sulaiman, 2002)

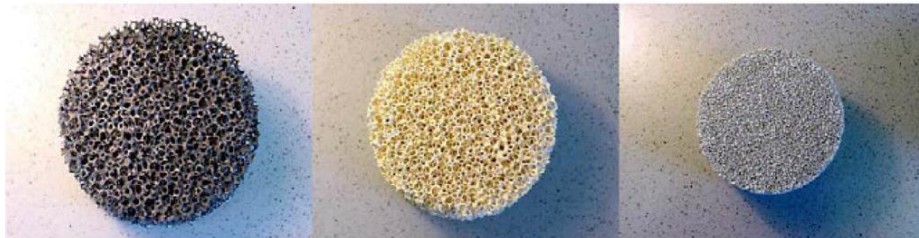


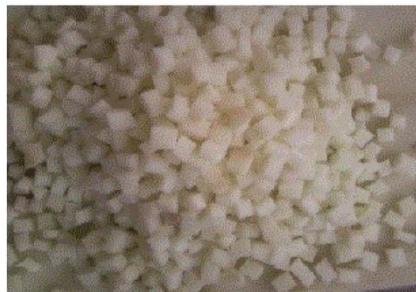
Figure 8. Porous ceramic pad (Al-Sulaiman, 2002)



Palm fruit fiber



Charcoal pieces



Shredded latex foam



Jute fiber

Figure 9. Pad materials (Al-Sulaiman, 2002)

2.11. Design considerations/choosing the right technology

Before making a decision, it's critical to consider the cooling requirements thoroughly and measure them against a variety of other aspects (**Odesola and Onyebuchi, 2009**) The following checklist may be useful in selecting the best design:

1. It is necessary to install a cooling system. Different foods require different chilling temperatures.
2. The average relative humidity of the area that requires cooling. Evaporative cooling will not be a viable choice if the relative humidity is continually high, so another system must be considered. Evaporative cooling may be effective if the relative humidity is low.
3. A windy area that necessitates cooling. If there is limited wind, evaporative cooling may not be the greatest solution. Where the cooling system to be used, there must be a sufficient supply of water. Evaporative cooling may be possible if this is easily available.
4. Access to the materials and skills required to construct the cooler.
5. If commercial systems are not too expensive, this technology may be a preferable option.

2.12. Physiological mass loss during storage

When tomatoes and carrots were stored in the evaporative cooling system chamber, mass loss was minimal, but it was maximal in ambient storage. The physiological mass reduction that the examined samples, tomatoes and carrots, experienced. As a result, the samples lost roughly 18 and 14 kg of mass, respectively. Contrary to this observation, tomatoes and carrots housed in the evaporative cooling cabinet retained their mass reasonably constant at 25kg after 2 weeks of storage, with only a 5 and 3kg mass loss for the studied samples after 2 weeks of storage, respectively (**Pessu, 2011**).

A porous evaporative cooler for carrot, spinach, and radish preservation. The cooler was created out of a 0.7 m³ brick construction that extended the storage life of a variety of produce. When compared to the control, vegetables in the evaporative cooler retained substantially more moisture after 7 days. The percent mass (%) loss of produce after 7 days is shown in **Table 2 (Dadhich *et al.*, 2008)**.

Table 2: Percent mass (%) loss of produce after 7 days (**Dadhich *et al.*, 2008**)

Product	Inside cooler	Outside cooler
Carrots	5%	50%
Spinach	8%	49%
Radish	12%	55%

2.13. Factors affecting the performance of a pad-suction impeller fan evaporative cooling system

The factors affecting evaporative cooling systems using pad-suction impeller fan system can be determined by several researchers (**ASHRAE, 1992; Liao and Chiu 2002; St-Pierre *et al.*, 2003 and Flores *et al.*, 2004**) as follows:

- Weather conditions.
- Pad material.
- Pad thickness and density.
- Pad face air velocity.

Cooling potential (T), saturation efficiency (SE), unit evaporative cooling performance (Unit ECP), and temperature humidity index (THI) are all key factors to consider when evaluating an evaporative cooling system.

2.13.1. Weather condition

ASHRAE (1992) reported that the efficiency of evaporative cooling is determined by the weather. The current outdoor dry and wet-bulb temperatures, as well as the system's requirements, influence system design. A simple household direct evaporative cooling system, for example, with an efficiency of 80%, will offer sufficient room conditions (given an adequate quantity of outdoor supply air and a well-designed exhaust system)

Campos *et al.*, (2002) used 13 years of data from the Maringa Meteorological Station, the potential for air temperature reduction through the deployment of an evaporative cooling system in the Maringa Parana region (Brazil). The potential for temperature reduction using evaporative systems was linked to the ambient temperature and relative humidity. Because of the low values of air relative humidity, the months with the best potential for temperature reduction were August, September, October, and November, according to the results. Despite being in the summer, the months of December, January, February, and March had a lesser potential for temperature reduction due to the occurrence of higher levels of air relative humidity. Evaporative cooling appears to be promising during the most important hours (13-18h), when the air temperature is at its greatest.

2.13.2. Pad material

Sharma and Kachru (1990) utilized evaporatively cooled sand stores, with a 5cm thick potato layer on the floor sandwiched between two 20cm thick sand layers to provide for evaporative cooling, 2.1m³ of water was sprayed on the sand every day. Wet sand was shown to be suitable for storing potatoes for up to 90 days under low atmospheric RH conditions, compared to 60 days in jute bags and even fewer in other storage methods such as bamboo baskets and piles.

Dzivama *et al.*, (1999) examined and tested at an ambient air temperature of 32°C and a relative humidity of 25%, four pad materials as pads for an active evaporative cooler: ground sponge, stem sponge, jute fibre, and charcoal. They discovered that the stem sponge performed best, with a temperature reduction of up to 18°C and a rise in air relative humidity of up to 84%. The produce remained in good physical condition for 18 days in the cooler, compared to 9 days under ambient settings, according to the results.

Abdel-Rahman (2000) evaluated and examined two types of evaporative cooling materials in greenhouse cooling systems, aspen fibres and long wheat straw are the materials used. He discovered that the cooling performance of both evaporative materials is nearly identical, with an average value of 22%. Both evaporative materials had maximum and minimum cooling performance values of 35% and 15%, respectively.

Liao and Chiu (2002) constructed a tiny wind tunnel for directly testing system performance and simulating pad-suction impeller fan evaporative cooling systems. Two different materials were tested as pads in a wind tunnel experiment: one made of thick fabric PVC sponge mesh 0.25cm diameter in pinhole and the other made of fine fabric PVC sponge mesh 0.75cm diameter in pinhole. This experiment looked at the effects of air velocity, watering rate, static pressure drop across pad, and pad thickness on evaporative cooling efficiency. The effectiveness of a fine fabric PVC sponge has been proven.

Jha and Kudos (2006) stated that the physical qualities of pads were investigated for optimizing cooling in an evaporatively cooled storage system, and it was discovered that partal wood savings was the best among the safeda, partal, and root pad for the greatest cooling effect in an evaporatively cooled storage system. With a thickness of 7mm of partal wood savings cooling, the greatest surface evaporation was found to be 14.87g of water per minute.

2.13.3. Pad thickness and density

Alchalabi (1996) compared between 10 and 20cm thickness of two types of vertical pad material in an evaporative cooling system. He stated that using a pad with a depth of 20cm and a pad face air velocity of 1.5m/s was the optimum option. At 20 and 10cm pad thicknesses, cooling effectiveness was 91% and 65% respectively.

Papa and El-Galabi (1997) studied the influence of pad thickness on a horizontally placed evaporative cooling system Palm fibres with a thickness of 9, 13, and 22cm were employed. They built the pad to serve as a dairy cow shelter's ceiling. They discovered that cooling efficiency was 70.1, 74.2, and 87.5% for pad thicknesses of 9, 13, and 22cm, respectively.

Dzivama *et al.*, (1999) pointed out at 6 cm pad thickness, 2.7 air suction velocity, and 90ml/s watering rate, the stem sponge worked well as a vertical pad cooler. The drop temperature was 12°C under the previous conditions, but the air relative humidity increased.

Liao and chiu (2002) studied three different vertical pad thickness namely 5, 10 and 15cm. Industrial materials were used to make these pads. The researchers discovered that the thicker the pad, the better the cooling efficiency. Increasing pad thickness from 5 cm to 10cm to 15cm improves cooling efficiency by approximately 24% and 16%, respectively.

2.13.4. Pad face air velocity

Abdel-Rahman (2000) used aspen wooden fibers and long wheat straw as horizontal pad materials. The air velocities through the pads were 1m/s, with R^2 values of 0.62 and 0.54, respectively, for aspen hardwood fibres and temperature versus air velocity through the pad for long wheat straw.

2.14. Humidity rate:

Ganesan *et al.*, (2004) evaluated the influence of different water levels on the shelflife of brinjal in an evaporative cooler, determining that the shelf-life at room temperature, which was only 3 days, was increased to 9 days by adding 100 litres of water each day.

2.15. Optimum temperatures and relative humidity for storing vegetables and fruits

The majority of fruits and vegetables prefer to be stored at a temperature above freezing (**FAO, 1995**).

Alexandre *et al.*, (2012) indicated that chilling temperatures (1-10°C) induce several physiological problems in the cell, resulting in chilling injury and death. By eliminating the field heat as quickly as possible after harvesting, the storage life can be extended.

Tropical and sub-tropical plants and some tissues of temperate origin plants are injured by exposure to temperature below 12°C (**Saltveit and Morris, 1990**). However, (**Alexander *et al.*, 2012**), indicated that Chilling temperatures (1-10°C) produce a variety of physiological problems in cells, leading to chilling injury and death.

Most green vegetables and temperate fruits, including citrus fruits, are not chill sensitive and can be stored at temperatures between 0 and 2°C for long periods of time without losing their visual quality. Meanwhile, tropical and subtropical fruits, as well as a number of root vegetables, are chill sensitive and can be damaged by extreme cold. As a result, they're frequently stored at temperatures of 13°C or above, while some can be safely stored at temps as low as 5°C if chilled rapidly after harvest. Low temperature does not completely remove such spoiling agents, but it considerably decreases their activity, making it a realistic method of keeping perishable food in their natural state which otherwise is not possible through heating as shown in **Tables 3, 4 and 5** (**Chopra *et al.*, 2003**).

Table 3. Recommended temperature, relative humidity and storage life of fruits (**Chopra *et al.*, 2003**)

Fruit	Temperature (°C)	Relative humidity (%)	Approx. storage live (weeks)
Custard apple	7–10	85–90	1–2
Guava	5–10	90	2–3
Jackfruit	11–12.8	85–90	3–5
Mango	13	95–90	2–3
Pineapple	7–13	85–90	2–4
Pomegranate	0–5	90–95	2–3 months

Table 4. Temperatures and relative humidity that are crucial for certain fruits and vegetables (**Chopra *et al.*, 2003**)

Products	Temperature °C	Relative humidity %	Maximum storage time Recommended (ASHRAE handbook 1998)	Storage time in cold stores for vegetables in tropical countries
Apple	0–4	90–95	2–6 m	–
Beetroot	0	95–99	–	–
Cabbage	0	95–99	5–6 m	2 m
Carrots	0	98–99	5–9 m	2 m
Cauliflower	0	95	2–4 w	1 w
Cucumber	10–13	90–95		
Eggplant	8–10	90–95		
Lettuce	1	95–99		
Leeks	0	95	1–3 m	1 m
Oranges	0–4	85–90	3–4 m	
Pears	0	90–95	2–5 m	
Pumpkin	10–13	70–75		
Spinach	0	95	1–2 w	1 w
Tomatoes	13–21	85–90		

Table 5: Optimal storage conditions for diverse produce are recommended for increased shelflife and best eating quality (Odesola and Onyebuchi, 2009)

Commodity	Temperature (°F)	Relative Humidity (%)	Storage Life
Apples, late season	30–38	95	2–6 months
Beet, bunched	32	98–100	10–14 days
Beet, topped	32	98–100	4–6 months
Broccoli	32	95–100	10–14 days
Brussels Sprouts	32	95–100	3–5 weeks
Cabbage	32	98–100	3–6 weeks
Carrot, bunched	32	95–100	2 weeks
Carrot, mature	32	98–100	7–9 months
Cauliflower	32	95–98	3–4 weeks
Celeriac	32	97–99	6–8 months
Celery	32	98–100	2–3 months
Garlic	32	65–70	6–7 months
Horseradish	30–32	98–100	10–12 months
Kale	32	95–100	2–3 weeks
Kohlrabi	32	98–100	2–3 months
Onion, dry	32	65–70	1–8 months
Parsnip	32	98–100	4–6 months
Pears	34–36	95	2–4 months
Pepper, sweet	45–55	90–95	2–3 weeks
Potato, late	50–60	90–95	5–10 months
Radish, winter	32	95–100	2–4 months
Rutabaga	32	98–100	4–6 months
Squash, winter	50	50–70	Variable
Tomato, ripe	46–50	90–95	4–7 days
Turnip	32	95	4–5 months

System performance at different affecting factors for some evaporative coolers and different studies as listed in **table 6**.

Table 6: System performance at different affecting factors for some evaporative coolers (**Odesola and Onyebuchi, 2009**)

S/no	Author	Pad material	Pad thickness/mm	Air flow rate/(m·s ⁻¹)	Cooling efficiency/%	Cooling capacity/W	Energy efficiency ratio	Evaporation loss/%	Ambient condition	Room condition
1	Jain, D ^[21]	Wood shave	50	3.0 intake air	85-90	2125 - 4500	-	-	21-33°C 15%-40%RH	17-25°C, 50% -75%RH
2	Abenoet al ^[42]	Jute	0.9	-	127	-	-	-	31.5°C 67.5%RH	25°C 90%RH
3	Mogaji and Fapetu ^[47]	Jute	60	4.3 intake air	-	-	-	-	26-32°C 18%-31% RH	16-26°C 33%- 88%RH
4	Manuwa and Odey ^[22]	Jute	25	0.51-1.37	93.5	-	-	-	20.6-33.3°C 65%-95%RH	22-26°C 95%-98%RH
		Latex foam	25	0.69-1.25	91.4	-	-	-	20.6-33.3°C 73%-93%RH	22 -25.5°C 91%-97%RH
		Charcoal	25	0.98-1.45	91.3	-	-	-	20.6-33.3°C 61%-90%RH	22.5-24.5°C 92-97%RH
		Wood shave	25	0.35-1.125	91.9	-	-	-	20.6-33.3°C 74%-94% RH	22.3-26.5°C 98%RH
5	Ndukwu ^[25]	Wood shave	80	-	20-92	1207	-	-	32-40°C 40.3%RH	24-29°C 92%RH
6	Ndukwu et al ^[28]	Palm fruit Fiber	30	4.0	98	2,529	-	-	29.9-37°C 34%-73%RH	23.2°C 85.6%-96.8%RH
7	Anyanwu ^[23]	Coconut husk	50	1.5	-	-	-	-	28-35°C 70%-90%RH	22.3-26.8°C

2.16. Developments of image processing fields

"Image processing" is an important process that extracts expressive information from grey scale or color (RGB) spectrum (**Agrawal et al., 2013**).

A digital image is split into various sections, or objects, during the segmentation operation in order to extract and understand the related information. In latest years, such technique has been extensively reflected in many key fields, such as medical imaging (**Taher et al., 2013**) remote sensing (**Ghamisi et al., 2014**), and pattern recognition (**Pal et al., 1993**).

Coster et al., (2005) determined the grain size after removing noise using linear filtering, and the grain boundaries were enhanced with a morphological gradient filter. Watershed transform thresholding and grain segmentation were also done.

Low-level processes on digital images are referred to as image preprocessing, and they are used to correct degradations and improve important qualities for high-level processes. Blur correction, illumination correction, filtering, morphological operations, noise removal, thresholding, segmentation, point processing, edge detection, and other techniques are commonly used, and each can be further categorized. **(Raja et al., 2014).**

Chen et al., (2010) told that image processing is used to detect cracks on the rail's surface automatically. An adaptive threshold technique was utilized to extract the crack region from the image, and a dynamic template based on the shape of the crack was employed to detect the continuous crack boundary and estimate the crack length.

The raw images are changed with a subset of those procedures in vegetable and fruit image processing, depending on the character of applications. In the image processing of vegetables and fruits, attribute extraction, background equalisation, and contrast enhancement are required on a regular basis **(Kondo, 2010).**

In recent years, hyperspectral imaging has been proposed as a viable method for identifying a variety of agricultural goods, combining the advantages of imaging and spectroscopy to obtain spectral and image information concurrently. Injuries to fruits and vegetables are included **(Ariana and Lu, 2010).**

With good digital image quality, an automated approach of image processing and mathematical morphology to assess grain size, grain boundaries, and size distribution was recorded in an ASTM standard. The image quality is affected by a variety of elements such as illumination, noise, low contrast, poorly defined grain boundaries, and pores. Correctly differentiating grain boundaries and pores results in a high-quality microstructure **(Peregrina et al., 2013)**

George (2015) told that the threshold level for separating necessary items (foreground) from background in a picture remains a crucial stage in imaging research. In recent years, there have been numerous research studies demonstrating the efficacy of computer vision-based attitudes for precision grading of vegetables and fruits in the food business.

Jhavar (2016) employed a recognition-based method to define orange maturity with a single color photograph of a fruit.

Based on the quantification of total soluble solids (TSS), hardness qualities, and pH, multispectral pictures were used to estimate the quality of pomegranate (**Khodabakhshian, 2017**).

2.16.1. Visual Performance

The resolution (quality of vision) of the retina is not uniform (or the field of view). In most animals, each eye has a centre region that gives superior resolution and is used to fixate and inspect an object of interest. Robotic operations based on visual instructions have become increasingly popular in modern production in recent years. Everyone's attention has been drawn to visual servoing as an active visual technology. The use of computer vision data to control the movements of a robot is known as visual servo control (VS) (**Darwish et al., 2017**).

The visual data can be received through a camera mounted directly on a robot manipulator or on a mobile robot, in which case the camera moves as the robot moves, or from a camera positioned in the workspace and watching robot motions from a fixed point. Other concepts, such as many cameras mounted on pan tilt heads and observing robot motion, can be explored. The robotic task to be completed can be represented in terms of virtual linkages (or fixtures) between the camera and the observed

objects, or it can be expressed directly using primitive constraints like point-to-line constraints (which states that an observed point must lie on a specific line) **Hager (1997)**.

Some issues, however, remain unresolved: In general, a single-camera based attitude assessment approach cannot create a transformation matrix with absolute scale. In the low-cost development trend of modern smart factories, the stereo attitude estimation approach, which uses the stereo disparity relationship to infer depth, requires at least two cameras, which raises system pricing. Furthermore, the distance between the two cameras restricts this method; if the distance is too short, the long-range target estimating accuracy suffers (**Tang *et al.*, 2019**).

Nyman *et al.*, (2010) showed that images with a low quality rating were reported differently from images with a high quality rating, reflecting a paradigm shift in the subjective decision-making space as a function of desire. To put it another way, low-quality images are assessed using a different set of rules and phrases than high-quality ones as shown in **Figure10**.

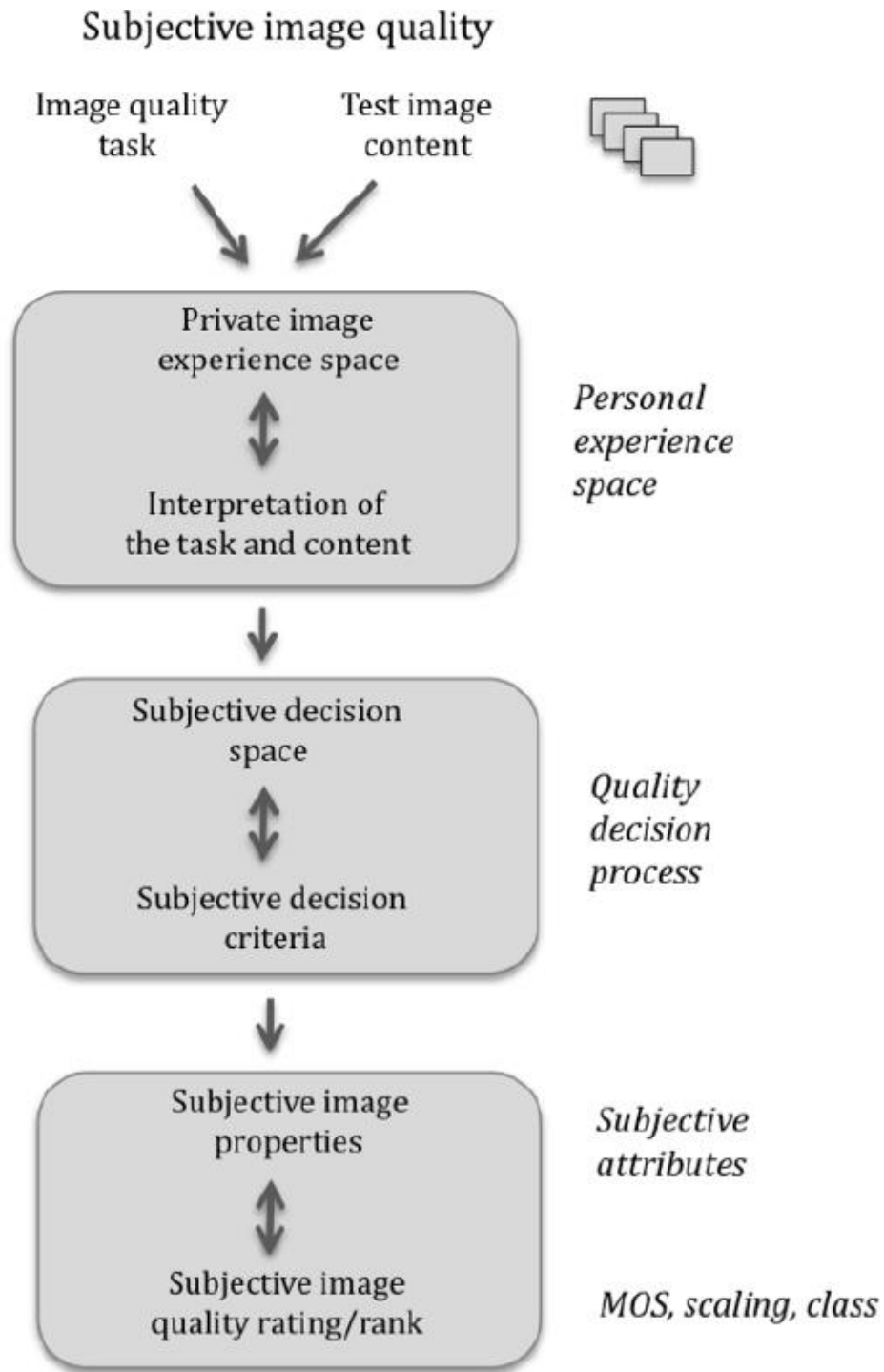


Figure 10. Main components of the subjective image quality decision process (Nyman *et al.*, 2010).

2.16.2. Machine Vision

Machine vision differs from animal vision in that it is not universal, but rather is specifically developed for a certain purpose or function. This aim can be quite specific, such as detecting faults in a manufactured object, verifying numerous specifications (such as shape and color), or controlling dynamic processes in production (filling a receptacle). As a result, the machine vision system's architecture will likely be highly limited, with parameters that are precisely tuned to the task at hand. Because of their capacity to collect both RGB images and depth information, RGB cameras have been used in a variety of sectors. These features serve as a guide for resolving the problem of target depth estimation in a visual servoing system (**Lin *et al.*, 2018**).

2.16.3. Machine Vision Application Using 3-D Imaging

The resolution and precision are determined by the sensor. More significantly, it establishes whether the data contains 2-D or 3-D scene information. The acquired data and the intended object model are described using object representations. During the matching stage, the descriptions are also utilized to figure out what the various properties of the scene's objects are. In real-time online operations, matching algorithms are employed to resolve ambiguities between input data and model descriptions. The target object's orientation and location information can be computed for future robot tasks once the match has been established. (**Anthes *et al.*, 1993**).

The following difficulties must be addressed by system designers in order to realize such vision systems: (1) the data collection sensor type, (2) the procedures for matching the object descriptions acquired from the input data to the intended object model, and (3) the strategies for describing the gathered data and the object (**Christoudias *et al.*, 2002**) .

Pabitra *et al.*, (2004) reported that machine vision is an important topic in the field of machine intelligence systems. A computer vision system's purpose is to comprehend picture input and use the extracted information to perform a high-level task. Typical application tasks include the assembly or inspection of industrial items, the navigation of autonomous vehicles, and the analysis of microscopic images.

Cyganek (2008) reported that one of the most significant aims of these activities is to recognize and locate a certain object in the scene. Thing recognition refers to the general difficulty of identifying the intended object. The objects in the following scenarios should be located by an ideal computer vision system: (1) Items can have arbitrary and complex shapes, (2) they can be seen from numerous perspectives, and (3) they can be partially concealed by other objects in the scene. In a manufacturing environment, a machine vision system like this can be used to determine the location of grab sites for a robot manipulating an object during assembly or inspection of parts.

2.16.4. Computer vision system

Traditional computer vision systems first appeared in the late 1960s and are now widely used in aerospace, industrial automation, security inspections, intelligent transportation systems, medical imaging, military applications, robot guidance, autonomous vehicles, food quality and safety inspection, and other fields. The images captured by RGB color cameras are centred around RGB wavelength because standard computer vision systems account for primary colors: red, green, and blue (RGB). Many properties such as texture, form, color, size, and flaws can be graded and assessed automatically by utilizing a computer vision system. However, some flaws are difficult to notice because their texture and color are comparable to skin (**Lorente *et al.*, 2012**).

Arman and Aggarwal (1993) reported that in an offline approach, a description of a standard item is established as the model object. The same description approach is used to represent the input data in an online process as it is in an offline process. The input object description and the model description are compared at the matching stage. In following applications, the object's location as well as its posture information are used. The main issues involved in the building of a computer vision system are described in the introduction section. The general paradigm of a computer vision system is depicted in **Figure 11**. The system includes both online and offline processes. In an offline procedure, a description of a standard item is established as the model object. The same description approach is used to represent the input data in an online process as it is in an offline process. The input object description and the model description are compared at the matching stage. In the following applications, the object's location as well as its posture information are used.

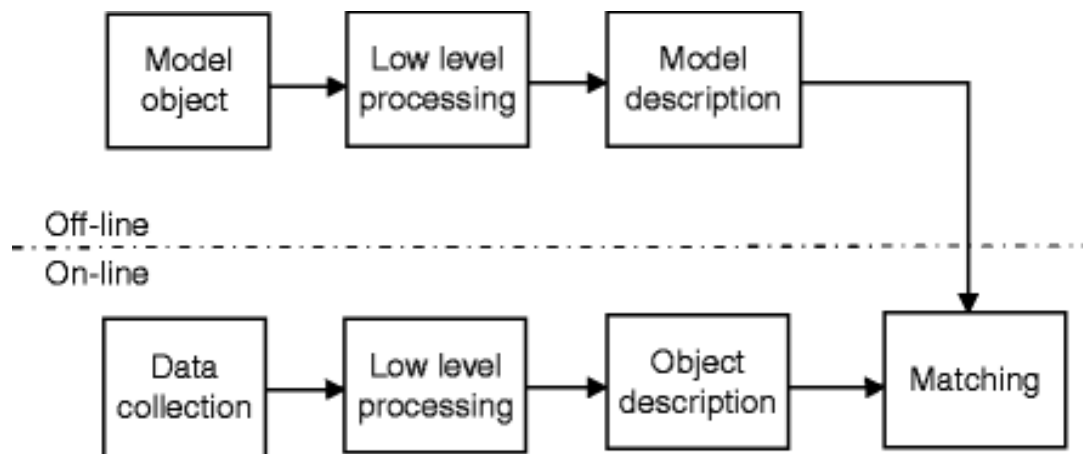


Figure 11. A general paradigm in computer vision **Arman and Aggarwal (1993)**

2.16.5. Low-Level Processes:

For the required high-level procedures, the collected range images must be represented using symbolic descriptions. In the first stage, the input images are partitioned based on the type of input data and the high-level processes. Contour information is also important for 3-D object recognition since the ideal vision system must be able to recognise any shaped object from any view direction. The fundamental low-level procedures in 3-D object recognition are segmentation and edge detection. Range scanners collect data from various spots on an object's surface. To obtain segmentation and edge detection, surface features such as surface normal and surface curvature are used **Brophy (1990)**.

Segmentation is the process of grouping pixels into one of several disjoint sets, each of which has a similar feature. Because it helps partition an image array into low-level elements, segmentation is most commonly utilized in range image analysis and recognition. In general, there are two types of segmentation methods for range photos. The first is based on area features, while the second is based on edge data. Unlike typical 2-D intensity image processing, range image processing uses three basic types of edges in 3-D range images.

Anthes et al., (1993) told that these sorts of edges include step edges, which are discontinuous in depth value, roof edges, which are discontinuous in surface normal, and curvature edges, which are discontinuous in a variety of surface normal. It's more difficult to recognise edges in range photos than it is in intensity photographs. Because the roof and curve edges do not correspond to depth discontinuity. A lot of studies on edge detection in range images have been published. The edge detection methods are divided into two classes to extract all three types of edges in range photos. Different operators or

techniques are used to extract different types of edges in the first class of methods. A merging process is then used to obtain final edge results (Arman and Aggarwal, 1993).

2.17. Imaging Devices

Bao *et al.*, (2005) told that in range image data collection, the pixel information within an image provides at least the relative distances from a sensor to the imaged points on objects. Images acquired using structured light, triangulation, or stereo pairs are frequently analysed to obtain range data. These image-gathering techniques make use of industry-standard CCD cameras, need a regulated lighting condition, and are limited to the geometric characteristics of imaged objects. In contrast, laser radar technology offers another feasible method for gathering range picture data.

Some factors, such as camera exposure duration, focal length, light intensity, image size, and convey speed, must be adjusted prior to image acquisition in order to obtain accurate data (Zou *et al.*, 2010).

2.18. Image processing techniques

Range image processing can be approached in a variety of ways. There are numerous ways in this area, and there are different methodologies for each imaging attribute description. Two approaches are presented: (1) edge detection and (2) region segmentation.

2.18.1. Edge Detection

For high-level machine vision tasks, range image processing extracts the 3-D geometrical properties of objects. In range photos, the edge feature is an important 3-D feature. In contrast to standard 2-D intensity image processing, range images have basically three sorts of edges: step edges that are discontinuous in depth value, roof edges that

are discontinuous in surface normals, and curve edges that are discontinuous in a variety of surface normals. A first-order derivative feature is the surface normal. Local 3-D features obtained with lower-order derivatives are more resistant to picture noise than those obtained with higher-order derivatives. One of the most common geometrical connections used to extract 3-D surface features is the angle between neighbouring surface normal (**Zhao, 2012**).

Fan et al., (1987) told that **Figure 12a** depicts the original range image with a size of 404 122 pixels. **Figure 12b, c** shows the matching intensity image as well as a 3-D presentation in light mode. This image contains a variety of edges, including step edges and roof edges of both concave and convex forms. **Figure 12d** depicts the MAF map. The MAF map depicts the surface angle features. The initial edges retrieved from the MAF map are shown in **Figure 12e**. The one-pixel-width margins in the range image are retrieved and presented in **Figure 12f** after expansion and thinning processing. To ensure that the edge points are correctly located, the edge image in **Figure 12f** is superimposed onto the original range image in **Figure 12a** to produce an accuracy verification as shown in **Figure 12g**. The edge points are checked based on the ground truth and they are found to be accurate.

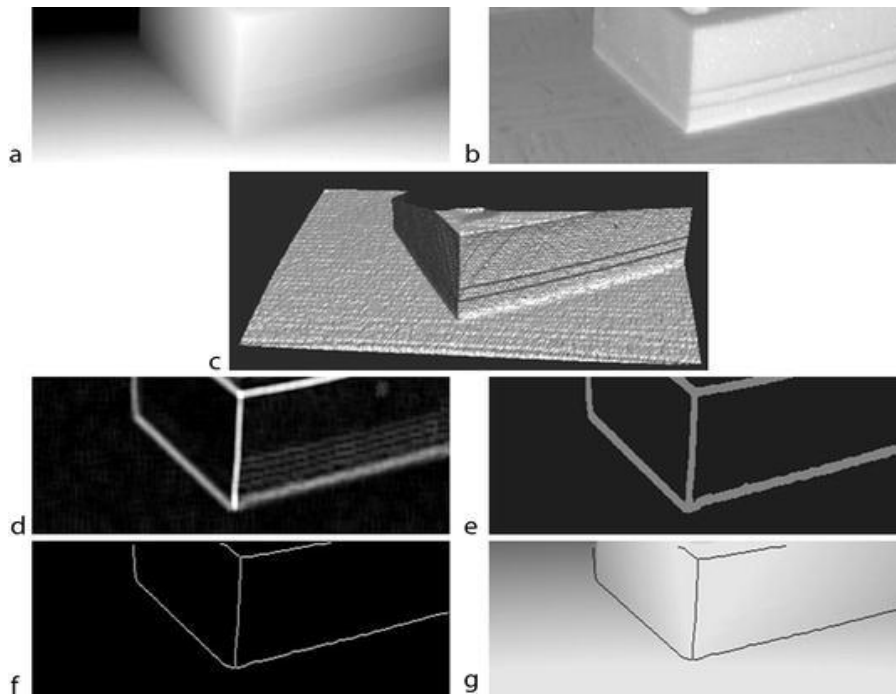


Figure 12. (a) The original range image of a packaging part; (b) the corresponding intensity image; (c) the 3-D display for showing image noise; (d) the MAF map of (a); (e) initial edge result; (f) the final edge result after expansion and thinning processing of (e); (g) a superimposed image of (a) and (f) to show edge localization accuracy (Fan *et al.*, 1987)

2.18.2. Region Segmentation

Segmentation is the process of grouping pixels into one of several disjoint sets, each of which has a similar feature. To acquire usable descriptions of 3-D scenes, many machine vision approaches now use range pictures. As it helps separate an image array into low-level components, segmentation is most commonly utilized in range image analysis and recognition. For range photos, there are two types of segmentation approaches. The first is based on area features, while the second is based on edge data. Pixels with similar qualities are clustered together in region-based segmentation methods. Surface fitting and feature clustering are two techniques that are often used to examine region properties for range image segmentation. Techniques for growing

in a certain region First, choose a set of seed regions, then grow them by iteratively merging nearby regions with similar attributes (**Fan *et al.*, 1987**). Another segmentation procedure is shown in **Figure 13**. The original intensity and range of images of a box are shown in **Figure 13 a, b**. The image has a resolution of 298 x 187 pixels. **Figure 13c** shows the range image in a 3-D display mode. The image noise is readily visible. The gradient histogram is shown in **Figure 13d**. Due to image noise and jump edges, the main peak areas and some random distribution areas can be seen. **Figure 13e** depicts the initial region grouping result. Small patches and jump edges are wrongly organised. Using the merge procedure, these regions are merged into their neighbouring regions. The final segmentation result is shown in **Figure 13f**.

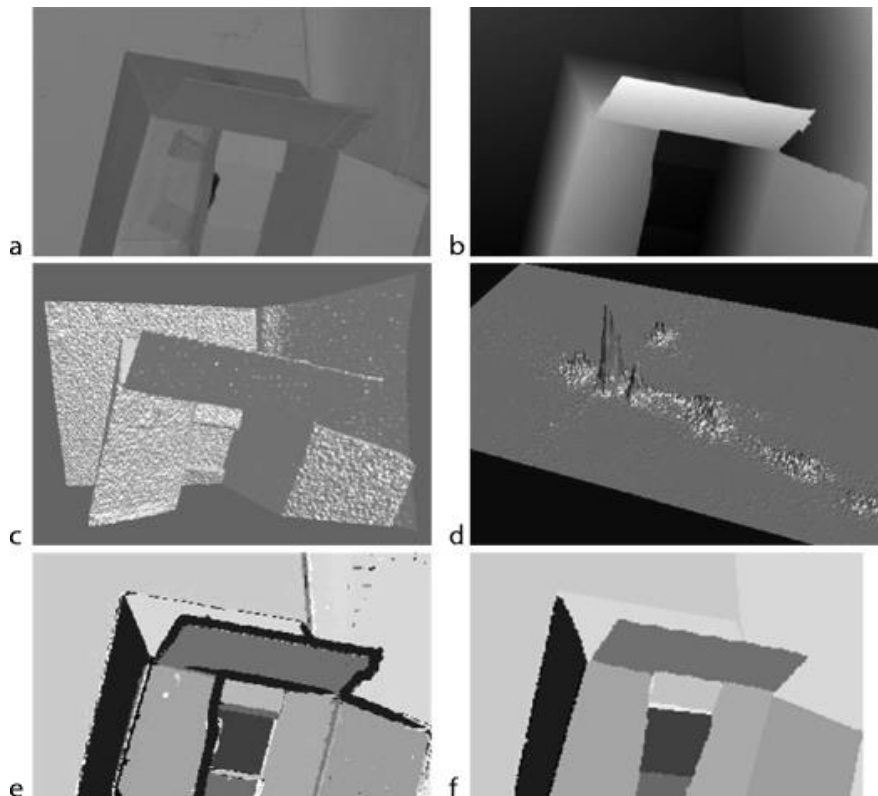


Figure 13. A box segmentation example. (a) original intensity image; (b) corresponding range image; (c) 3-D display for exhibiting image noise; (d) gradient feature space; (e) initial region grouping result; (f) final segmentation result after applying the merge process (**Fan *et al.*, 1987**)

2.19. Morphological image processing

The morphological procedures are a collection of image processing operations based on forms that are used to fill in any gaps in the grain boundaries borders. This process adjusts each pixel's sensitivity to the image's specific forms by altering the values of the other pixels in the image. In this study, the basic essential morphological procedures of erosion, dilation, and closure are applied. With a spatial low pass filter, the dilation process is mostly employed to fill in the holes. The additional pixels at the grain boundaries connect the missing pixels to form a continuous shaped object (**Adams and Bischof, 1994**).

Photographic pictures are the primary source of data and information in agriculture, but estimating or processing photographic data numerically is difficult. As a result, digital image processing technology aids in the processing of images and the attempt to extend their analysis. In the subject of agriculture, image processing has a variety of uses, such as land identification ([Erdenee *et al.*, 2010](#)).

The blurring is caused by a shift in the pixel intensity level at that particular spot. During artificial neural network-based segmentation of fruits from the canopy, a combination of texture and color features was also investigated. The viability of these methods for picture segmentation is described in the preceding approaches for post or real-time image processing. Nonetheless, there are a number of drawbacks to these approaches. For example, the RGB color model is device dependent, and pixel values change dramatically when different imaging sensors are used. Such models become unreliable for illumination color shift or shading conditions due to chrominance and luminance mixing (**Shaik *et al.*, 2015**).

2.19.1. Morphological Image Processing based Segmentation

Binary images might have a lot of flaws. Noise and textures buckle binary zones created by simple thresholding in some situations. Morphology refers to a broad range of image processing processes that alter images based on their forms. It is one of the data processing methods that can be used in picture processing. It offers a wide range of applications, including texture analysis, noise reduction, and boundary extraction (**Serra, 1982**).

The goal of morphological image processing is to eliminate all of these flaws while keeping the image's structure. Morphological operations are mainly focused on binary images since they rely on the related ordering of pixel values rather than their numerical values, but they may also be applied to grey scale images when the light transfer functions are unknown and so the absolute pixel values are ignored (**Khan and Thakur, 2012**).

2.19.2. Grey Scale morphological analysis

Sternberg (1978) discussed the application of such morphological approaches to industrial inspection duties. Small positive-contrast grey level patches in an image are typically smoothed with this method. **Haralick (1987)** found that using neighbourhood minimum and maximum functions, binary morphological processes may be readily extended to interpret grey scale imagery.

Heijmans (1991) gives a thorough examination of grey scale morphological operators, demonstrating how binary morphological operators and thresholding approaches can be used to create a large number of useful grey scale morphological operators.

2.20. Illumination correction techniques

For many image and machine vision applications, scene illumination is one of the most crucial aspects that determines success or failure. Irrelevant information can be removed, the contrast of important visual features improved, and the sensor signal-to-noise ratio improved with the right lighting. Defects in the optics and imaging hardware can cause apparent fluctuations in scene lighting, reducing the resilience and dependability of vision systems even with optimum illumination. Due to the \cos^4 law and vignetting, optical losses increase dramatically from the centre of the field to the edge. Sensitivity fluctuations (shading) in imagers are common as a function of spatial position (**Kleinemeier, 1985**).

Adaptive thresholding with invariant illumination adaptive thresholding, like morphological filters, can be tweaked for illumination invariance. Working with a density representation makes separating the illumination and reflectance components of an image in a variety of situations simple. The goal of illumination-invariant adaptive thresholding, once again, is to ensure that if a feature in a bright area surpasses the threshold, an analogous feature in a dim area will similarly exceed it. The threshold at every given place in the image using adaptive thresholding is based on a local average, which is commonly obtained by low-pass filtering the original image (**Cielo, 1988**).

Daut and Zhao (1989) told that morphological processing has also been used to compensate for lighting differences. By suppressing dark features at higher spatial frequencies, a closure operation can produce an image that is a good estimate of background illumination in some applications. A high pass filtered image is created by calculating the difference between the background image and the original image.

2.21. Histogram Features

The intensity histogram of all or portion of a picture is the basis for this valuable texture analysis method. Moments, entropy dispersion, mean (an estimate of the average intensity level), variance (a measure of the dispersion of the regions intensity), mean square value or average energy, skewness (the third moment that indicates the histograms symmetry), and kurtosis are all common histogram properties (cluster prominence or peakness). This naturally leads us to investigate the co-occurrence approach to texture measurement. A number of texture measures (also referred to as texture attributes) have been developed to describe the co-occurrence matrix numerically and allow meaningful comparisons between various textures (**Haralick, 1997**).

Wang et al., (2008) told that to do image preprocessing for rail surface-defect identification, researchers used the learning partial differential equation of a Gaussian blurred image. This technology substantially reduced image blur and enhanced fault detection accuracy.

Marmol and Mikrut (2012) obtained the collected head position information from image and laser data, retrieved data from the track edge's auto-approximation mode, fed back the position in space with high-precision laser data, and determined the position of the rail head in the digital image. This approach was more versatile, but it didn't work well with low-contrast backgrounds.

Taştimur et al., (2015 and 2016) processed morphological aspects of the rail surface-defect image were used to process video data in real time. This approach proved more efficient and resilient under a variety of lighting situations.

Innovative camera hardware and circuitry can also deal with variations in lighting. The use of polarised HSI, for example, can separate the absorption and scattering components without the need for any prior data processing (**Xu *et al.*, 2019a and Xu *et al.*, 2019b**)

At the intersection of agriculture, technology, and plant science, digital phenotyping is becoming an important study domain (**Awada *et al.*, 2018 and Liu *et al.*, 2019**).

Digital phenotyping's main goal is to use advanced non-destructive sensing techniques and information technology infrastructure to automate the extraction of structural and physiological features. Hyperspectral imaging is a frequently used technology in the digital phenotyping area (HSI) (**Mishra *et al.*, 2017**).

The majority of HSI's uses were in remote sensing. Close-range HSI, on the other hand, has recently emerged as a possible technique for in-situ non-destructive fast plant assessment (**Li *et al.*, 2014, Lowe *et al.*, 2017 and Mishra *et al.*, 2017**).

Electromagnetic radiation (EMR) can be reflected, transmitted, and absorbed when it strikes the surface of a plant (**Mishra *et al.*, 2017**).

The amount of reflection when EMR interacts with the plant is determined by the plant's physicochemical characteristics (**Mishra *et al.*, 2020a and Mishra *et al.*, 2020b**).

Mishra *et al.*, (2017) told that the reflected spectrum from a plant across a given wavelength range is referred to as the spectral signature, while the average reflectance is referred to as the plant's reflectance. These spectral signatures are obtained using spectrophotometers and hyperspectral cameras. A spectrophotometer can offer spectral data on a tiny region of a plant at a specific place. Spectrophotometers have a high

spectrum resolution, but they don't provide any spatial information. In terms of both the spatial and spectral features of an item, a hyperspectral camera may capture high resolution data.



Materials & Methods

3.MATERIALS AND METHODS

In the present investigation, an evaporative cooling system was developed and tested for Jew's Mallow storage after harvesting at Rice Mechanization Center (RMC) at Meet Eldeebah village, Kafr Elsheikh Governorate, Egypt, during the summer season of 2017.

3.1. Materials

3.1.1. Evaporative Cooler Manufacturing

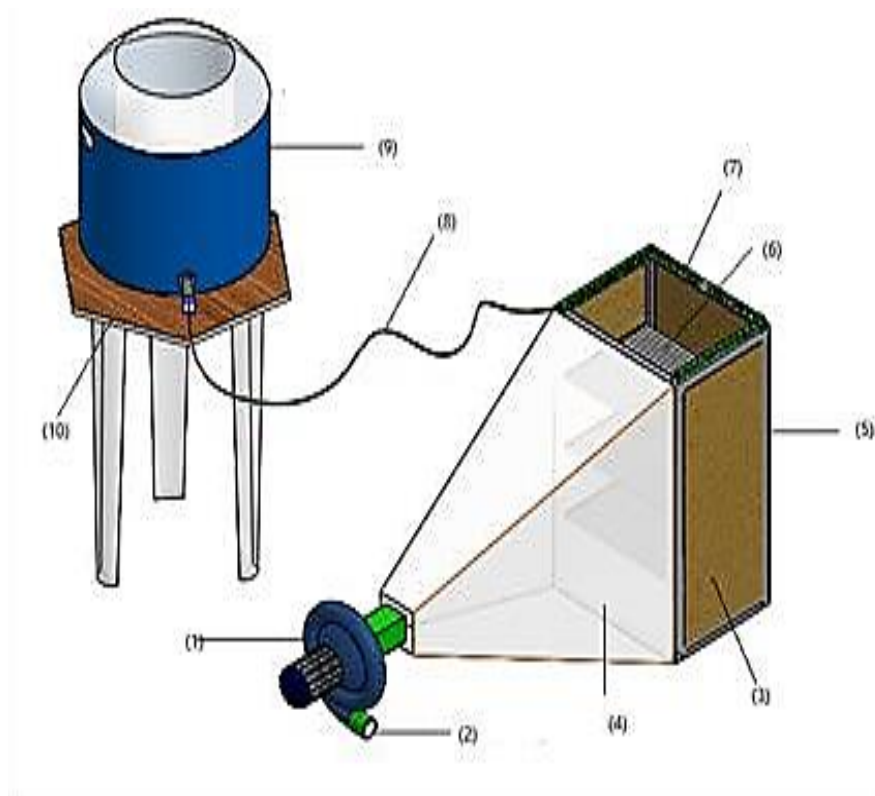
Design of evaporative cooling system technology requires considerable information such as economic worth, physical realization, financial feasibility...etc., one has to consider factors such as materials, components and their design steps, components and their combination, and its adaptability for customers.

The evaporative cooler consists of frame, suction impeller fan, water tank, plastic sheet and jute fiber as shown in **Figures 14 and 15**. Ripe fresh Jew's Mallow (variety of Alaskndrany) was used in this study. The crops were collected from a private farm in Kafr Elsheikh Governorate.

3.2. Experimental setup

The evaporative cooler unit was mainly developed to simulate the pad suction impeller fan evaporative cooling system. Four steel angles of 1m length were used to connect the suction impeller fan (has an operating voltage of 220V, 0.85kW, 50Hz and 4cm of diameter) with the evaporative cooler's storage room (test section of 0.55m long, 0.35m wide and 1m height) which was constructed from welded steel angles (30x30mm) to form the connection between suction impeller fan and a storage room. This connection creates a quadrilateral pyramid shape; where one wall side of the storage room geometrically shown as a pyramidal base and the suction impeller fan as pyramidal top. The

constructed pyramidal tunnel was covered with plastic sheet to keep the airflow. Evaporative cooler was covered with jute fiber (7cm and 10cm as thickness of pad material). Evaporative cooler pad (ECP) was assembled under a manifold tube for pad wetting which is connected with a tank of water.



- | | |
|----------------------------------|---------------------------|
| 1) Suction impeller fan | 2) Outlet air |
| 3) Jute fiber | 4) Plastic sheet |
| 5) Metal frame | 6) Shelves |
| 7) Watering network | 8) Water hose |
| 9) Water tank (with float valve) | 10) Table of 50 cm height |

Figure 14. Solid view of the experimented evaporative cooler

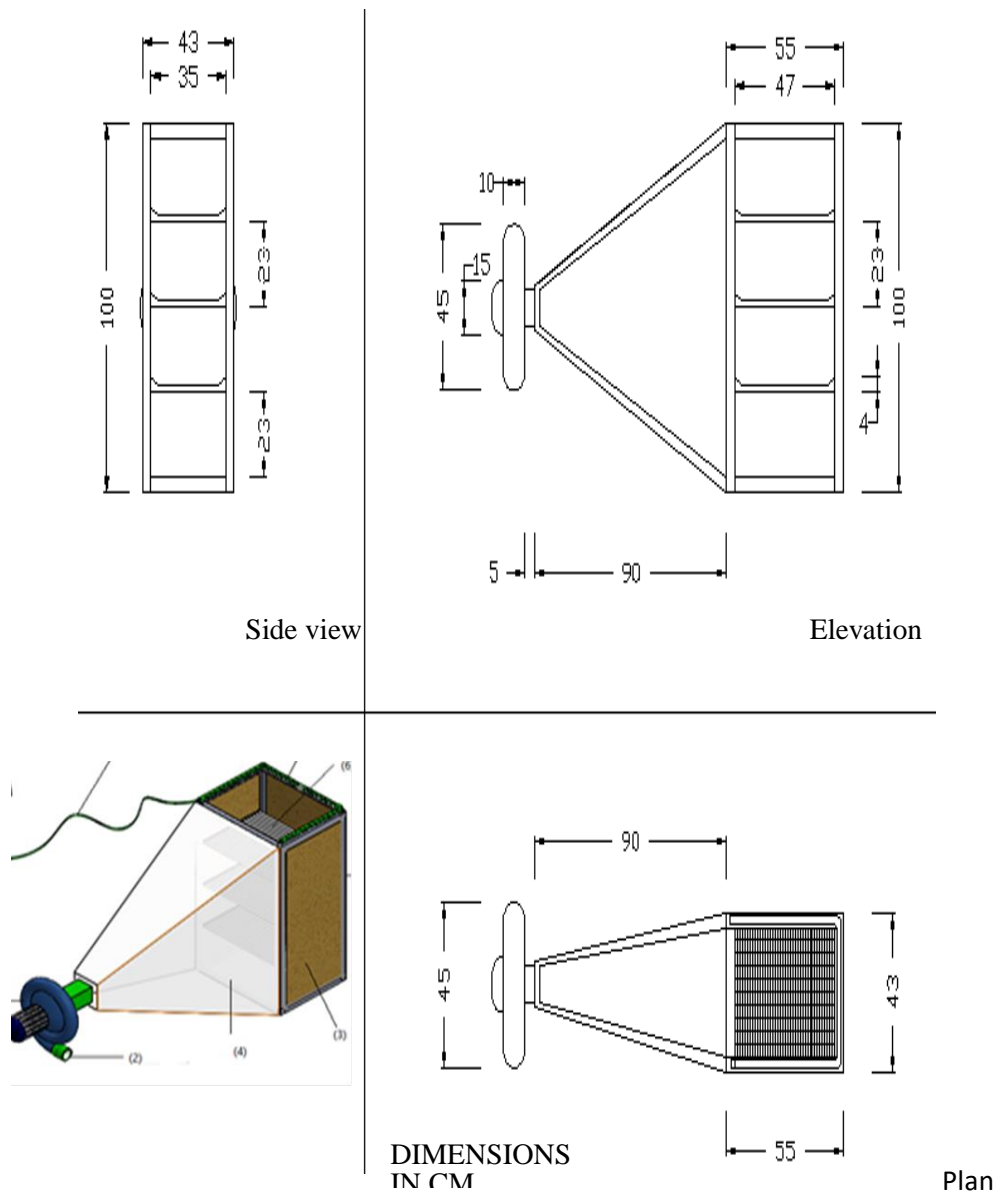


Figure 15. Engineering drawing of the experimented evaporative cooler

3.3. Experimental procedures and measurements

3.3.1. Air relative humidity and temperature

Air temperature and the relative humidity inside and outside evaporative cooler were measured by using air temperature and relative humidity meter. Temperature and relative humidity data of the evaporative cooler were collected each two hours interval. The evaporative cooling process started at 8:00AM and continued up 5:00 PM every day.

3.3.2. Instantaneous Jaw's Mallow mass

Initial mass of Jaw's Mallow was measured by the normal balance during the experimental evaporative cooling process. The loss of moisture content can also be achieved by acknowledging the reduction in Jaw's Mallow mass at initial condition and after every hour.

3.4. Imageries Acquisition procedures

Leaves were picked visually based on a wide range of greenness intensity, which varied related to nutrient deficiencies, plant position, and leaf age. A CCM-200 metre was used to determine the Chlorophyll Content Index, which was measured three times at the same location on each leaf and averaged. For imagery features analysis, a leaf disc was extracted from the same location as the measurement. Ripe Jew's Mallow was used in the study and was collected from a private farm in Kafr Elsheikh Governorate. All foreign materials, such as dust, dirt, immature, and damaged pieces, were removed from the fresh leaves.

3.4.1. Imagery Process and Analyses Techniques

By maximising the variance function between classes, Otsu's image thresholding technique returns the ideal threshold of a given image. On grayscale and color photos, this method has already proven to be effective. For color image segmentation, Otsu's methodology is used with the use of the **RGB** histogram. Each color pixel in the image is a mixture of Red, Green, and Blue in **RGB** space, and the data space size for that comparable image is $[0, L-1]^3$ ($R = [0, L-1]$, $G = [0, L-1]$, and $B = [0, L-1]$). Despite this, the empirically developed segmentation technique can be formalised as follows:

Allow L intensity degrees in the field $[0,1,2,\dots, L-1]$ for a certain RGB image.

Formerly, the probability distribution h_i^c can be shaped as:

$$h_i^c = \frac{h_i^c}{N} \sum_{i=0}^{L-1} h_i^c = 1 \quad \text{Eqn 1}$$

Where i is a specific intensity degree in the scope $\{0 \leq i \leq L - 1\}$ for the color constituent(C), $C = \{R,G,B\}$, N is the whole pixel numbers in the image, and h_i^c is the pixels number for the matching intensity level i in constituent C . Obtained results can be predicted by using the **equation 2**. CCM-200 output is the radiation transmission ratio of a Light Emitting Diode (LED) centered at 931 nm to radiation transmission of LED run at 653 nm according to the used manual of CCM-200, **Equation2**.

$$\text{Chlorophyll Content Index(CCI)} = \frac{\% \text{ transmission } 931 \text{ nm}}{\% \text{ transmission } 653 \text{ nm}} \quad \text{Eqn 2}$$

Because of CCI has no direct association to chlorophyll content, CCI values generated by the CCM-200 are just relative indicators of chlorophyll concentration. CCI values have been used to settle chlorophyll prediction equations in several studies (**Richardson *et al.*, 2002**, **Jifon *et al.*, 2005**, **Goncalves *et al.*, 2008** and **Cerovic *et al.*, 2012**).

3.4.1.1. The output of the CCM-200

The ratio of transmission of radiation from a light emitting diode (LED) cantered at 931 nm to transmission of radiation from an LED cantered at 653 nm is the output of the CCM200 (CCM200 user handbook). The chlorophyll content index is the name given to this ratio (CCI).



Figure 16. Opti-Sciences CCM-200

3.4.1.2. Standard B-H Table

Standard B-H table established by **Horsfall and Barratt (1945)**, **Table 7** was used to convert the output of CCM-200 (CCI) and its corresponding value of B-H mean index to wilting percent.

Table 7. Standard B-H mean and its corresponding value of wilting percent

0-2.9 B-H Mean*	Wilting Percent, %	3-5.9 B- H Mean*	Wilting Percent, %	6-8.9 B- H Mean *	Wiltin g Percen t,%	9-11 B- H Mean*	Wilting Percent %
0-0	0.0	3.0	9.2	6.0	63.1	9.0	97.4
0.1	0.2	3.1	9.9	6.1	64.4	9.1	97.7
0.2	0.4	3.2	10.5	6.2	67.2	9.2	97.9
0.3	0.7	3.3	11.1	6.3	68.4	9.3	98.3
0.4	1.0	3.4	11.9	6.4	71.2	9.4	98.4
0.5	1.3	3.5	12.6	6.5	72.8	9.5	98.5
0.6	1.6	3.6	13.4	6.6	74.3	9.6	98.7
0.7	1.9	3.7	14.8	6.7	75.1	9.7	98.9
0.8	2.1	3.8	15.6	6.8	76.2	9.8	99.0
0.9	2.4	3.9	16.8	6.9	78.5	9.9	99.1
1.0	2.6	4.0	17.3	7.0	80.5	10.0	99.2
1.1	2.8	4.1	18.9	7.1	82.4	10.1	99.3
1.2	3.1	4.2	20.6	7.2	83.6	10.2	99.3
1.3	3.3	4.3	23.3	7.3	85.4	10.3	99.4
1.4	3.5	4.4	26.2	7.4	86.3	10.4	99.5
1.5	3.7	4.5	28.1	7.5	89.1	10.5	99.5
1.6	3.9	4.6	29.4	7.6	90.2	10.6	99.6
1.7	4.2	4.7	31.9	7.7	91.4	10.7	99.7
1.8	4.5	4.8	33.4	7.8	92.7	10.8	99.8
1.9	4.7	4.9	36.1	7.9	93.3	10.9	99.9
2.0	4.9	5.0	38.3	8.0	94.5	11.0	100
2.1	5.1	5.1	42.5	8.1	94.9		
2.2	5.4	5.2	45.3	8.2	95.3		
2.3	5.8	5.3	46.9	8.3	95.8		
2.4	6.0	5.4	49.2	8.4	96.1		
2.5	6.4	5.5	51.8	8.5	96.5		
2.6	6.8	5.6	54.2	8.6	96.7		
2.7	7.4	5.7	56.1	8.7	96.9		
2.8	8.2	5.8	58.3	8.8	97.0		
2.9	8.6	5.9	59.6	8.9	97.3		

* Dimensionless

3.4.1.3. Visualization of leaves color gradient (Chlorophyll Content)

Recognizing color distribution in Jew's Mallow leaves is very important to evaluate the chlorophyll content and eventually wilting percent of leaves. To estimate CCI in various leaves, the models were used to display and map each pixel of the RGB pictures in the form of a chemical image. A linear color scale is used to display the resulting chemical image or prediction map, with the CCI or wilting percent linearly matched to the color scale. Then, by evaluating the color variations in the constructed map, the expected distribution of CCI may be simply evaluated. All of the steps in the visualization process were carried out with the help of a Matlab (Version 2009a, the Mathworks Inc., Mass, USA).

3.4.1.4. Morphological operations

Several morphological operators were incorporated into the system to increase segmentation accuracy by reducing various noises. Each of the categorised photos was first transformed to greyscale before being thresholded and converted to a binary image. To reduce minor noise, smaller blobs were removed from the image. In addition, a hole-filling operator was used to fill the image's microscopic holes.

3.5. Investigated variables

The performance of evaporative cooler was experimented under the effect of the following parameters:

1. Three different levels were selected of superficial air velocity of 0.13, 0.17 and 0.21m/s,
2. Three different levels of watering rate of 1, 2 and 4ℓ/h,

3. Two different levels pad thicknesses of 7 and 10cm, Variables were tested to show their effect on air relative humidity and temperature and instantaneous mass of Jew's Mallow with homogeny distribution on shelves of 7cm depth.

3.6. Instruments and data acquisition of the evaporative cooling unit

3.6.1. Air temperature and relative humidity measurements

Air temperature and relative humidity inside and outside evaporative cooler were measured by a digital temperature and humidity meter model chino HNK. They were measured and recorded during the period started from 9:00 AM to 5:00 PM. **Figure 17** shows an overall feature of the air relative humidity meter used for the experimental work.



Figure 17. A digital air temperature and relative humidity meter

3.6.2. Instantaneous Jew's Mallow mass meter

The digital balance model NBT-A200 was used for weighing yield of mallow inside and outside the evaporative cooler (maximum mass is 2kg with accuracy 0.01g) **Figure 18** shows an overall feature of the normal balance.



Figure 18. A digital balance of mass meter

3.6.3. Air velocity measurement

A digital anemometer (with temperature measurement) was used for measuring the exhausted air velocity at suction impeller fan outlet, m/s, with a range from zero to 50m/s (AM- 4838 made in Japan). **Figure 19** shows an overall feature of the air velocity meter used for the experimental work.

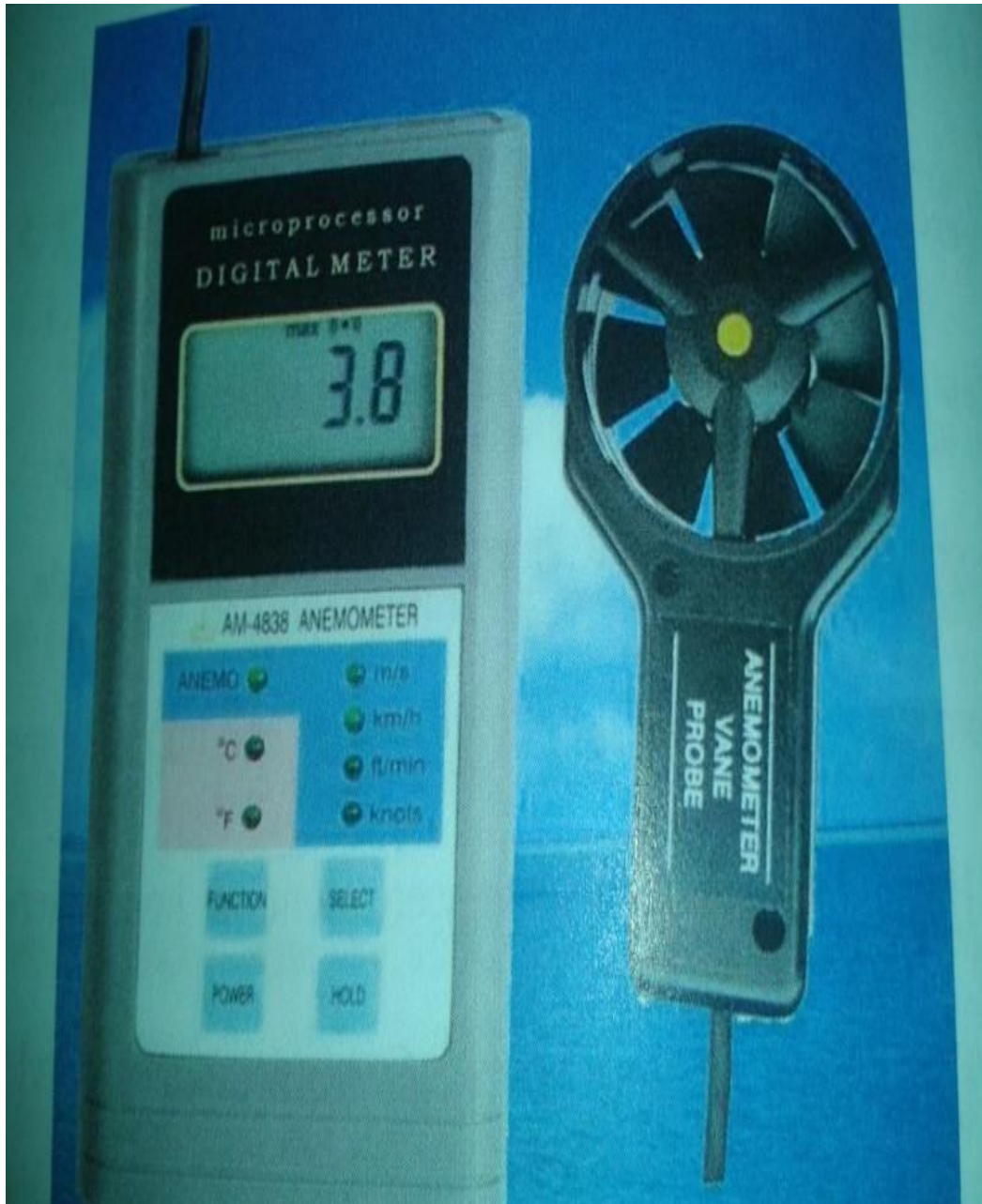


Figure 19. An anemometer of air velocity meter

3.7. Performance evaluation of evaporative cooler

3.7.1. Superficial air velocity calculations and regulations

Superficial air velocity facing pad surface has a potential effect on the thermal of evaporative cooler performance. The efficiency of a suction impeller fan and pad cooling system depends on air moving through the cooling pad. To achieve the highest thermal performance of the evaporative cooler, superficial air velocity facing and passing through

the whole surface of wetted pad must have been determined. The following formulas were used firstly to calculate and regulate the superficial air velocity levels during the experimental runs, **Table 8**;

- a. Airflow rate at suction impeller fan outlet, m³/s:

$$Q = A_f \cdot V_f \quad \text{Eqn 3}$$

- b. Superficial air velocity at pad section, m/s:

$$V_p = \frac{Q}{A_p} \quad \text{Eqn 4}$$

Table 8. Calculated superficial air velocity

Measured exhausted air velocity, m/s	Airflow rate at suction impeller fan outlet, m ³ /s	Superficial air velocity at pad section, m/s
1.5	0.1884	0.13
2.0	0.2512	0.17
2.5	0.314	0.21

3.7.2. Cooling potential of the evaporative cooler

The cooling potential of the evaporative cooler can be expressed as temperature reduction and can be estimated using the following equation:

$$\Delta T = T_{db} - T_c \quad \text{Eqn 5}$$

The averaged cooling potential was calculated for each experimental treatment.

3.7.3. Saturation efficiency inside evaporative cooler

Saturation efficiency can be determined by calculating the saturation potential at the same time of process (**Hellickson and Walker, 1983**). The averaged saturation efficiency of each treatment was estimated. It

was calculated from the following formula:

$$SE = \frac{T_{db}-T_c}{T_{db}-T_{wb}} \times 100 \quad \text{Eqn 6}$$

Multiple non-linear regression equations were developed to predict the influence of pad thickness and superficial air velocity together on cooling air temperature and relative humidity for various pad configurations.

3.7.4. Mass loss of Jew's Mallow analysis

The mass loss of Jew's Mallow can be calculated as a percent of original mass. Initial and final mass of the Jew's Mallow was determined at time zero and after storage inside the evaporative cooler. The mass loss percentage was determined using the following equation (**Abdur Rab *et al.*, 2012**) as:

Mass loss, % =

$$\frac{\text{Mass of fresh mallow} - \text{Mass after storage interval}}{\text{Mass of fresh mallow}} * 100 \quad \text{Eqn 7}$$



Results & Discussion

4. RESULTS AND DISCUSSION

The heat inside the product has to be removed to prevent it from deterioration. The amount of heat to be removed from the Jew's Mallow depends on the required storage temperature. Proper design, fast cooling, and relative humidity control in cooling environment can extend the period of fresh appearance of the product. The results of the experiments are given in Figures show the effect of superficial air velocity on air relative humidity, cooler temperature and Jew's Mallow instantaneous mass at different pad watering rates and thicknesses of jute fibre. As superficial air velocity increased from 0.13 to 0.21m/s, relative humidity and air temperature were found to increase and decrease, respectively. The air temperature was lower inside evaporative cooler than the ambient. However, the instantaneous mass reduction percentage of Jew's Mallow was found to decrease as superficial air velocity increased from 0.13 to 0.21m/s. The instantaneous mass was found to decrease slowly inside evaporative cooler compared by stored Jew's Mallow under the ambient conditions.

4.1. Evaporative Cooler Performance

Figures from 20 to 34 show that as superficial air velocity increased from 0.13 to 0.21m/s, watering rate increased from 1 to 4ℓ/h and pad thickness of 7cm, relative humidity and air temperature were found to increase from 84.2 to 87.4% and decrease from 23.9 to 22.1°C, respectively. Meanwhile, the instantaneous mass of Jew's Mallow decreases with the mass reduction percentage of 4.2%.

4.1.1. Relative humidity inside evaporative cooling system

Figures 24 and 32 also show that at pad watering rate of 4ℓ/h, superficial air velocity of 0.21m/s and pad thickness of 10cm, air relative

humidity and air temperature were found to be increased to 98.7% and decreased to 20.2°C, respectively. The instantaneous mass was found to be decreased to 699g with a mass reduction percentage of 0.85%.

Figures from 25 to 32 show the relationship between air relative humidity and daytime for the three superficial air velocities of 0.13, 0.17 and 0.21m/s, three watering rates of 1, 2, and 4ℓ/h and pad thicknesses of 7cm and 10cm, respectively. It can be noticed that air relative humidity increases with the increase of superficial air velocity and watering rate. Air relative humidity was found to be increased from 87.4 to 98.7% for pad thickness of 7 and 10cm, respectively.

The experiments were spread over several weeks, in order to display the environmental conditions.

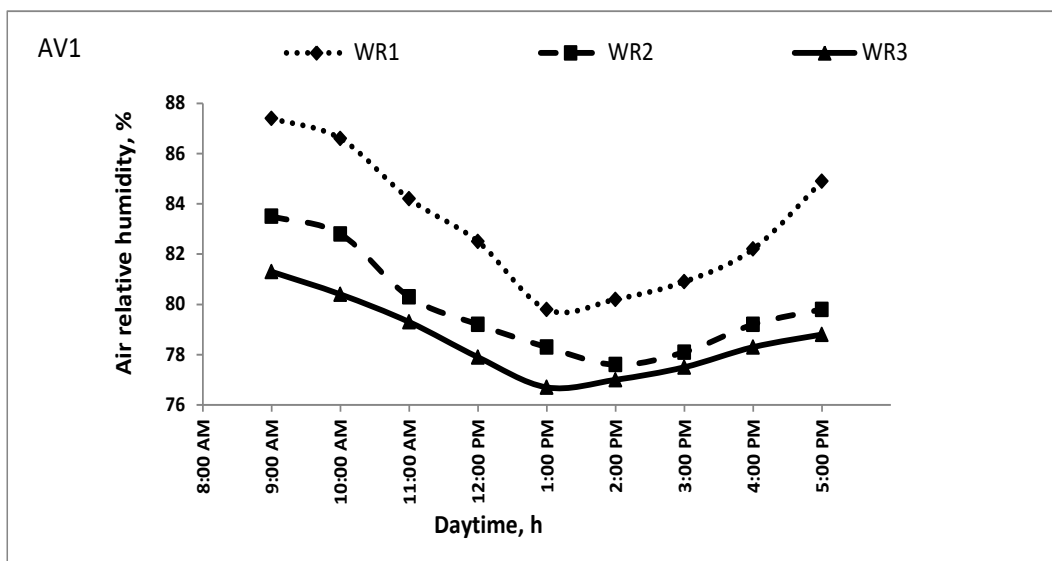


Figure 20. Air relative humidity behavior under superficial air velocity of 0.21m/s, three watering rates of 1, 2, and 4ℓ/h and pad thickness of 7cm

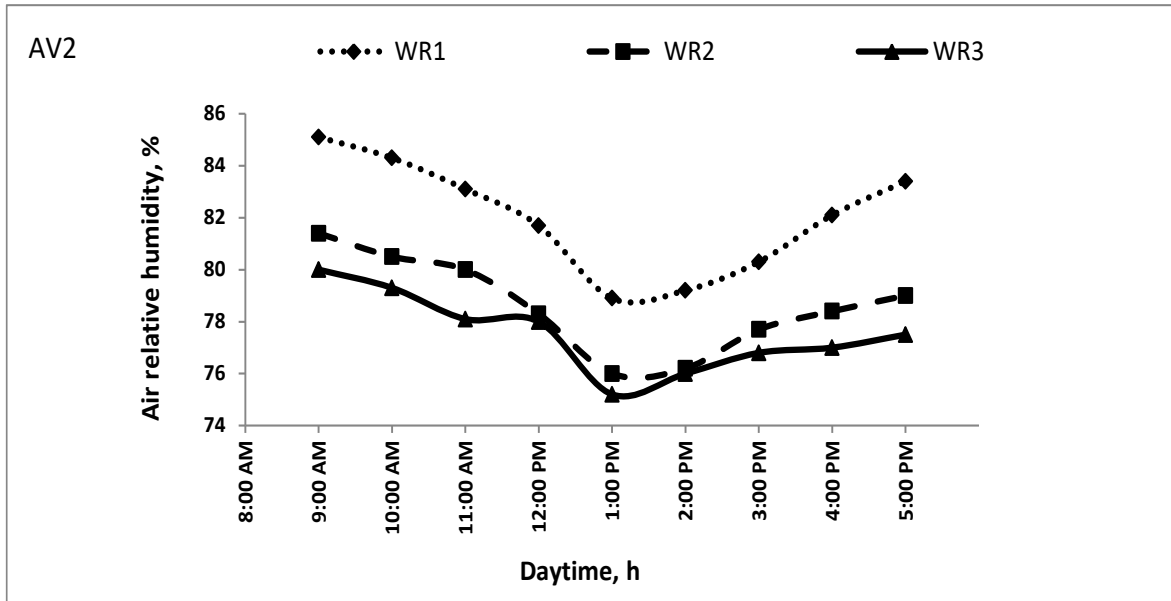


Figure 21. Air relative humidity behavior under superficial air velocity of 0.17m/s, three watering rates of 1, 2, and 4ℓ/h and pad thickness of 7cm

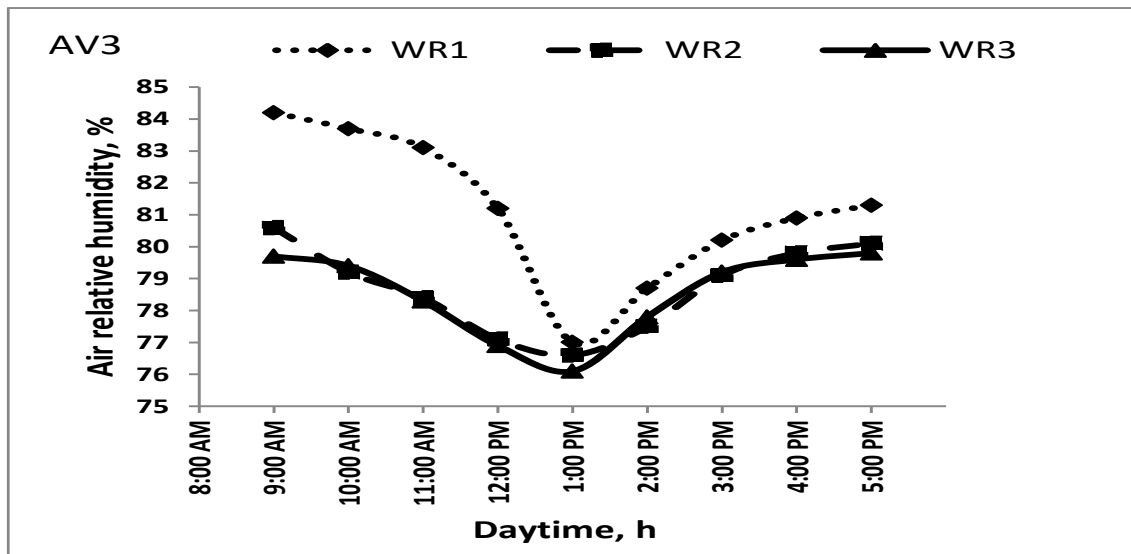


Figure 22. Air relative humidity behavior under superficial air velocity of 0.13m/s, three watering rates of 1, 2, and 4ℓ/h and pad thickness of 7cm

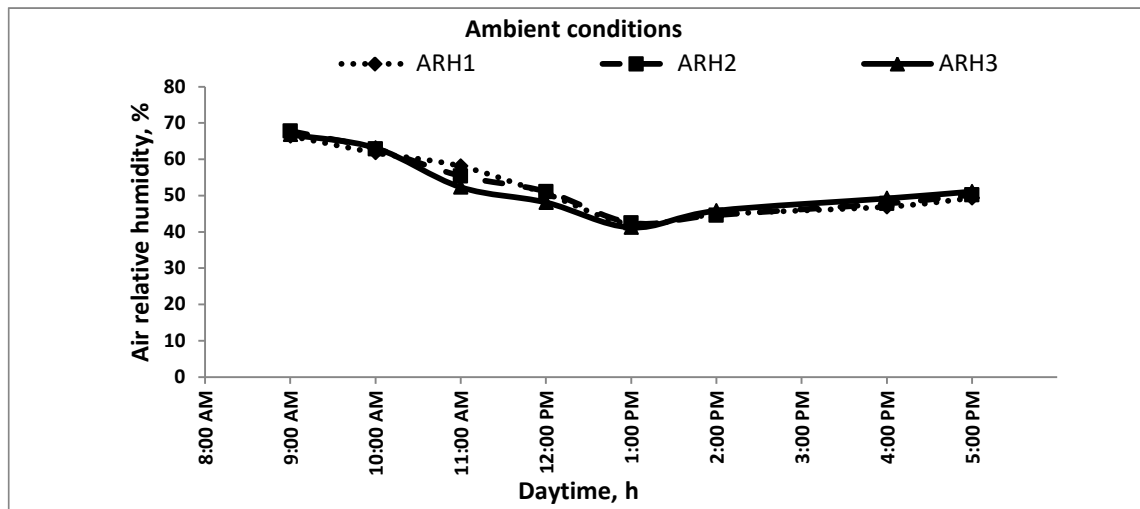


Figure 23. Air relative humidity behavior under the ambient conditions on a typical first summer day

Relative humidity levels inside the evaporative cooler without cooling system was observed and recorded applied during sunny days.

The relative humidity inside the evaporative cooler decreased with increasing outside temperature. At all point the relative humidity inside the evaporative cooling system when the system was not operating it was lower than the relative humidity when evaporative cooling system was operating.

The lower values of relative humidity of the evaporative cooler was 42.1% which occurred at midday.

The moisture content of the atmosphere is nearly constant during hot summer days. The relative humidity is lowest in the afternoon when the temperature is maximum, and the lower the humidity, the stronger the evaporative cooling effect. The inside relative humidity of the evaporative cooler increased as compared with outside environment. As water evaporates, it absorbs energy from the surrounding environment and rising moisture content.

The relative humidity inside evaporative cooling system has the same behavior as ambient relative humidity the periods from 1:00 to 3:00

pm were characterized by decreasing levels of humidity while the relative humidity during the morning from 9:00 am to 12:00 pm was exhibited with high relative humidity levels.

The changes in relative humidity inside the evaporative cooling system are a function of several factors influencing the air ability to evaporate and carry water. Thus, the air relative humidity inside the evaporative cooling system was affected by several factors, such as operating conditions and outside relative humidity.

The effect of different pad thickness on the hourly variations of air relative humidity have been tested for several days. When the system operated under the 10cm of pad thickness, the relative humidity achieved was higher than that obtained with less pad thickness (7cm). the relative humidity was ranged from 98.7 to 87.4% for two pad thickness.

From **Figure 24** it was found that maximum relative humidity recorded at the evaporative cooling system was 98.7% at superficial air velocities of 0.21m/s and 4ℓ/h and pad thicknesses of 10cm.

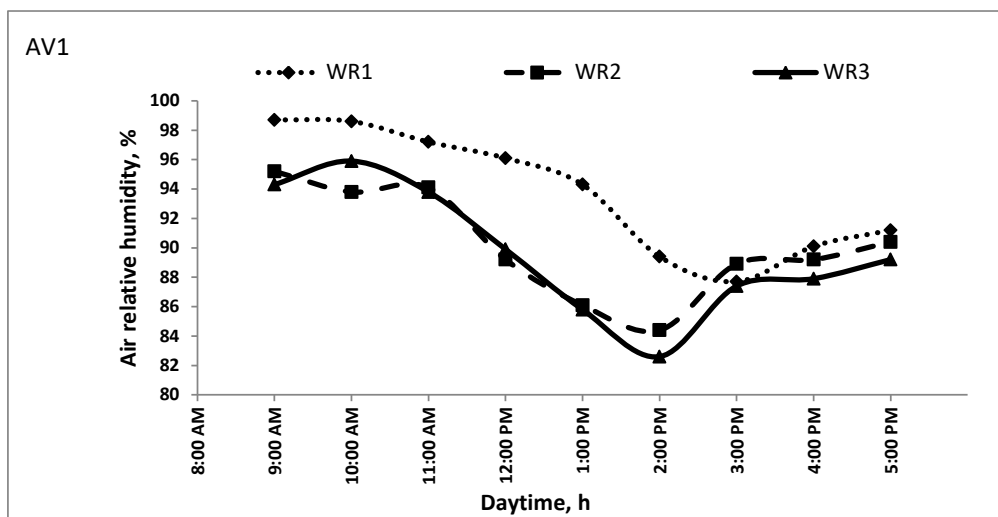


Figure 24. Air relative humidity behavior under superficial air velocity of 0.21m/s, three watering rates of 1, 2, and 4ℓ/h and pad thickness of 10cm

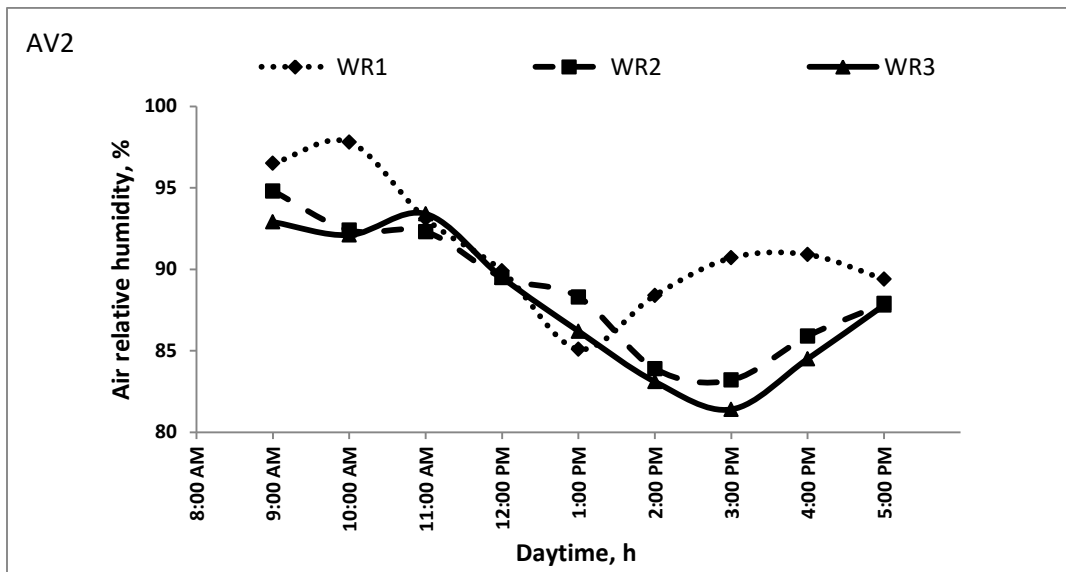


Figure 25. Air relative humidity behavior under superficial air velocity, AV2, of 0.17m/s, three watering rates of 1, 2, and 4ℓ/h and pad thickness of 10cm

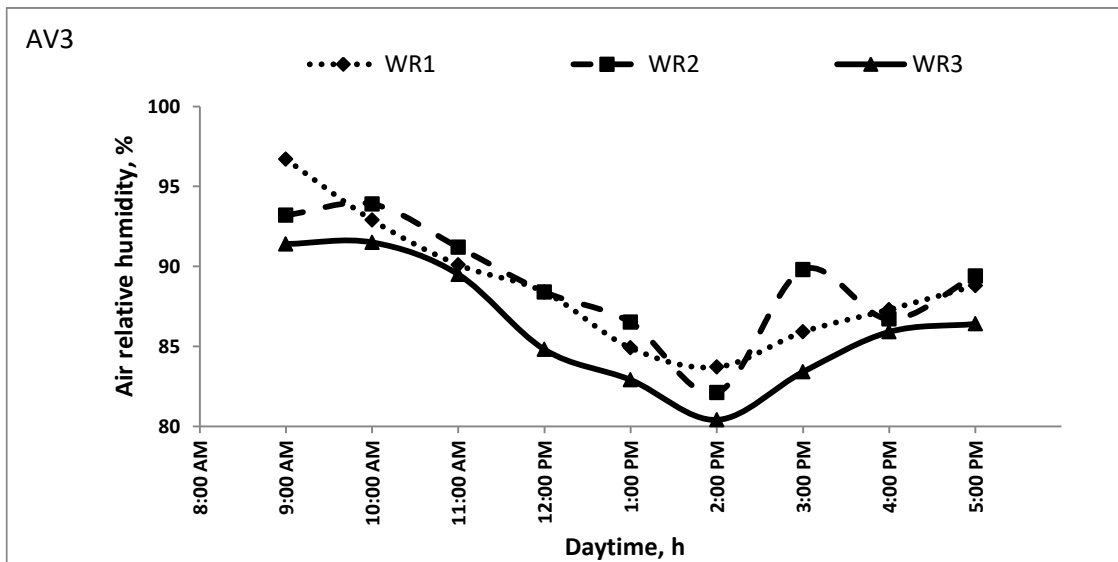


Figure 26. Air relative humidity behavior under superficial air velocity of 0.13m/s, three watering rates of 1, 2, and 4ℓ/h and pad thickness of 10cm

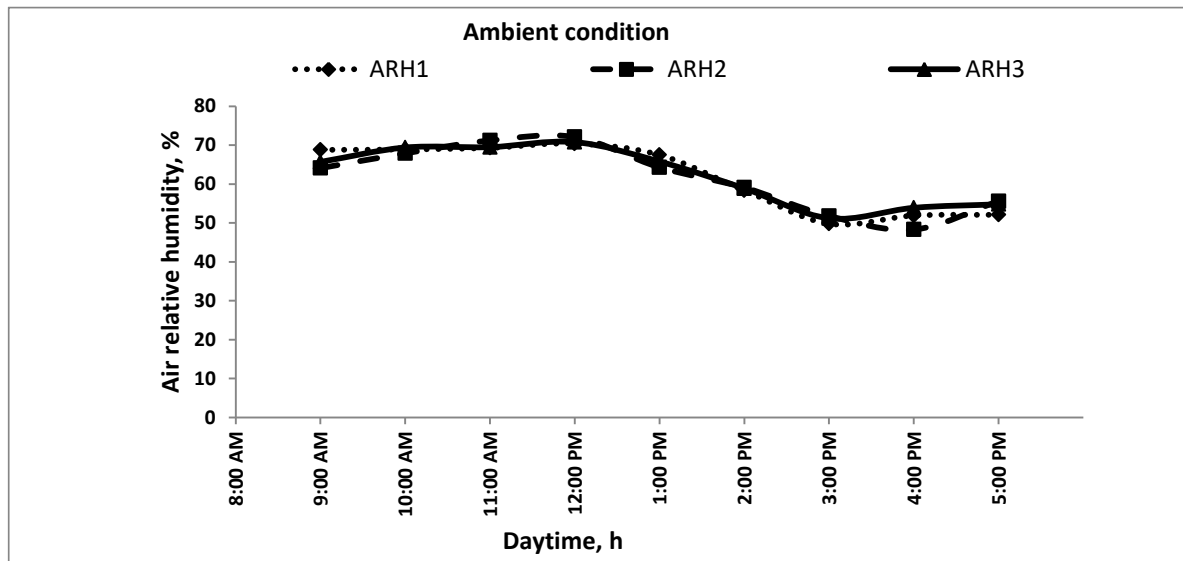


Figure 27. Air relative humidity behavior under the ambient conditions on a typical first summer day

The experiments were spread over several weeks, in order to display the environmental conditions; the first day for each state has been selected for the diagrammatic representation. **Figure 27** shows the ambient air relative humidity during clear sunny day. It was noted that the periods from 9:00 AM to 1:00 PM were characterized by sharp drop of air relative humidity.

Reducing the heat stress inside the evaporative cooling system

Evaporative cooling and the suction impeller fan-pad system were chosen to reduce heat stress inside the experimental evaporation cooler. Also, new alternative and economical pad material was adapted and investigated.

The proposed suction impeller fan-pad combined with watering rate for cooling. The watering rate and the cooler pad which tends to reduce the cover heat as well as to reduced inside air stratification temperatures.

4.1.2. Air temperature inside evaporative cooling system

Suction impeller fan-pad evaporative cooling system was investigated in the present study to enhance the internal environment of experimental evaporative cooling system during summer time. New pad material was adapted and use in this investigation.

The ability of cooling system to microclimate the environment conditions inside the evaporative cooler is affected by several factors such as: pad material, pad thickness, air velocities, outside climatic parameters and cooling system arrangement. Inside air temperature have the same behavior as outside whereas the maximum temperature occurred during the period of 1:00 to 3:00 pm by the end of the day the evaporative cooler temperatures stay below that of outside .

Figures from 28 to 35 show the relationship between air temperature and daytime for three superficial air velocities (0.13, 0.17 and 0.21m/s), three watering rates (1, 2, and 4ℓ/h) and pad thicknesses of 7cm and 10cm. In general, air temperature decreases with the increase of superficial air velocity and watering rate. Air temperature was found be decreased from 22.1 to 20.2⁰C for pad thicknesses of 7cm and 10cm, respectively

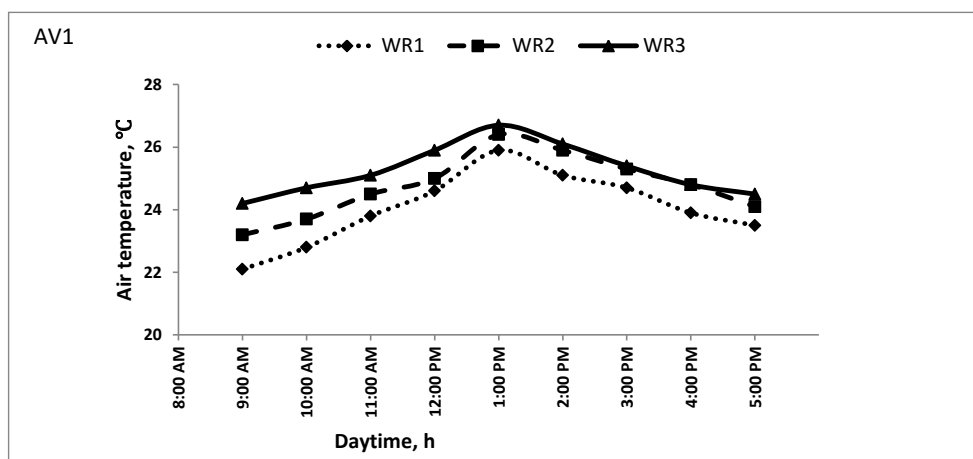


Figure 28. Air temperature behavior under superficial air velocity of 0.21m/s, three watering rates of 1, 2, and 4ℓ/h and pad thickness of 7cm

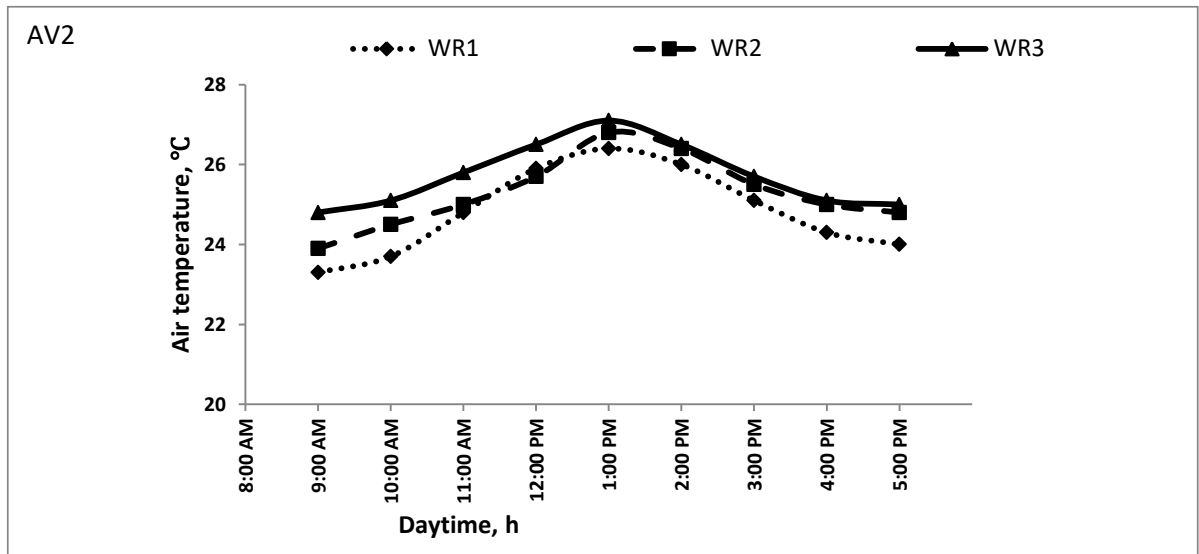


Figure 29. Air temperature behavior under superficial air velocity of 0.17m/s, three watering rates of 1, 2, and 4ℓ/h and pad thickness of 7cm

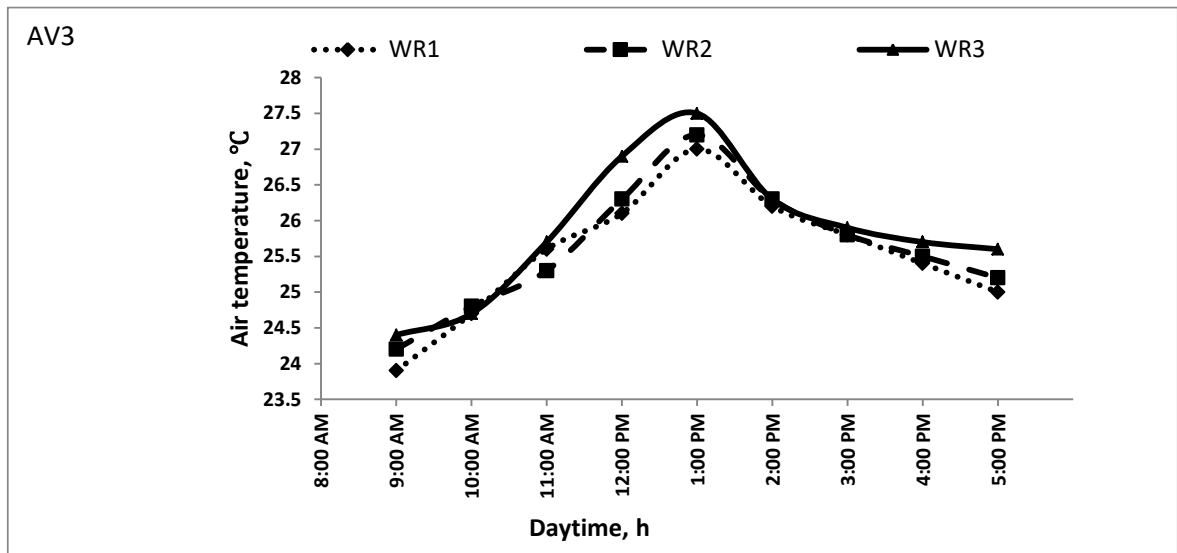


Figure 30. Air temperature behavior under superficial air velocity of 0.13m/s, three watering rates of 1, 2, and 4ℓ/h and pad thickness of 7cm

4.1.3. Temperature patterns inside evaporative cooler without cooling system.

The effect of ambient conditions on the environment inside the experimental evaporative cooler was observed and data were recorded when evaporative cooler was not provided with any cooling system.

Figure 31 shows that when the evaporative cooling system was not operating, the air temperature was little higher than before midday by 31.2 to 35.7°C.

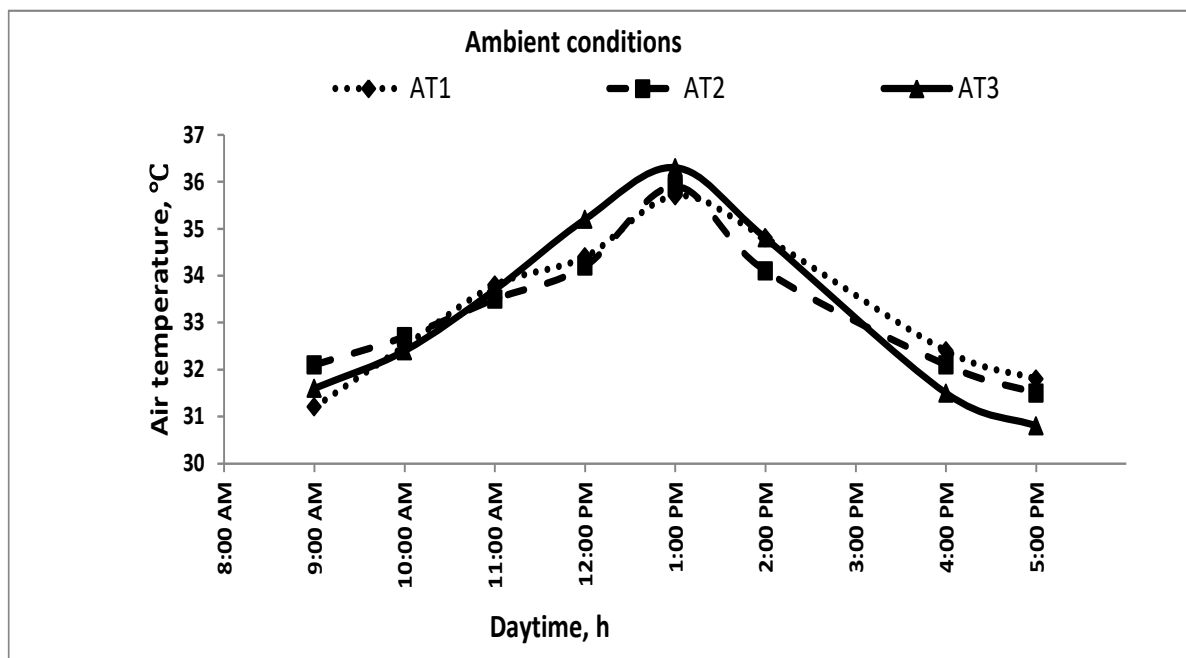


Figure 31. Air temperature behavior under the ambient conditions on a typical first summer day

Cooling potential for evaporative cooling system:

It was observed that the temperatures measured inside the evaporative cooling system remains below that of outside due to evaporative cooling. the inside temperature was closer to ambient air condition as compared to asituation with no cooling, and then the cooling effect started to increase. The maximum difference in temperature occurred at the midday when the outside relative humidity at its minimum value.

Values of temperature reduction differ with operating conditions as well as pad thickness, pad material, air velocity and watering rate.

Figures 32, 33 and 34 show the difference of temperature reduction that estimated from the investigated system as function of input experimental parameters. The temperature reduction resulted inside the evaporative cooling system under pad thickness of 10cm and other same operation conditions was higher than that operated under pad thickness of 7cm and same other operating conditions by 0.9°C so the investigated cooling system is passed upon using new alternative evaporative cooling pad.

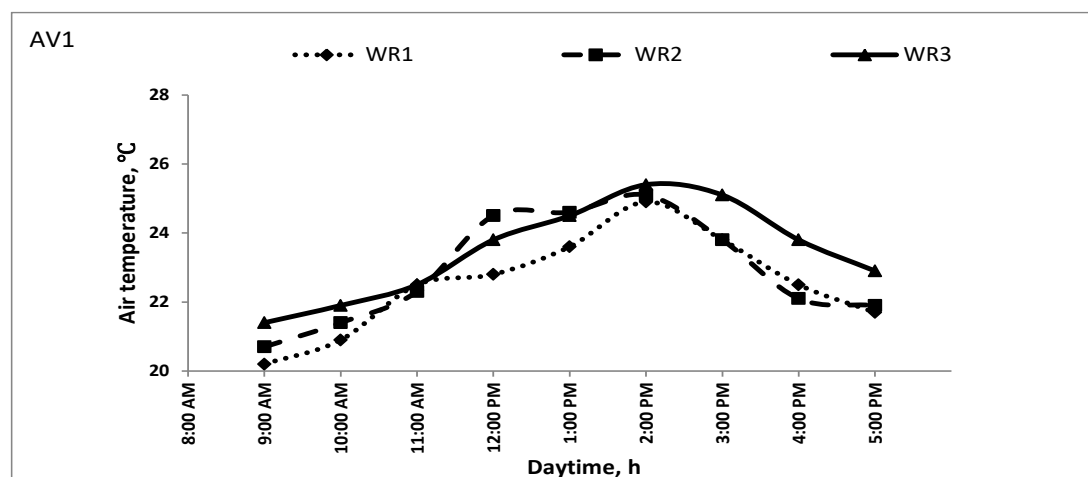


Figure 32. Air temperature behavior under superficial air velocity of 0.21m/s, three watering rates of 1, 2, and 4l/h and pad thickness of 10cm

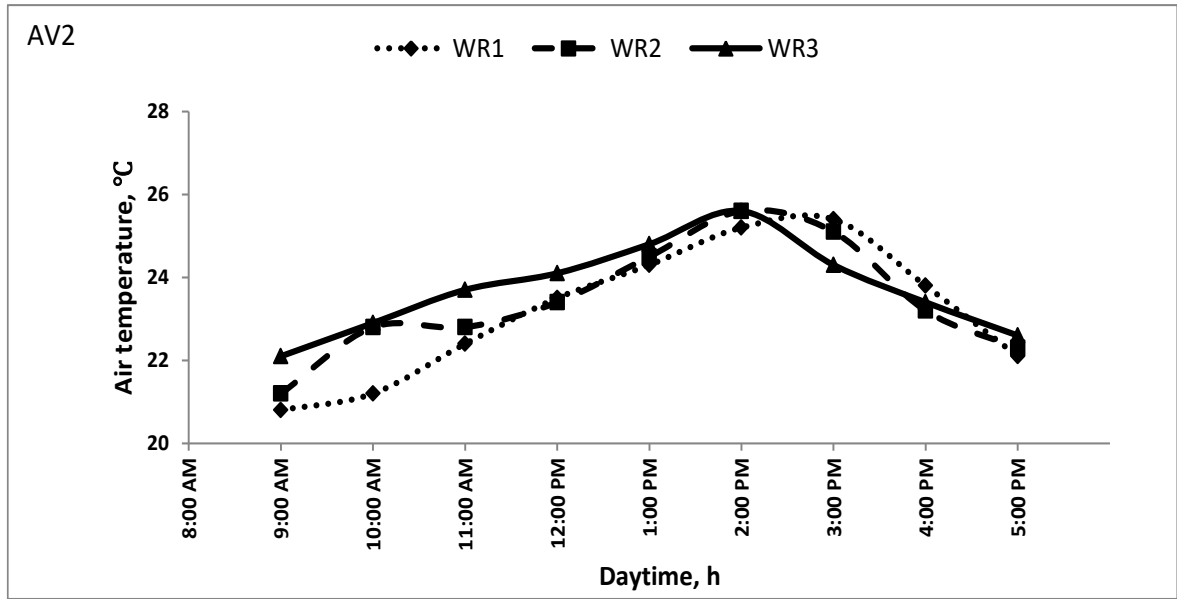


Figure 33. Air temperature behavior under superficial air velocity of 0.17m/s, three watering rates of 1, 2, and 4ℓ/h and pad thickness of 10cm

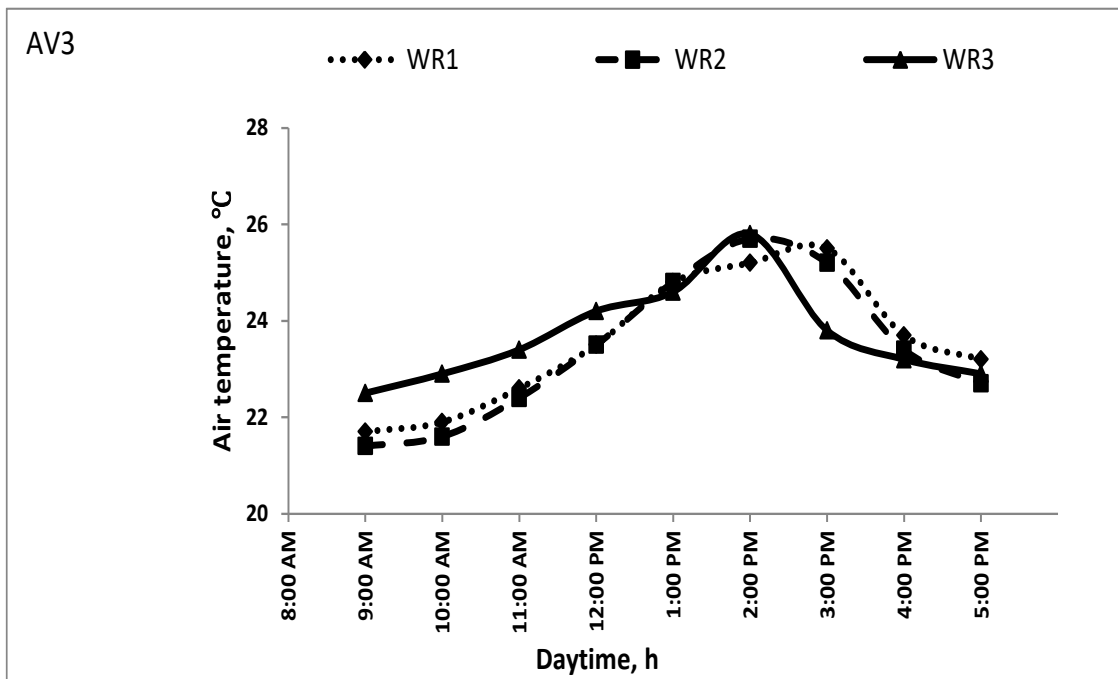


Figure 34. Air temperature behavior under superficial air velocity of 0.13m/s, three watering rates of 1, 2, and 4ℓ/h and pad thickness of 10cm.

The maximum ambient temperature occurred at midday where the relative humidity was at its minimum value. The highest ambient relative humidity occurred on the early morning time. It begins to decrease slowly with the time and reached its minimum value at noon and thereafter increased again.

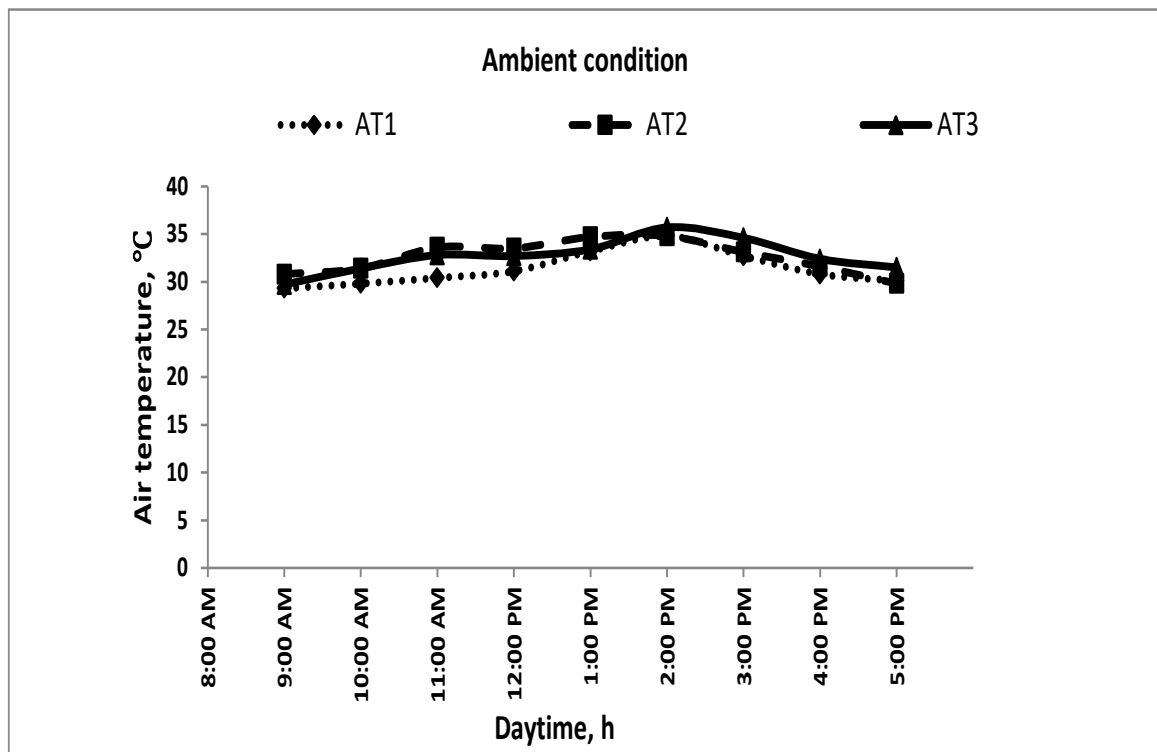


Figure 35. Air temperature behavior under the ambient conditions on a typical first summer day.

4.1.4. Instantaneous mass of Jew’s Mallow inside evaporative cooling system

Figures from 36 to 59 show the relationship between instantaneous mass and daytime at watering rates of (1, 2 and 4ℓ/h), superficial air velocity of (0.21, 0.17 and 0.13m/s) and two different pad thicknesses of 7 and 10cm. Pad thickness affect tremendously the instantaneous mass reduction. Instantaneous mass reduction percentage was found to be lower by 4.2 to 0.85% for pad thickness of 7 and 10cm, respectively.

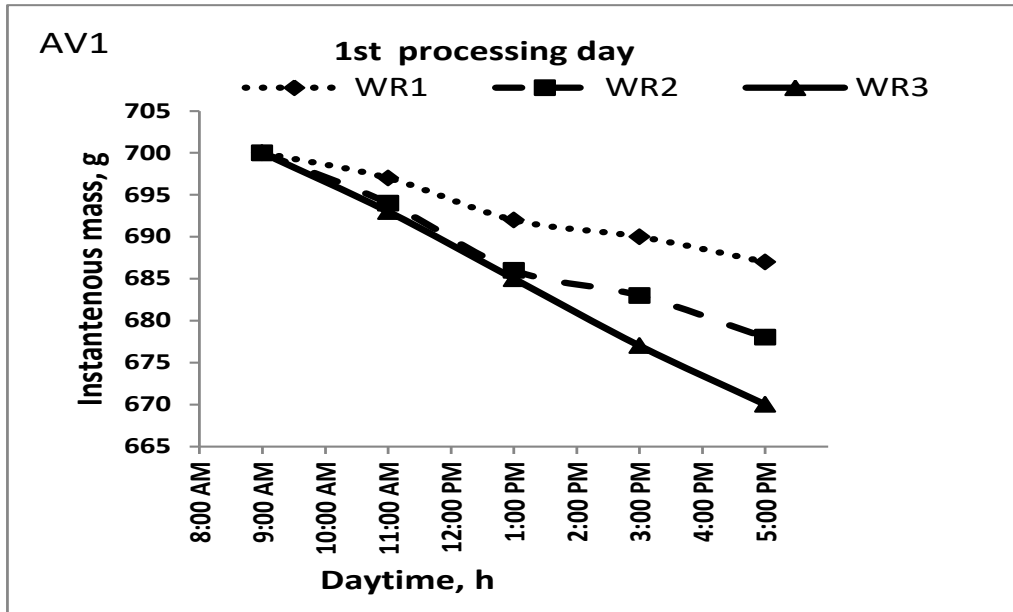


Figure 36. Instantaneous mass behavior under the superficial air velocity of 0.21m/s, three watering rates of 1, 2, and 4ℓ/h and pad thickness of 7cm for the first processing day.

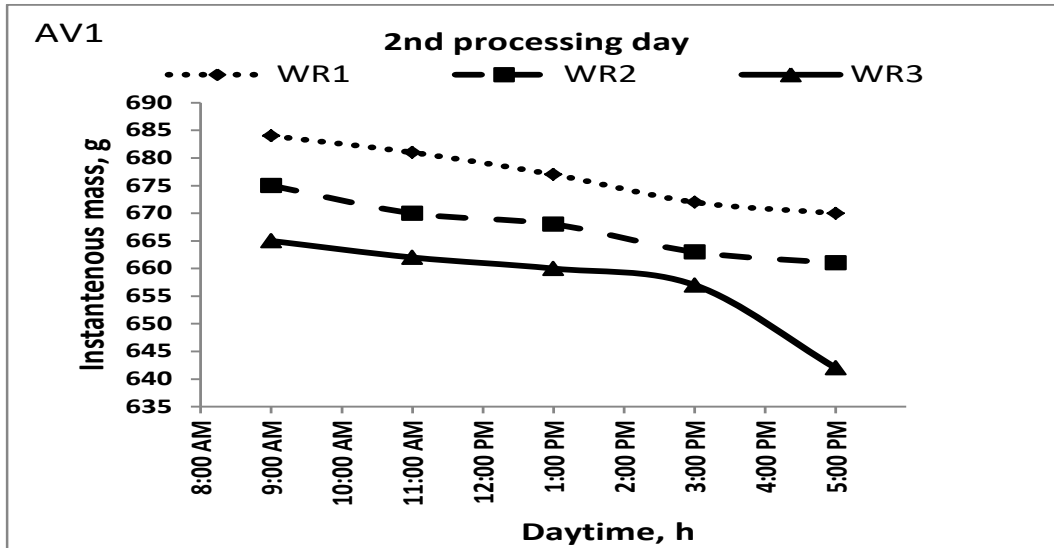


Figure 37. Instantaneous mass behavior under the superficial air velocity of 0.21m/s, three watering rates of 1, 2, and 4ℓ/h and pad thickness of 7cm for second processing day

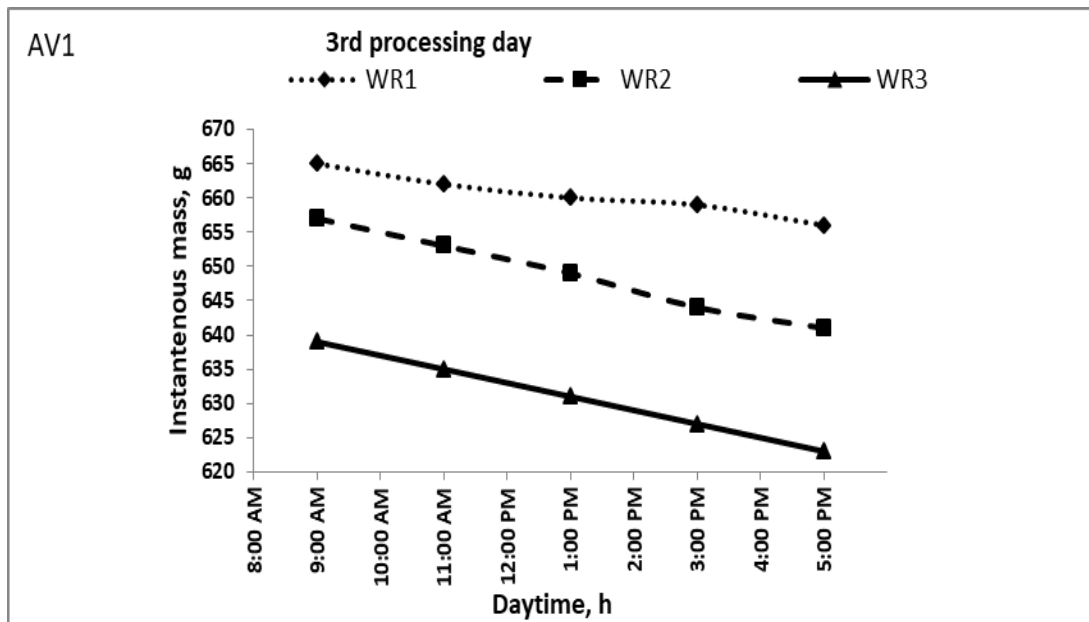


Figure 38. Instantaneous mass behavior under the superficial air velocity of 0.21m/s, three watering rates of 1, 2, and 4ℓ/h and pad thickness of 7cm for the third processing day.

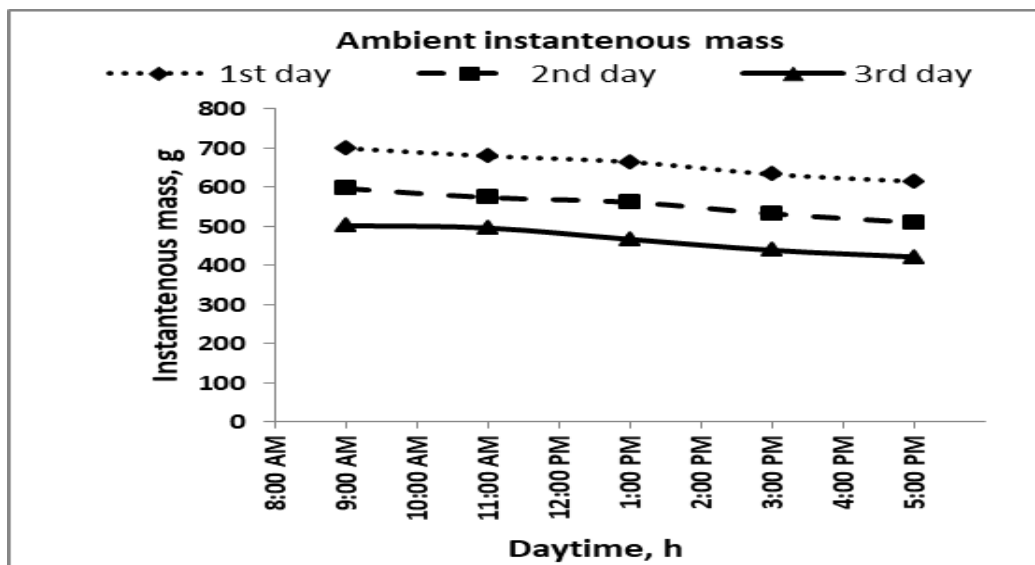


Figure 39. Instantaneous mass behavior under the ambient conditions for the first, second and third processing days.

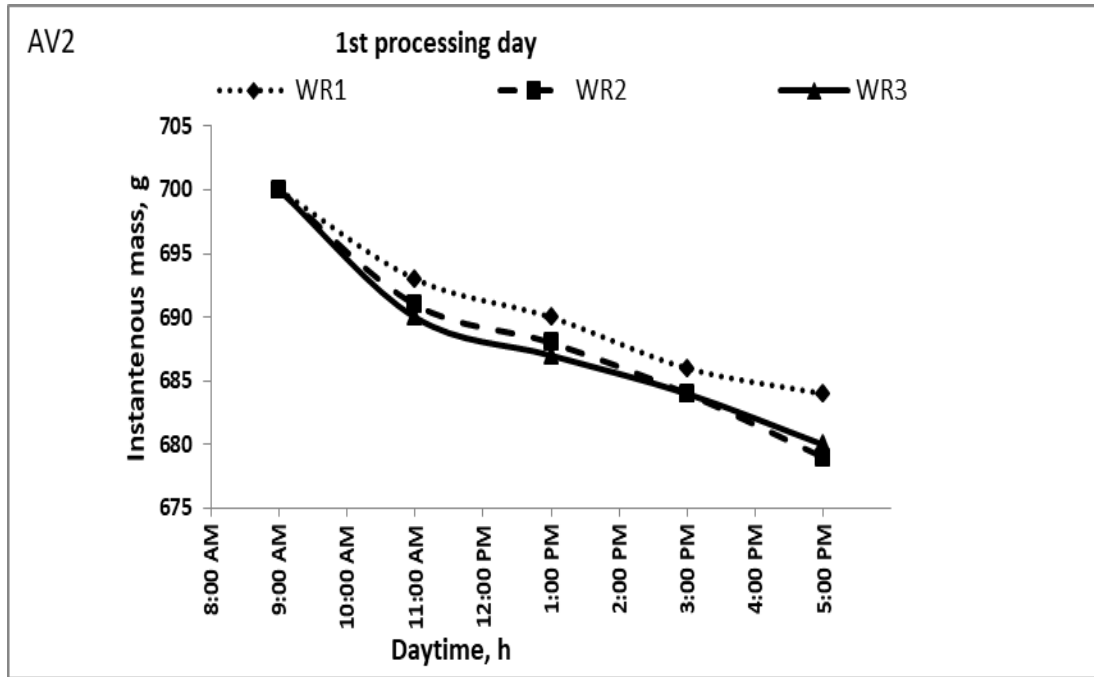


Figure 40. Instantaneous mass behavior under the superficial air velocity of 0.17m/s, three watering rates of 1, 2, and 4ℓ/h and pad thickness of 7cm for the first processing day

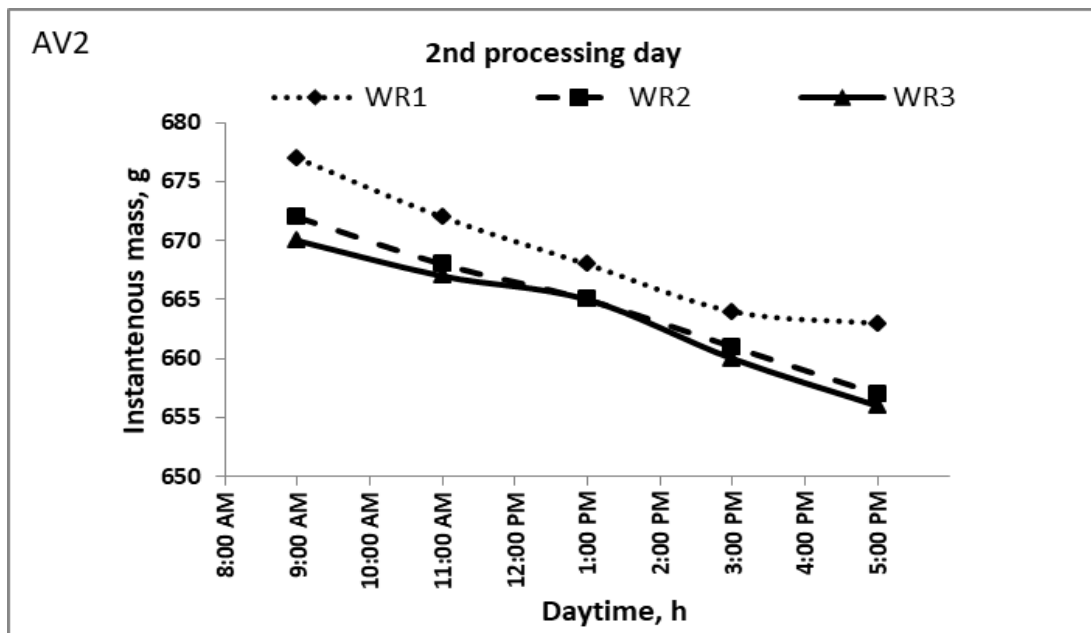


Figure 41. Instantaneous mass behavior under the superficial air velocity of 0.17m/s, three watering rates of 1, 2, and 4ℓ/h and pad thickness of 7cm for the second processing day

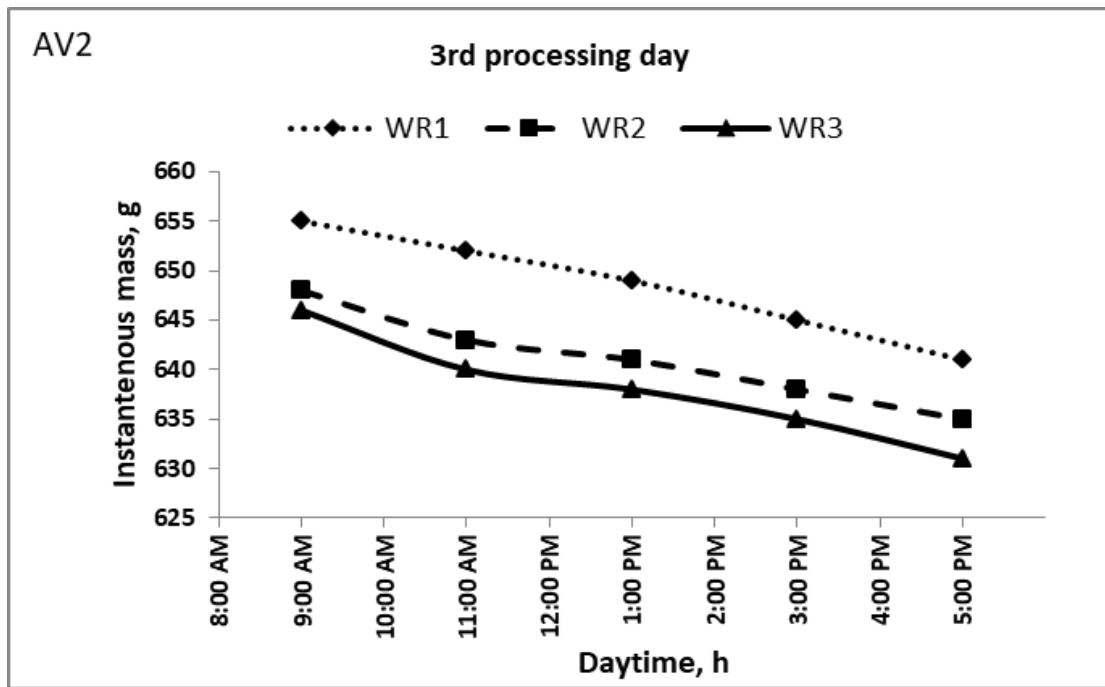


Figure 42. Instantaneous mass behavior under the superficial air velocity of 0.17m/s, three watering rates of 1, 2, and 4ℓ/h and pad thickness of 7cm for the third processing day

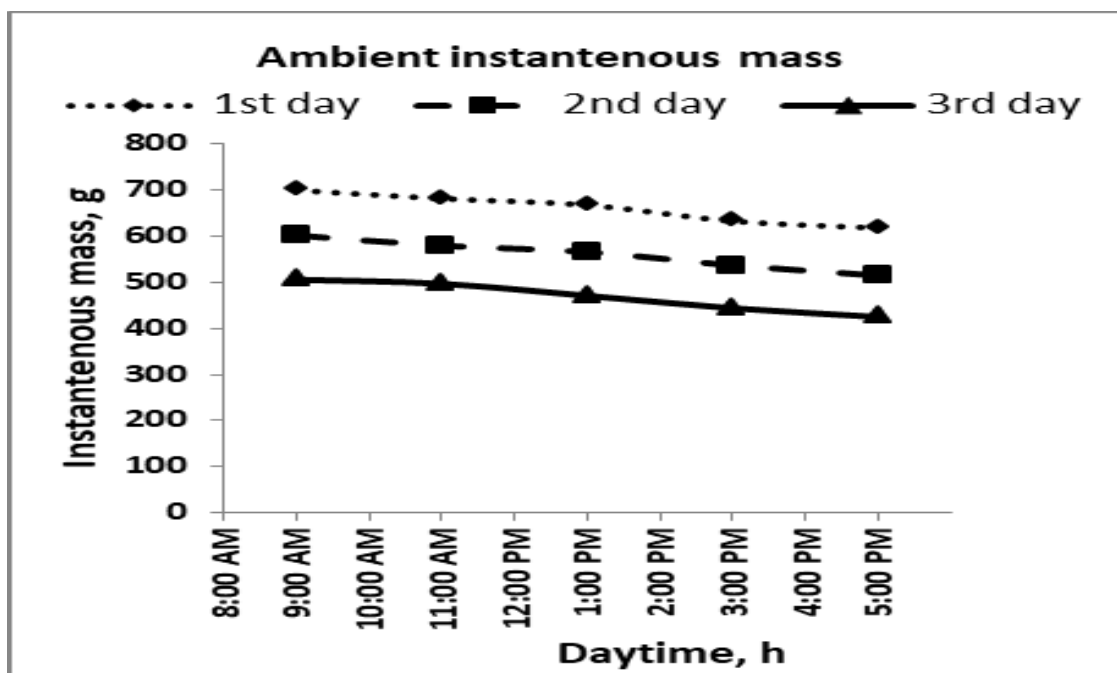


Figure 43. Instantaneous mass behavior under the ambient conditions for the first, second and third processing days

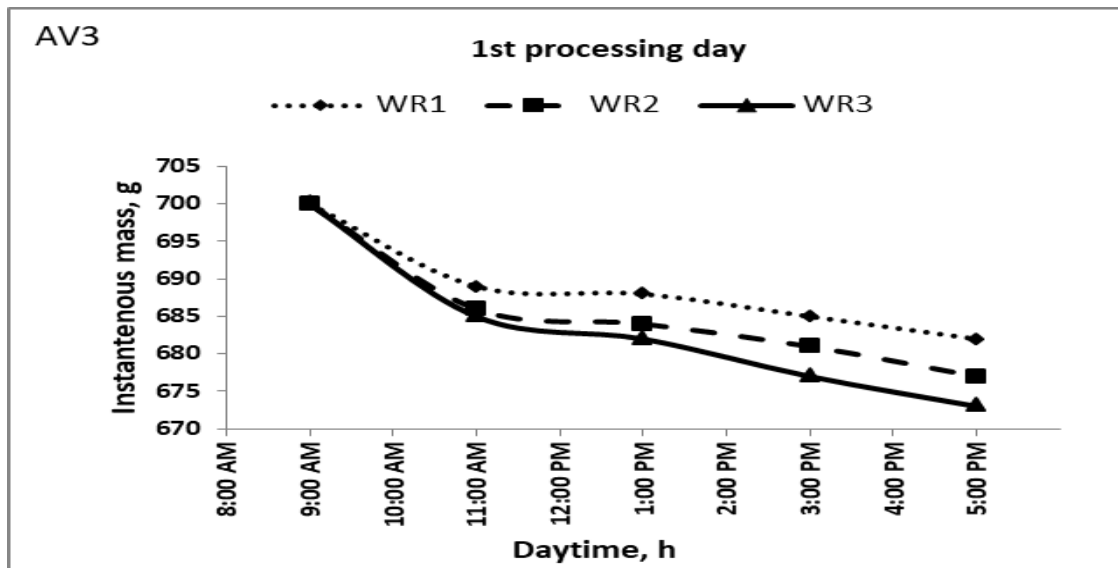


Figure 44. Instantaneous mass behavior under the superficial air velocity of 0.13m/s, three watering rates of 1, 2, and 4ℓ/h and pad thickness of 7cm for the first processing day

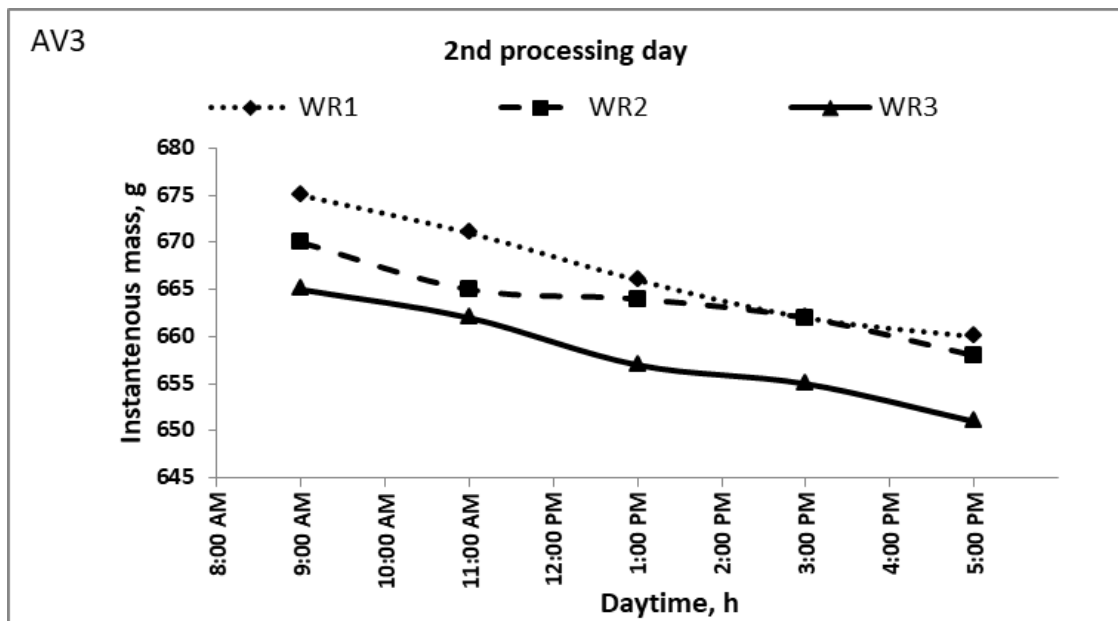


Figure 45. Instantaneous mass behavior under the superficial air velocity of 0.13m/s, three watering rates of 1, 2, and 4ℓ/h and pad thickness of 7cm for the second processing day

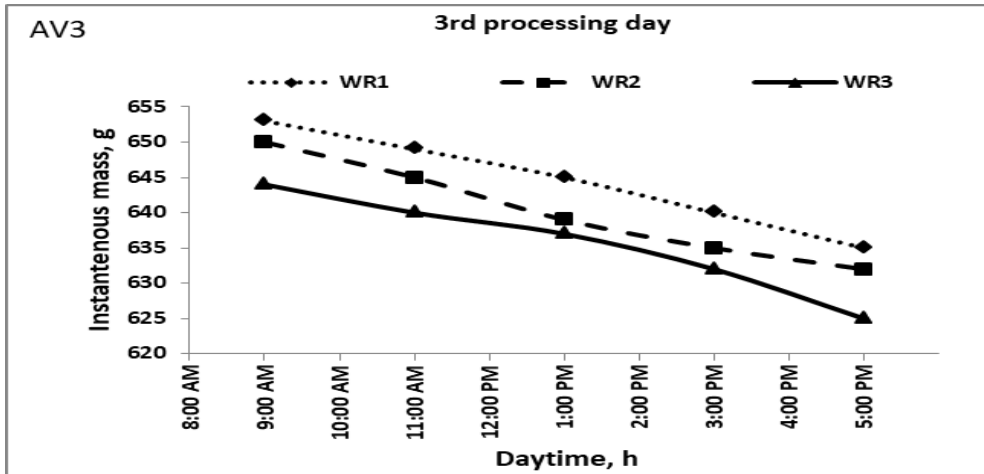


Figure 46. Instantaneous mass behavior under the superficial air velocity of 0.13m/s, three watering rates of 1, 2, and 4ℓ/h and pad thickness of 7cm for the third processing day

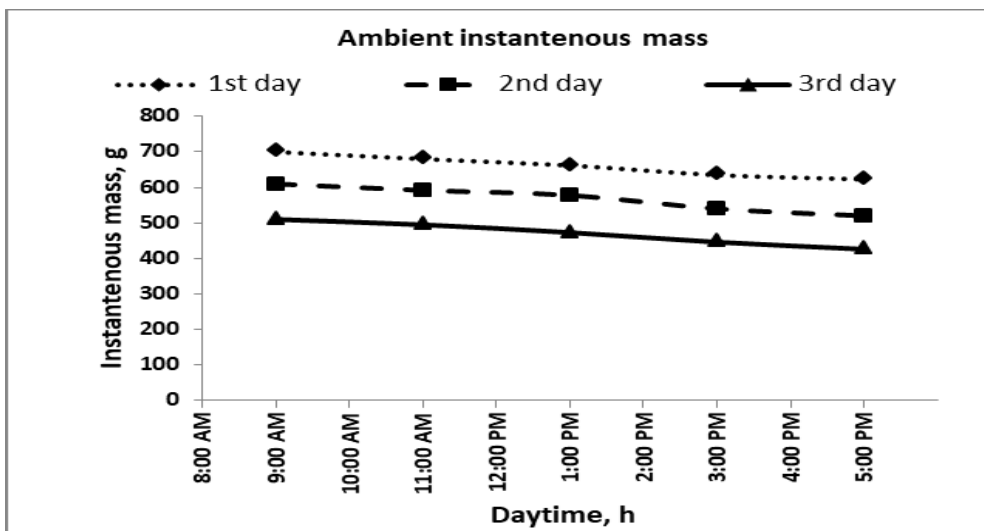


Figure 47. Instantaneous mass behavior under the ambient conditions for the first, second and third processing days

On several days, the effect of pad thickness on mass loss was investigated. As a result of the diverse climatic conditions, it was difficult to draw a comparison between the results.

Figures from 36 to 59 show that For two pad thickness, the best recorded results were achieved with air velocity of 0.21m/s and watering rate of 4ℓ/h but lowest reductions of mass are obtained with a thicker pad (10 cm) was 0.1%.

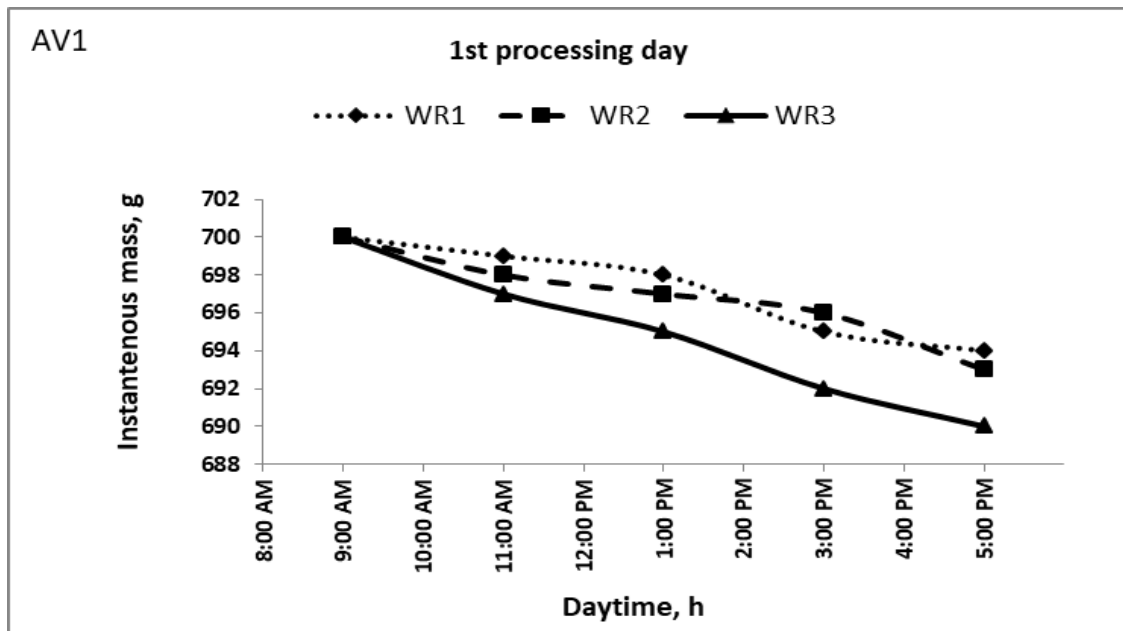


Figure 48. Instantaneous mass behavior under the superficial air velocity of 0.21m/s, three watering rates of 1, 2, and 4ℓ/h and pad thickness of 10cm for the first processing day.

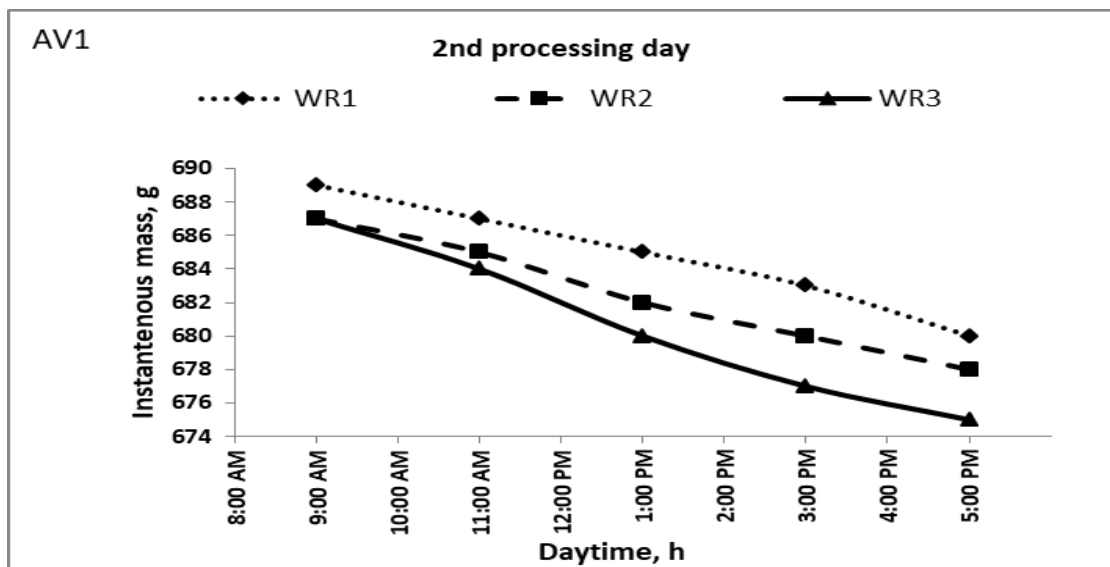


Figure 49. Instantaneous mass behavior under the superficial air velocity of 0.21m/s, three watering rates of 1, 2, and 4ℓ/h and pad thickness of 10cm for the second processing day

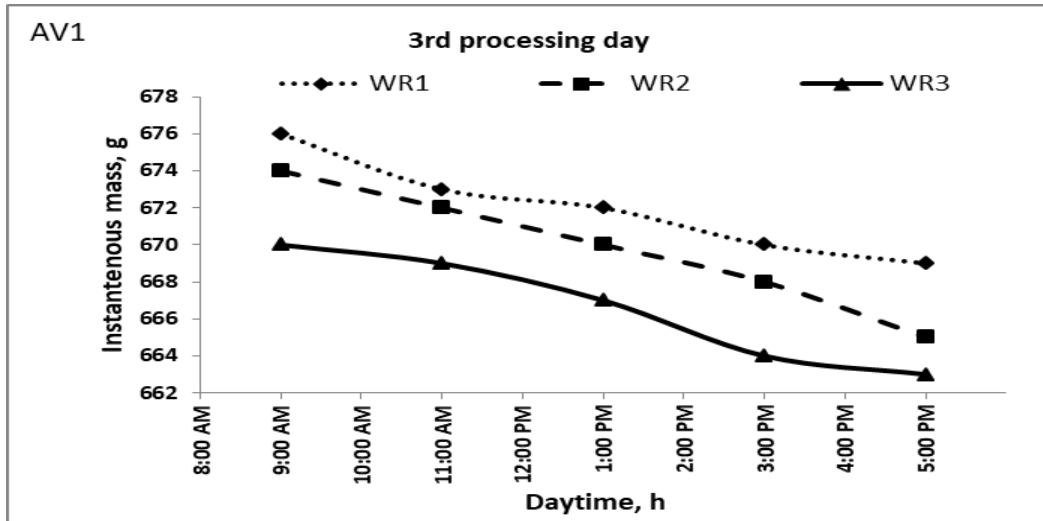


Figure 50. Instantaneous mass behavior under the superficial air velocity of 0.21m/s, three watering rates of 1, 2, and 4ℓ/h and pad thickness of 10cm for the third processing day.

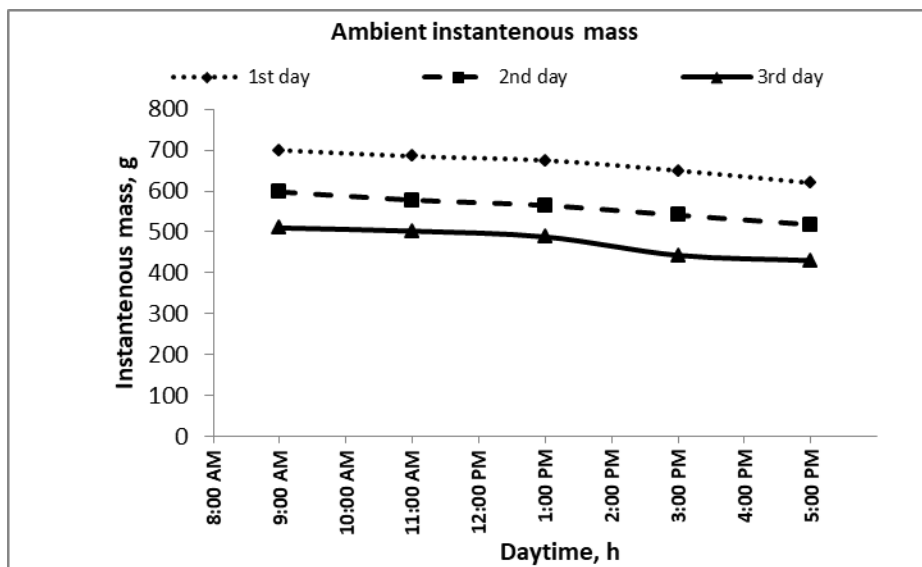


Figure 51. Instantaneous mass behavior under the ambient conditions for the first, second and third processing days

Figures 52 through 55 show the variation of effect of evaporative cooling system at superficial air velocity of 0.17m/s results indicated that the average reduction of mass were 0.2, 1.3 and 2.8% for watering rate of 4ℓ/h. but watering rate of 2ℓ/h average reduction were 0.3, 1.8 and 3.2%. then results indicated that average reduction of mass were 0.4, 2.0 and 3.7% at 1ℓ/h.

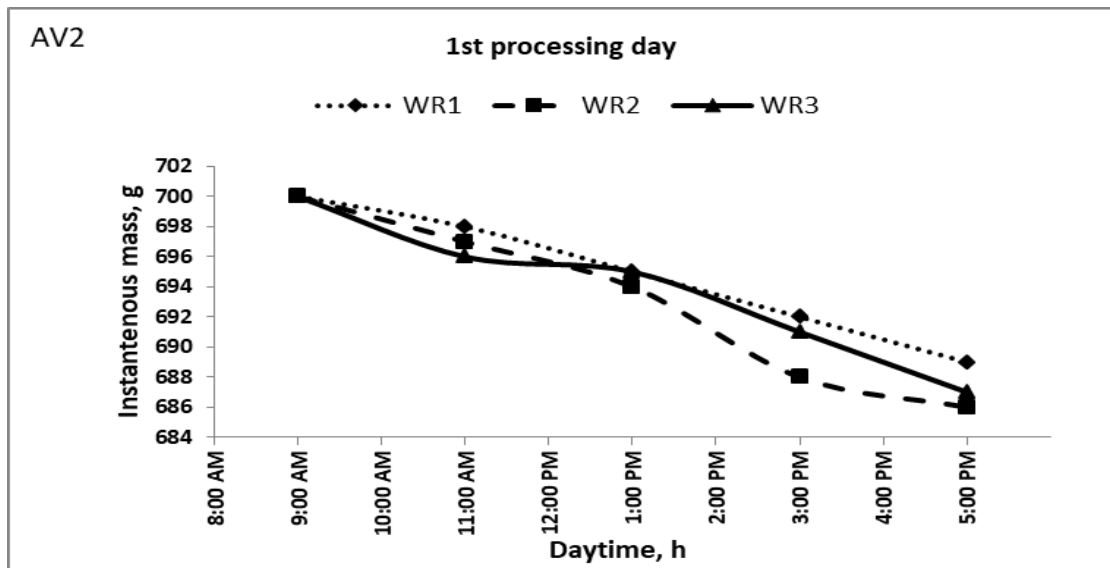


Figure 52. Instantaneous mass behavior under the superficial air velocity of 0.17m/s, three watering rates of 1, 2, and 4ℓ/h and pad thickness of 10cm for the first processing day

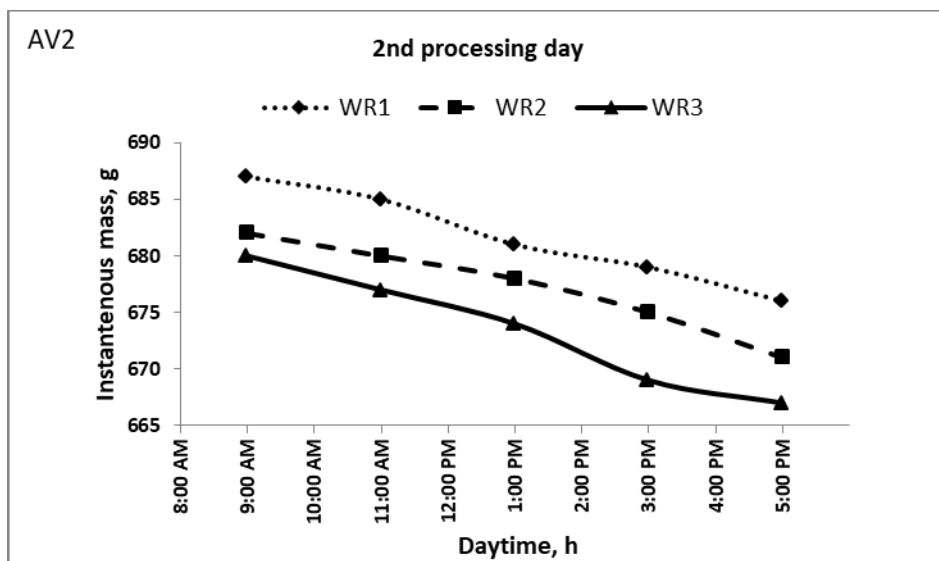


Figure 53. Instantaneous mass behavior under the superficial air velocity of 0.17m/s, three watering rates of 1, 2, and 4ℓ/h and pad thickness of 10cm for the second processing day

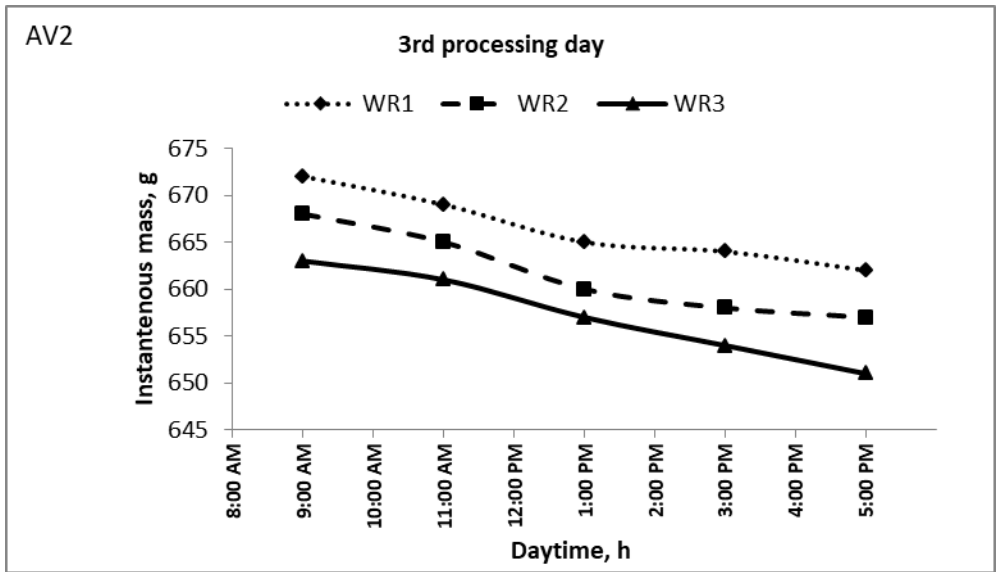


Figure 54. Instantaneous mass behavior under the superficial air velocity of 0.17m/s, three watering rates of 1, 2, and 4ℓ/h and pad thickness of 10cm for the third processing day

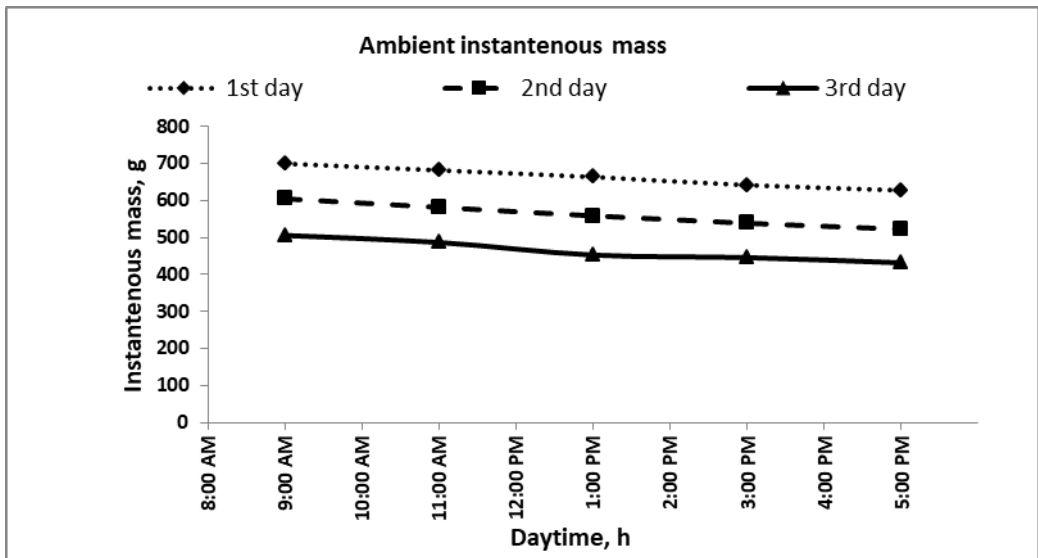


Figure 55. Instantaneous mass behavior under the ambient conditions for the first, second and third processing days

The evaporative cooling system's performance is based on data collected from the demonstration system. The greater cooling efficiency can be achieved at the lower temperature and high air relative humidity

Figures 56 through 59 show the variation of effect of evaporative cooling system at superficial air velocity of 0.13m/s results indicated that the average reduction of mass were 0.5, 1.6 and 3.2% for watering rate of 4ℓ/h. but watering rate of 2ℓ/h average reduction were 0.6, 2.0 and 3.5%. then results indicated that average reduction of mass were 0.8, 2.3 and 4.0% at 1ℓ/h.

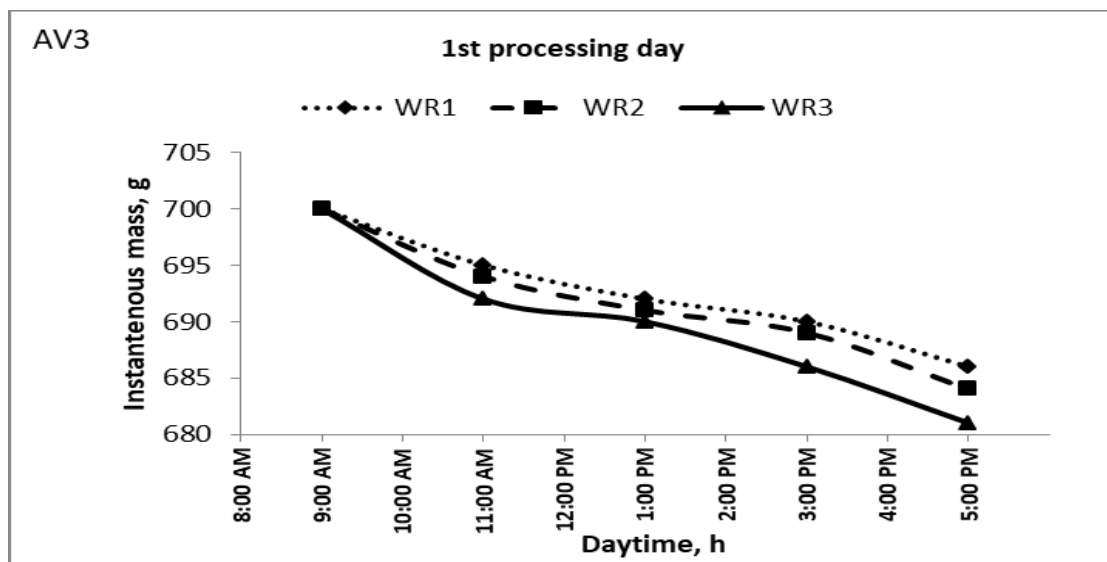


Figure 56. Instantaneous mass behavior under the superficial air velocity of 0.13m/s, three watering rates of 1, 2, and 4ℓ/h and pad thickness of 10cm for the first processing day

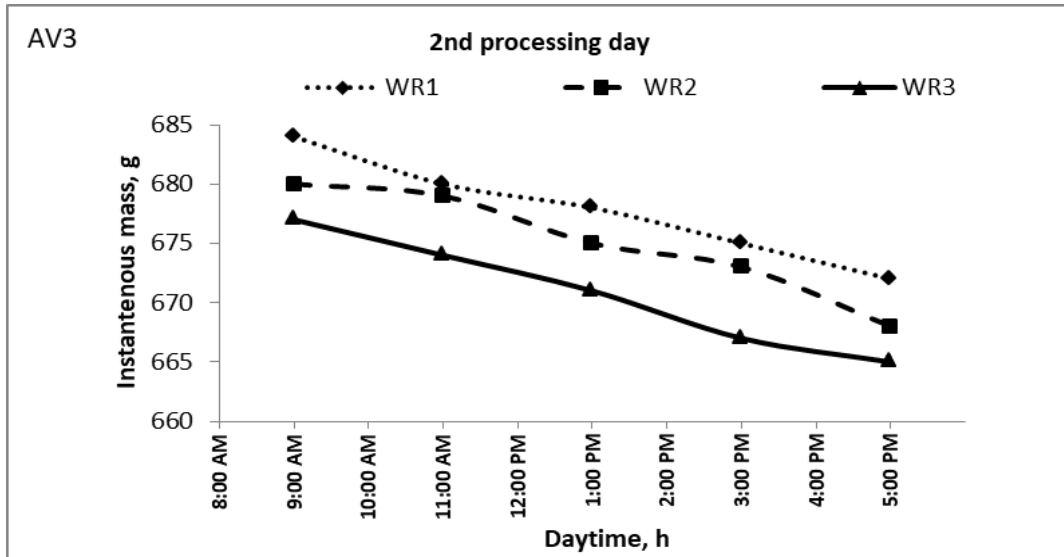


Figure 57. Instantaneous mass behavior under the superficial air velocity of 0.13m/s, three watering rates of 1, 2, and 4ℓ/h and pad thickness of 10cm for the second processing day

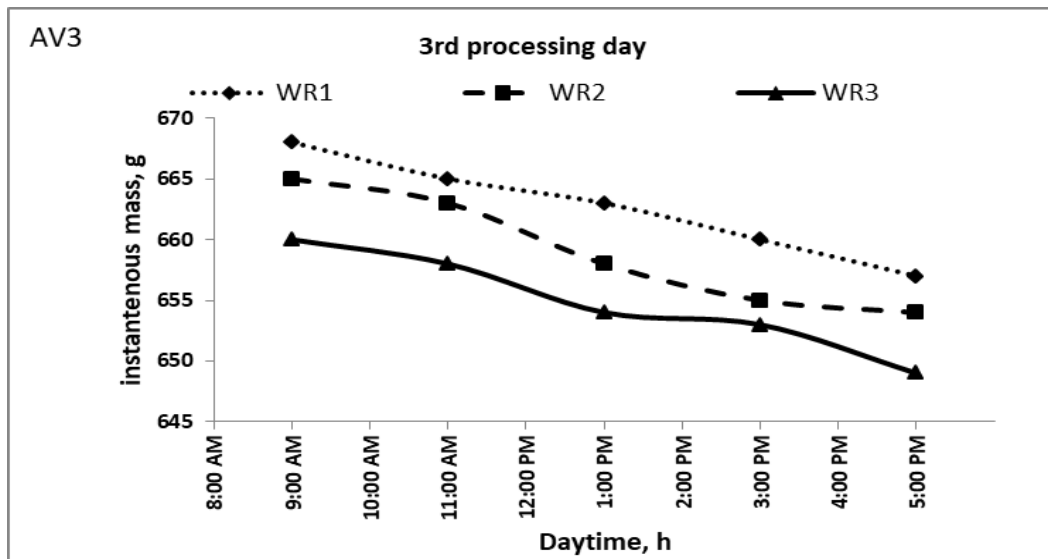


Figure 58. Instantaneous mass behavior under the superficial air velocity of 0.13m/s, three watering rates of 1, 2, and 4ℓ/h and pad thickness of 10cm for the third processing day

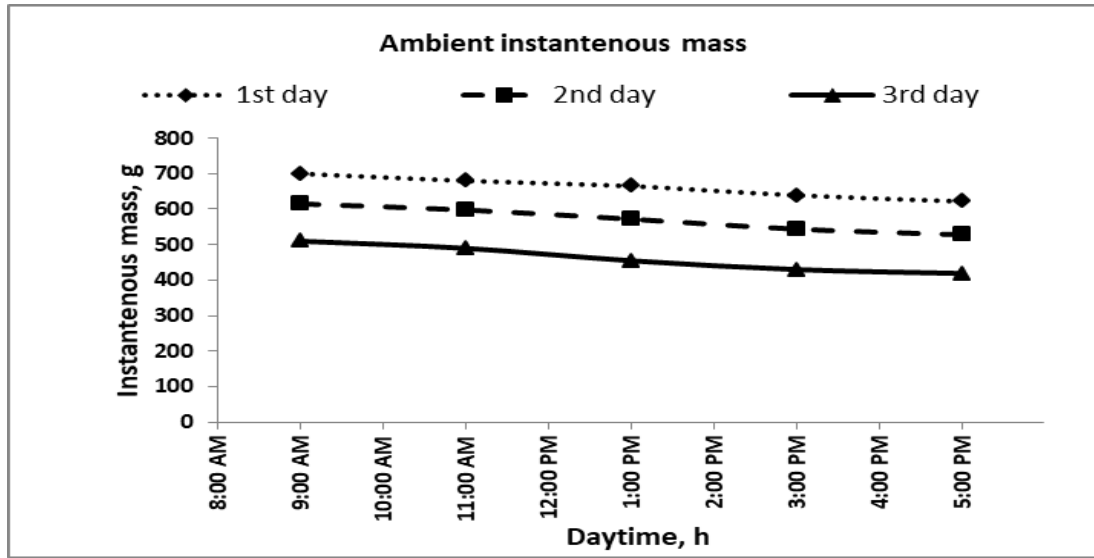


Figure 59. Instantaneous mass behavior under the ambient conditions for the first, second and third processing days

4.2. The predicted air temperature and relative humidity of evaporative cooler

Under ambient conditions of air relative humidity and temperature illustrated that air relative humidity and temperature inside the evaporative cooler can be predicted by using the **equations** of **8** and **9**, respectively. Boundary conditions should be considered for model applications listed in **Table 9**

$$\begin{aligned}
 RH = & -135.4AV^2 - 0.261WR^2 + 0.25PT^2 & R^2 & \text{Eqn 8} \\
 & + 82.67AV + 3.248WR + 1.38AV.WR & = & 0.987 \\
 & - 1.11AV.PT - 0.066WR.PT + 56.7
 \end{aligned}$$

$$\begin{aligned}
 T_c = & -88.54AV^2 + 0.225WR^2 - 0.03489PT^2 & R^2 & \text{Eqn9} \\
 & + 41.04AV - 0.74856WR & = & 0.971 \\
 & - 5.2223AV.WR - 1.25AV.PT \\
 & + 0.0151WR.PT + 24.51
 \end{aligned}$$

Table 9. Boundary conditions of the developed model application

<i>No.</i>	<i>Item</i>	<i>Boundary values</i>
1	Weather conditions <ul style="list-style-type: none">• Air temperature• Relative humidity	29-37°C 40-74%
2	Superficial air velocity	0.13-0.21m/s
3	Watering rate	1-4 ℓ/h
4	Pad thickness of Jute fibre	7-10cm

Figures 60 and 61 compares the experimental data with those predicted by **Equations 8 and 9** for air temperatures and relative humidity of the evaporative cooler (inside the evaporative where the Jew's Mallow is stored). The prediction used the equations showed air temperature and relative humidity values banded along the straight line, which showed the suitability of the developed equations in describing the values of air and relative humidity of the evaporative cooler.

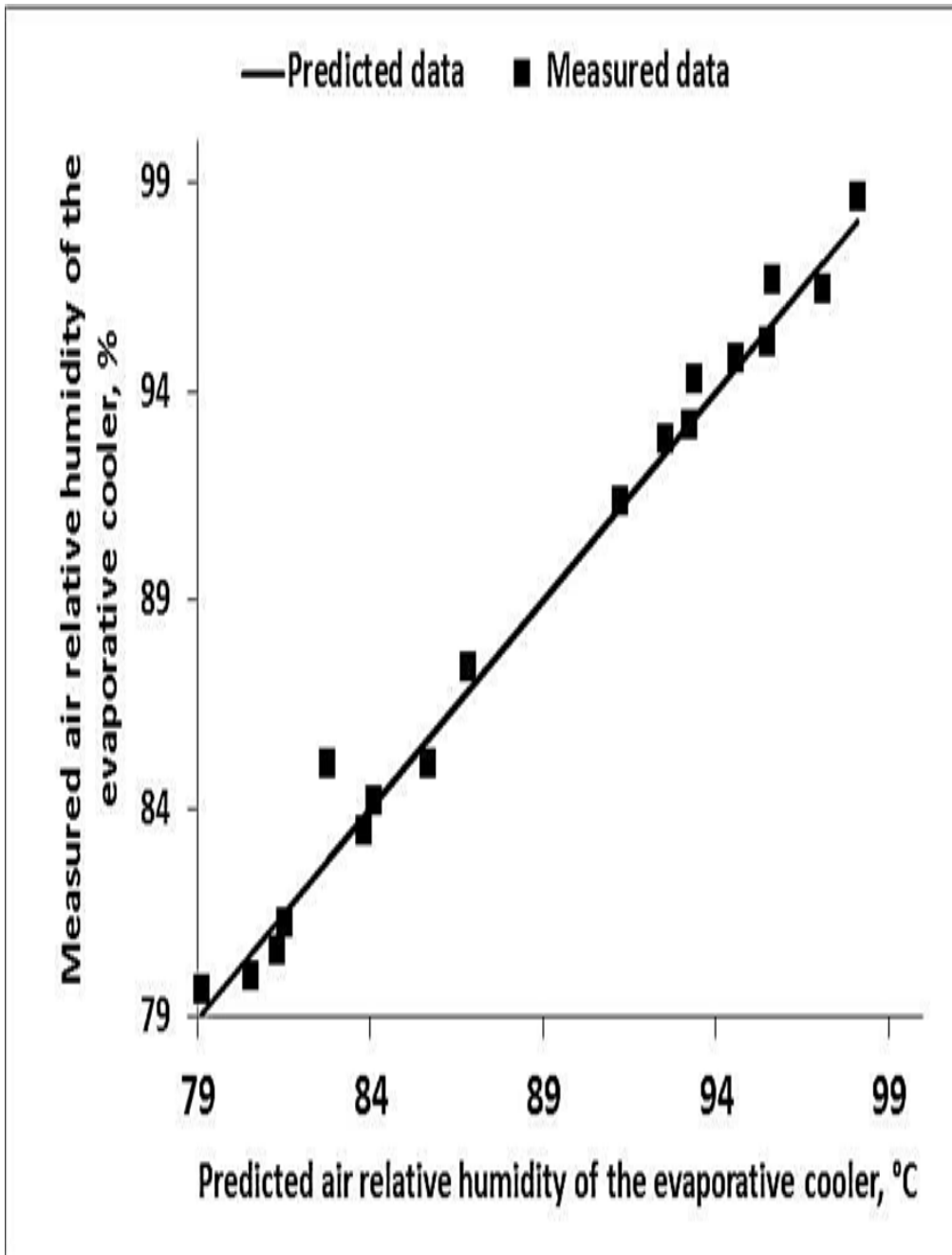


Figure 60: Scatter distribution of the measured versus the predicted relative humidity of the evaporative cooler by **Equation 8**

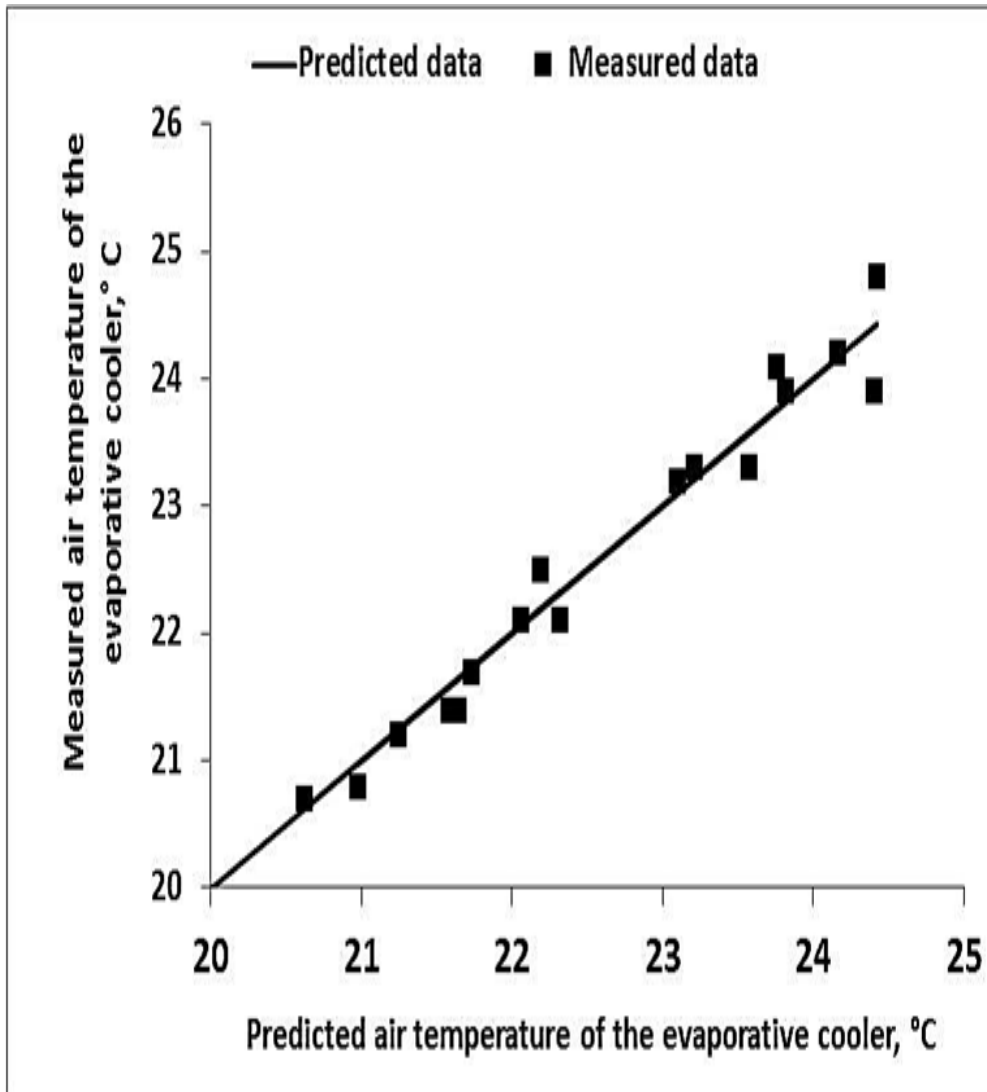


Figure 61: Scatter distribution of the measured versus the predicted air temperature of the evaporative cooler by **Equation 9**

4.3. Instantaneous mass reduction of Jaw's Mallow

4.3.1. Effect of ambient conditions on the instantaneous mass reduction of Jaw's Mallow

Figures from 62 to 64 show the instantaneous mass reduction during daytime at watering rate of 4ℓ/h and pad thickness of 10cm for the three superficial air velocities of 0.13, 0.17 and 0.21m/s. Instantaneous mass tends to gently decrease with the mass reduction percentage of 0.85, 1.5 and 2% at 1st processing day for 0.21, 0.17 and 0.13m/s, respectively. However under ambient conditions, it was dramatically decreased from 11.4, 11.1 to 10.2%.

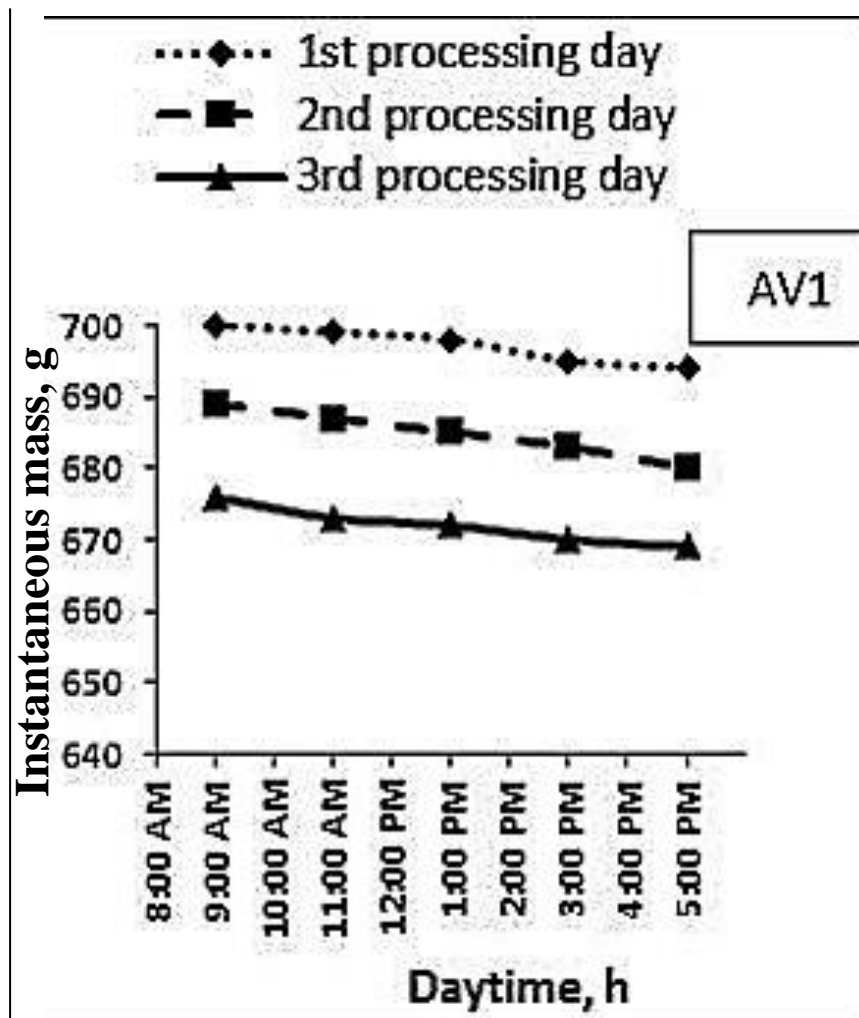


Figure 62. Instantaneous mass of Jew's Mallow in the evaporative cooler under: watering rate of WR1 and superficial air velocity of AV1 at pad thickness of 10cm

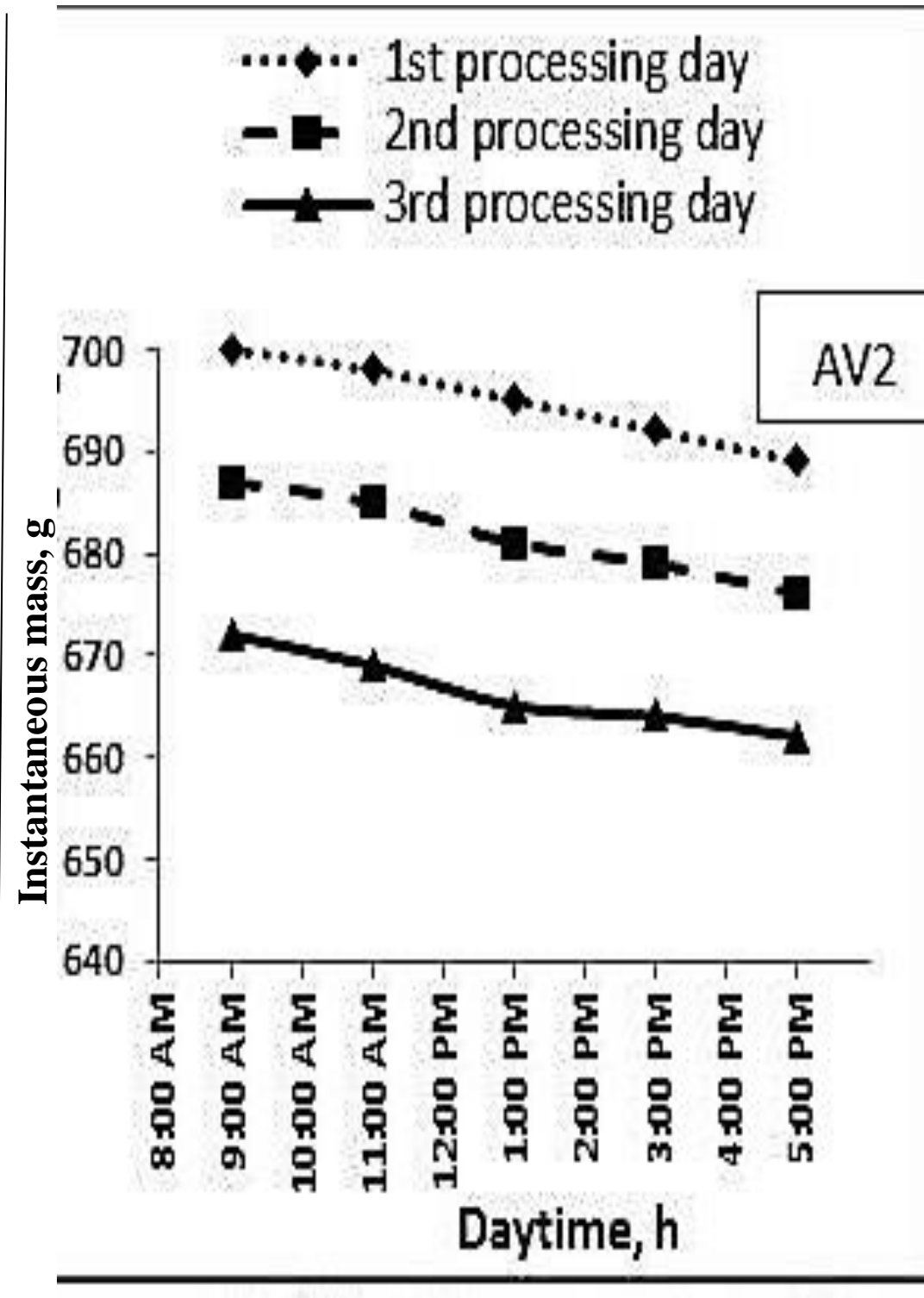


Figure 63. Instantaneous mass of Jew's Mallow in the evaporative cooler under: watering rate of WR1 and superficial air velocity of AV2 at pad thickness of 10cm

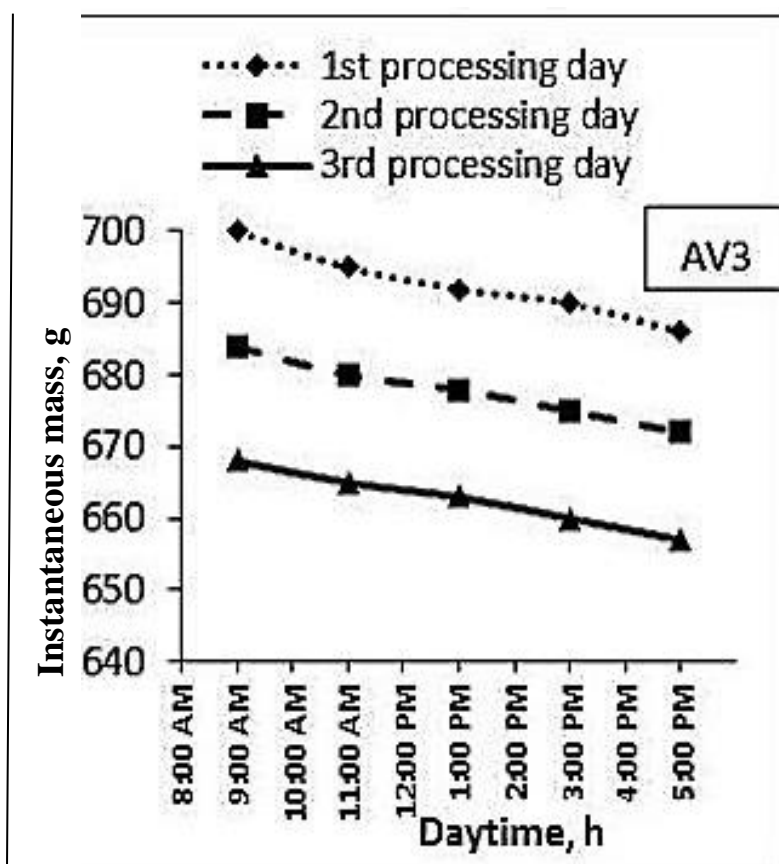

















Figure 64. Instantaneous mass of Jew's Mallow in the evaporative cooler under: watering rate of WR1 and superficial air velocity of AV3 at pad thickness of 10cm

4.4. Wilting percent values of different samples of Jew’s Mallow leaves was obtained by CCM-200 and converted to wilting percent according to the standard Table of Horsfall and Barratt (1945) as listed in Table 10.

Table 10. General Appearance, CCI and wilting percent measurements of some samples of Jew’s Mallow leaves

Whole leaf image						
CCI*	25.2	25.4	25.9	27.3	27.8	28.1
B-H**	0	0.1	0.2	0.3	0.4	0.5
Percent***	0	0.2	0.4	0.7	1.0	1.3
						
28.4	28.7	29	29.3	29.5	30.5	
0.6	0.7	0.8	0.9	1.0	1.1	
1.6	1.9	2.1	2.4	2.4	2.8	
			<p>* CCI measured by CCM-200</p> <p>** The values of B-H mean are used to calculate the wilting percent from the following table</p> <p>*** Wilting percent is obtained from the following table</p>			
32.4	32.9	33.8				
1.2	1.3	1.4				
3.1	3.3	3.5				


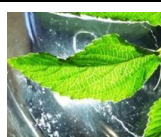



4.5. Chlorophyll Content Index measurements

CCI is calculated using the proportion of Near Infra-Red (NIR) to red wavelengths transmitted by the Opti-Sciences CCM-200 meter. Radiation transmission is non-linearly related to the amount of absorbing compound in leaf tissue and linearly related to compound absorbance (Atkins, 1990). Transmission of (NIR) radiation is not influenced by chlorophyll and is hence principally measured by the quantity of non-chlorophyll compounds, by presumption an even spreading of chlorophyll in leaves.

Measurements of General Appearance (GA)

Evaluation was done by considering the leaves' freshness and wilting, according to the following scale: 1= very weak, 2= weak, 3= average, 4= good and 5= excellent (Troncoso *et al.*, 2005). General Appearance, GA measurements were illustrated by **Figure 65**. It can be noticed that the appearance changes during the storage period under laboratory conditions of Jew's Mallow leaves. On the other hand, **Table 11** indicates the corresponding changes of CCI values for the same leaves.

Table 11. Six times daily measurements of CCI for five storing days under laboratory environment conditions

Daytime, h	CCI, ratio				
	1 st day	2 nd day	3 rd day	4 th day	5 th day
					
8	26.3	28	41.7	54.2	54.5
10	31.2	26.5	29.5	52.6	56.8
12	24.3	24.7	32.2	45.7	57.2
14	25	19.6	35.6	48.3	63.1
16	25.2	42.4	34.3	51.9	52.8
18	26.2	43.4	33.7	53.2	64.3

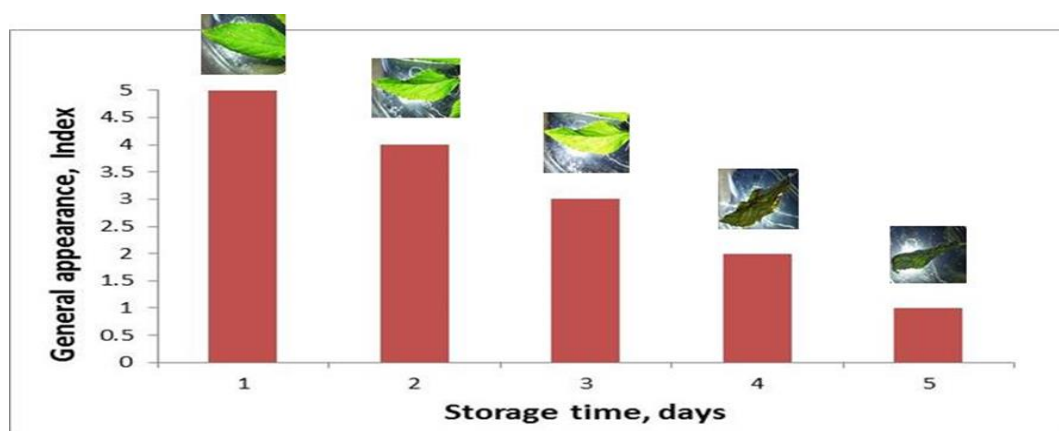


Figure 65. General Appearance from the first to the fifth experimental day

The experiment of image segmentation is implemented by Matlab R2010a. Procedures for implemented segmentation are followed up form Matlab central webpage. Segmented image and RGB histogram, are represented in **Figures 67, 68, 69** and **70** the RGB image segmentation is a complex problem due to the three unlike color rhythms of Red, Green

and Blue components. The histogram of a RGB image is more difficult than the grey scale histogram of the image. Searching for optimal threshold on such composite histogram is a hard assignment. Each color distribution should be distinctly analyzed using the RGB histogram, which may upsurge the computational period. The conforming optimal thresholds (R, G, B) are shown in the following **Figures 67, 68, 69** and **70**.

4.6. Morphological system for image processing

Morphological image processing is a procedure for adjusting pixels in an image. In the example of a Gray scale image, the pixels are defined by the binary numbers 0 and 1, and the procedure is carried out using complex image processing algorithms, or less complex calculations. It includes contracting and stretching as well as opening and closing. The goal of formalizing images is to remove unwanted defects or improve image quality. **Figure 66** shows the open process: The opening process of morphological analysis (A), original images (B), and wilting percent (C) is a process that erodes first and expands later. It is used to get rid of small objects in the image, separate objects at thin points, and smooth the outlines of larger objects without significantly changing the size of the objects. The opening process ability of images decreases to eliminate the small black spots just when the moisture content of the leaves decreases, which means that as wilting percent, increases the black area tends to be the predominant color in the image.


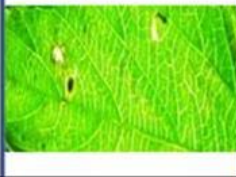






A	B	C
		0%
		2.1%
		2.8%
		3.5%

Figure 66. Morphological analysis (A), original images (B), and wilting percent (C) of *Corchorus olitorius* leaves images

4.7. RGB histogram for pixel intensity distribution

An image histogram is a type of histogram that expresses the distribution of the color value in a digital image. The graph consists of plotting the pixels number of each color degree. By looking at the graphic representation of a particular image, the viewer can, at a glance, judge the overall distribution of tonal values. Image histograms are found on many modern digital cameras. Photographers can use this feature in order to show the distribution of captured tonal values, and if a certain detail in the image has been lost due to too brightness or due to obscuring shadows. The x-axis (horizontal) of the graphic representation represents the various color values on the scale from zero (dark areas) to 255 (light areas), while the y-axis (vertical) represents the number of pixels in a specific color value. The left side of the x-axis shows the black parts, the middle side represents the medium Gray areas and the right side represents the light and pure white areas.

While the y-axis represents the size of the captured region in each of these areas. Therefore, the histograms of a very dark image will have most of its points on the left and middle side of the graph. On the contrary, a histogram of a very light image with few dark zones and / or shadows will have most of which are located in the right and middle part of the graph. **Figures 67, 68, 69 and 70** show RGB histogram that illustrates the color channels of the leaves sheets with different degrees of freshness. It is noticed that, the green channel on the right side of the horizontal axis, represents that the light color, which decreases with a decrease in the degree of freshness.

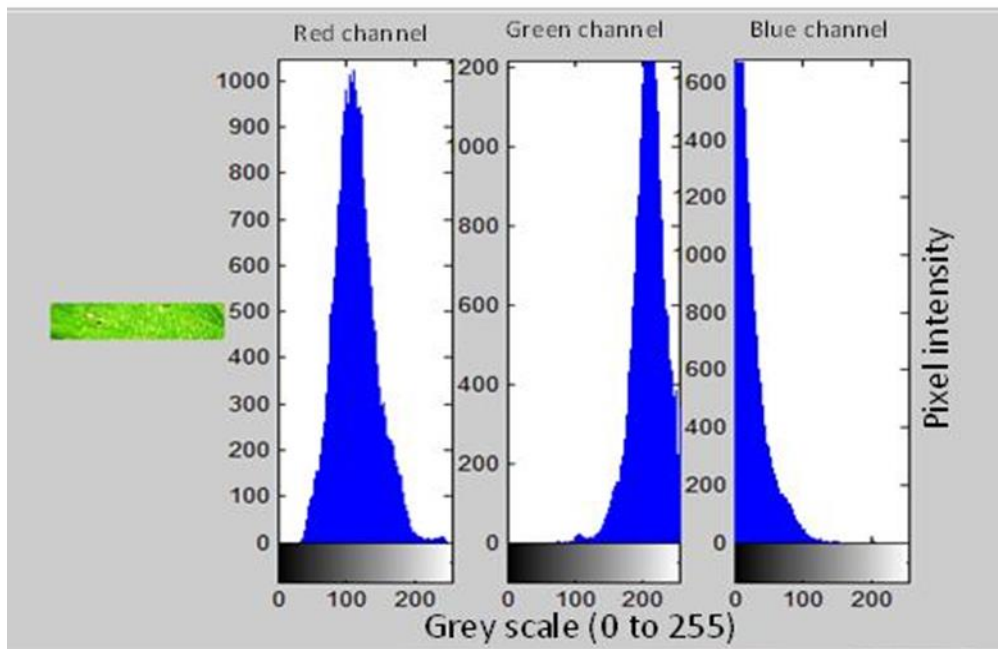


Figure 67. RGB pixel intensity histogram of leaf sample of 0.0% wilting percent

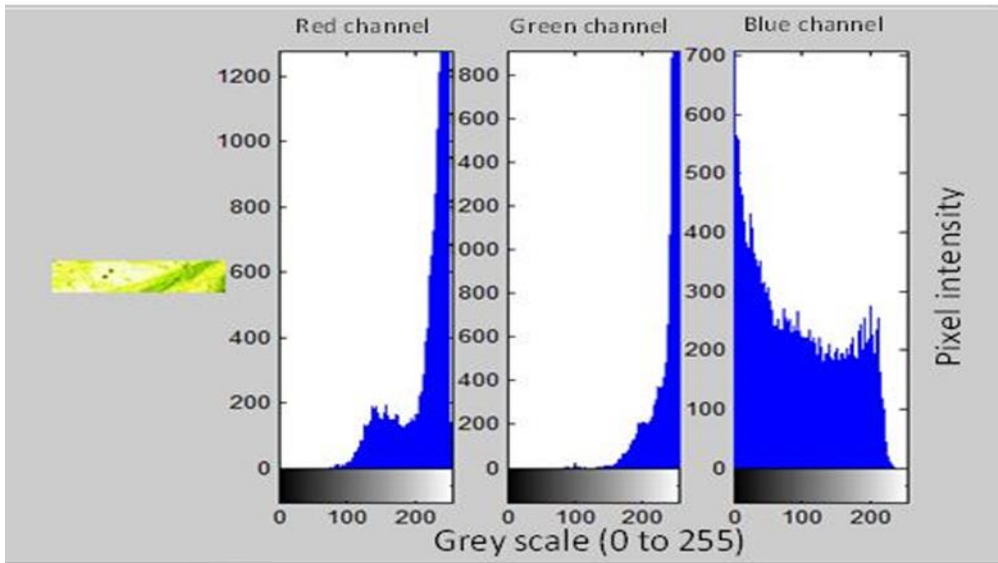


Figure 68. RGB pixel intensity histogram of leaf sample of 1.3% wilting percent

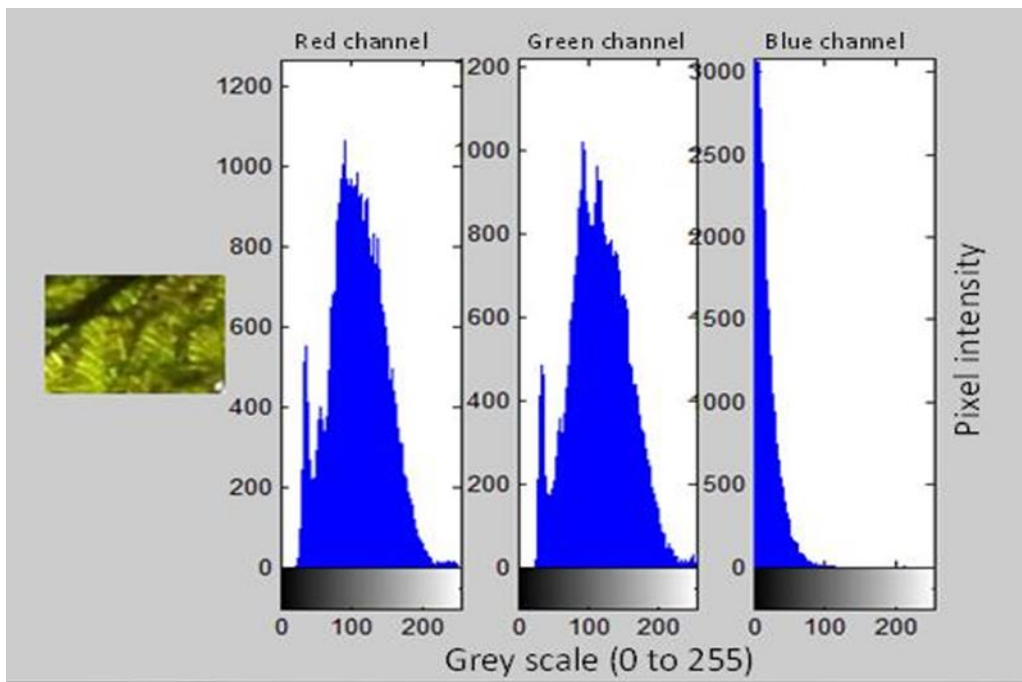


Figure 69. RGB pixel intensity histogram of leaf sample of 3.1% wilting percent

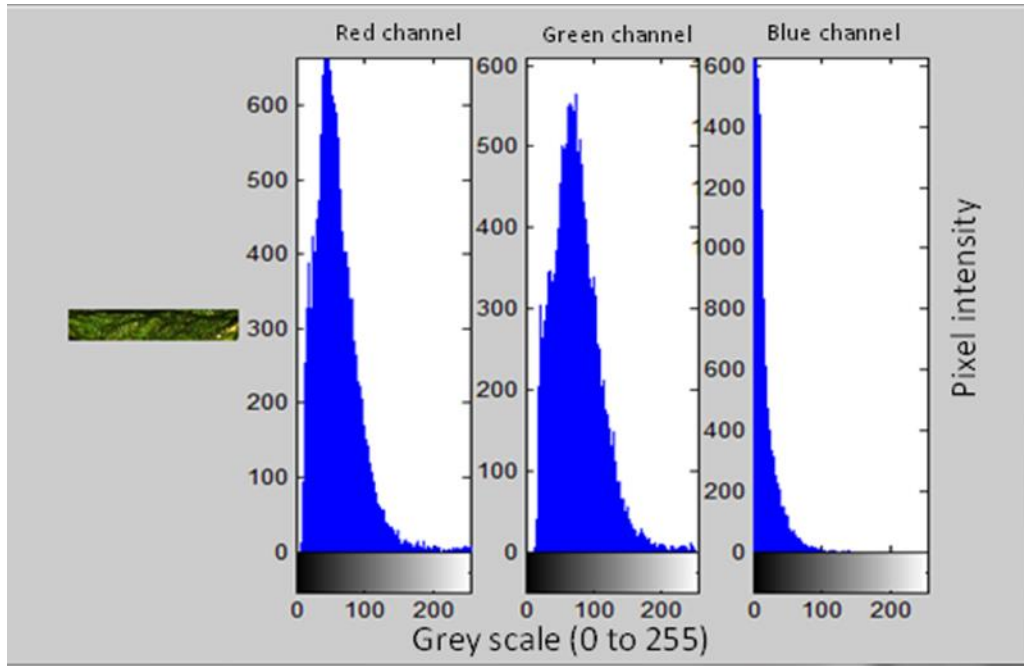


Figure 70. RGB pixel intensity histogram of leaf sample of 3.5% wilting percent

$$\begin{aligned}
 P, \% = & 18281.77E^2 + 0.018M^2 + 1.75D^2 - 281789E + 382.28M & \text{Eqn 10} \\
 & - 664.39D - 52.01EM + 68.39ED - 0.53MD & R^2 = 0.99 \\
 & + 1091100
 \end{aligned}$$

Where $P, \%$ is wilting percent, E , is the image pixel entropy, M , is mean pixel intensity value over the region of interest, and D is the standard deviation of pixel intensity. According to the data acquired from pixel intensity analysis for each freshness grade of Jew's Mallow, an expressive nonlinear multiple regression equation was developed, **Equation 10**. The equation can be used to predict the wilting percent according to image pixel intensity statistical analysis, for further leaf image classification processes. Comparing obtained data with those predicted by **Equation 10**, the prediction showed imagery characteristics values banded along the straight line, which showed that the suitability of the developed equations in describing the obtained results, ($R^2=0.99$).

Visualization of Jew's Mallow freshness by RGB color space model

A jet type color-map was used to determinate the degree of freshness of Jew's Mallow. The final pattern generated was transferred with optimal wavelengths for each pixel of the image, to predict the brightness degrees of all leaf samples. To depict the degree of freshness inside the sheets, the regression coefficients of the model were multiplied by the spectrum of each pixel in the image to form an expectation image called a distribution map. Pixels with the same spectral attitudes generated the same predicted value for luminosity gradients in the resulting distribution map, which were then displayed in the image with a comparable color. Brightness gradients ranging from high to low were displayed in a variety of colors ranging from green to black (color bar on the right in **Figure 71**). By completing a quality assessment and inspection, this technique benefits the Jew's Mallow sector. as it means monitoring the process in the primary stage of production. A new objective and quantitative technique for measuring the quality of Jew's Mallow products is now income to this technology.

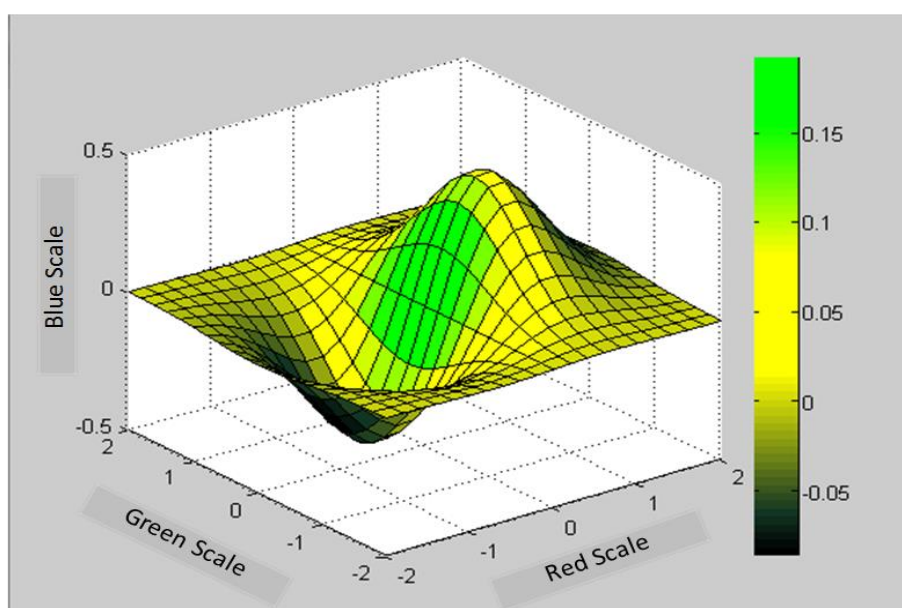


Figure 71. RGB color-map based on freshness degrees of Jew's Mallow



Summary and Conclusion

5. SUMMARY AND CONCLUSIONS

Evaporative cooling system leads to greater yields, higher quality, and the harvest season is extended.

Evaporative cooling is a type of cooling that is both environmentally friendly process and energy efficient because it simply employs water as a working fluid. Cooling system is considered to be a viable solution for growers in regions where worms or hot seasons may spread throughout most of the year. In Egypt, there are only two seasons : a mild winter and a hot summer.

Evaporative cooler is a flexible system. A lot of modifications can be applied to make the system more appropriately under different conditions. Using local pad materials, inexpensive, easy to find and efficient, such as jute fiber can be constructed to provide a cooling effect instead of commercial pad materials. These commercial pad materials are usually complicated to manufacture and they are costly and not rapidly available. On the other hand, the received product has some quality defects that need to be treated by sorting and grading. Leaves color is a vital characteristic that ensures product quality. So the suitable technology for leaves sorting is vision technology, which depends on image processing and pattern recognition. The sorting process is reliant on the integration of vision, appropriate software and mechatronics engineering. Image processing is an essential part of pattern recognition in logic design. Feature extractions and characteristic definition for each quality category of captured leaves images are necessary for machine and computer vision designs. The morphological analysis technique can rapidly discriminate among four classes of Jew's Mallow leaves.

The main objective of this current investigation is to control and quickly remove field heat stress appropriately and maintain the Jew's

Mallow at good storage environment by manufacturing an accessible compact evaporative cooler that has a potential storage quality monitoring tool.

The specific objectives are as follows:

1. Studying the thermal performance of the manufactured evaporative cooler under different levels of pad watering rates and pad thicknesses,
2. Investigating the influence of superficial air velocities of 0.13, 0.17 and 0.21m/s on the evolution of evaporative cooling process,
3. Developing an empirical equation for the evaporative cooling rate during Jew's Mallow storage, and
4. Extracting an appropriate imagery classifying features for further implementation in machine vision in Jew's Mallow (*Corchorus olitorius*) processing plants in Egypt.

In the present investigation, an evaporative cooling system was developed and tested for Jew's Mallow storage after harvesting at the Rice Mechanization Center (RMC) at Meet Eldeebah village, Kafr Elsheikh Governorate, Egypt, during the summer season of 2017. The evaporative cooler consists frame, suction impeller fan, water tank, plastic sheet and jute fiber. Ripe fresh Jew's Mallow (variety of Alaskndrany) was used in this study.

The crops were collected from a private farm in KafrElsheikh Governorate. The leaves were cleaned to remove all foreign materials such as dust, dirt, immature and damaged parts. Therefore, this research deals with the study of some research variables such as the air velocity, the rate of wetting pad and the thickness of the wetting pad on the efficiency and performance of the evaporative cooler. Three different

levels of air velocity of 0.13, 0.17 and 0.21m/s, watering rates of 1, 2 and 4ℓ/h and the thickness of the wetting pad of 7 and 10cm were determined.

It also deals with the study of the variables of classifying the visuals of mallow leaves according to the rules of general appearance, the measurement of primary colors and the ratio of black to white color for different wilting rates of mallow leaves. A large group of leaves under study were selected in terms of green intensity, which varies according to their environmental conditions. A CCM-200 optical meter was used to measure the chlorophyll content index of each leaf. This study was conducted in November of the year 2019 in the laboratory of the Department of Horticulture, Faculty of Agriculture, Kafr El-Sheikh University.

The efficiency indicators were as follows:

- 1- Decrease in temperature.
- 2- Relative humidity.
- 3- Mass of the stored Jew's Mallow.
- 4- The emergence of visual analytical differences between the different classification groups for Jew's Mallow leaves.

The obtained results can be summarized as follows:

1. At superficial air velocity of 0.21m/s, pad watering rate of 4ℓ/h, and pad thickness of 10cm, the achieved air relative humidity, air temperature and mass loss were of 98.7%, 20.2 °C and 0.85%, respectively
2. The storage under ambient conditions can dramatically decrease the Jew's Mallow mass to be 11.4%.

3. At optimum operating conditions, the modified evaporative cooler had cooling potential of 9.1°C at ambient air temperature of 29.3°C and air relative humidity of 68.8%.
4. An empirical mathematical model can predict the values of air temperature and relative humidity obtained by the modified evaporative cooler under different weather conditions of relative humidity and air temperature of 40-74% and 29-37°C, respectively, using the following equations;

$$\begin{aligned}
 RH = -135.4AV^2 - 0.261WR^2 + 0.25PT^2 + 82.67AV & R^2 & \text{Eqn 8} \\
 + 3.248WR + 1.38AV.WR - 1.11AV.PT & = 0.987 \\
 - 0.066WR.PT + 56.7 &
 \end{aligned}$$

$$\begin{aligned}
 T_c = -88.54AV^2 + 0.225WR^2 - 0.03489PT^2 + 41.04AV & R^2 & \text{Eqn 9} \\
 - 0.74856WR - 5.2223AV.WR - 1.25AV.PT & = 0.971 \\
 + 0.0151WR.PT + 24.51 &
 \end{aligned}$$

5. Leaf images were scaled from freshness to wilting according to the general appearance (GA) and wilting percentage rules.
6. A color map was created on the basis of the primary color scale (red, green and blue) to classify the mallow leaves from dark green, light green, yellow and finally black.
7. Morphological analysis of mallow leaves showed significant differences between the different classes based on the ratio of the area of black to white.
8. A non-linear polynomial regression equation was obtained, through which it was possible to predict the wilting rate of mallow leaves based on the statistical analysis of the pixel intensity distribution of the image of the mallow leaf:

$$\begin{aligned}
P, \% = & 18281.77E^2 + 0.018M^2 + 1.75D^2 - 281789E \\
& + 382.28M - 664.39D - 52.01EM + 68.39ED \quad R^2 = 0.99 \\
& - 0.53MD + 1091100
\end{aligned}$$

Applied recommendations:

The obtained results from the experiments indicated that the optimum performance of the modified evaporative cooler was at superficial air velocity of 0.21m/s, pad watering rate of 4ℓ/h, and pad thickness of 10 cm, to increase the safe storage period for fresh consumption or marketing.



References

6.REFERENCES

- Abdalla, A. M. E. 2009. Lower energy wind catcher assisted indirect evaporative cooling for building applications. Doctoral dissertation, University of Nottingham, UK, 1–211.
- Abdel-Rahman, G. M. 2000. Aspen wooden fibers and long wheat straw as evaporative materials for greenhouse cooling systems. *Misr Journal of Agricultural Engineering*, 17(3): 647-659.
- Abdur Rab.; S. Muhammad, U. K. Naqib, N. Khalid, A. Muhammad and K. K. Mansoor. 2012. Influence of storage temperature on fungal prevalence and quality of citrus fruit. *Pakistan Journal of Botany*, 44(2): 831-836.
- Acedo, A. L. 1997. Storage life of vegetables in simple evaporative coolers. *Tropical Science*, 37: 169–175.
- Adams, R and L. Bischof. 1994. Seeded region growing. *Pattern Analysis and Machine Intelligence*, 16(6): 641-647.
- Agrawal, S.; R. Panda; S. Bhuyan and B. K. Panigrahi. 2013. Tsallis entropy based optimal multilevel thresholding using cuckoo search algorithm, *Swarm and Evolutionary Computation*, 11: 16–30.
- Alchalabi, D. A. 1996. Computer – aided design for evaporative cooler systems and estimating number of air coolers in poultry houses. *AMA- Agricultural Mechanization in Asia, Africa and Latin America* , 27(4): 49-52.
- Alexandre, E. M.; T. R. Brandão and C. L. Silva. 2012. Efficacy of non-thermal technologies and sanitizer solutions on microbial load reduction and quality retention of strawberries. *Journal of Food Engineering*, 108(3): 417-426.

- Al-Sulaiman, F. 2002. Evaluation of the performance of local fibers in evaporative cooling. *Energy Conversion and Management*, 43: 2267-2273.
- Anthes, J.; P. Carcia; J. Pierce and P. Dressendorfer. 1993. Non-scanned Ladar imaging and applications. In: *Applied Laser Radar Technology*, 1936: 11–22.
- Anyanwu, E. E. 2004. Design and measured performance of a porous evaporative cooler for preservation of fruits and vegetables. *Energy Conversion and Management*, 45(13–14): 2187–2195.
- Ariana, D. P. and R. F. Lu. 2010. Hyperspectral waveband selection for internal defect detection of pickling cucumbers and whole pickles. *Computers and Electronics in Agriculture*, 74: 137–144.
- Arman, F. and J. Aggarwal. 1993. Model-based object recognition in dense-range image – a review. *ACM Computing Surveys*, 25:5–43.
- ASHRAE. 1992. American Society of Heating, Refrigerating and Air-Conditioning Engineers. Evaporative air cooling. In *Equipment Handbook*, Ch.46, Atlanta, Inc., 1791 Tullie Circle, N.E., Atlanta, GA 30329.
- Awada, L.; P. W. B. Phillips and S. J. Smyth. 2018. The adoption of automated phenotyping by plant breeders. *Euphytica*, 214(8): 1-15.
- Bao, G. Q.; S. S. Xiong and Z. Y. Zhou. 2005. Vision-based horizon extraction for micro air vehicle flight control. *IEEE Transactions on Instrumentation and Measurement*, 54(3): 1067-1072.
- Basiouny, M. A. and Abdallah, S. E. 2013. Influence of pad configuration on evaporative cooling system effectiveness inside a wind tunnel. *AMA- Agricultural Mechanization in Asia, Africa, and Latin America*, 44(4): 70-81.

- Bhardwaj, R. L and N. L. Sen. 2003. Zero energy cool-chamber storage of mandarin (*Citrus reticulata* blanco). *Journal of Food Science and Technology*, 40(6): 669–672.
- Bhatnagar, D. K.; M. L. Pandita and V. K. Shrivastava. 1990. Effect of packaging materials and storage conditions on fruit acceptability and mass loss of tomato. National Workshop on Postharvest Management of Fruits and Vegetables, March 14–16, Nagpur, India.
- Brophy, C. 1990. Effect of intensity error correlation on the computed phase of phase-shifting interferometry. *Journal of the Optical Society of America*. 7(4): 537–541.
- Campos, A. T.; E. S. Klosowski and E. Gasparino. 2002. Study of the air temperature reduction potential through the evaporative cooling system in the region of Maringa-PR Brazil. *Acta Scientiarum*, 24(5): 1575-1581.
- Cefola, M. and B. Pace. 2015. Application of oxalic acid to preserve the overall quality of rocket and baby spinach leaves during storage. *Journal of Food Processing and Preservation*, 39 (6): 2523-2532.
- Cerovic, Z. G.; G. Masdoumier; N. B. Ghazlen and G. Latouche. 2012. A new optical leaf-clip meter for simultaneous non-destructive assessment of leaf chlorophyll and epidermal flavonoids. *Physiologia Plantarum*, 146(3): 251-260.
- Chakraverty, A.; A. S. Mujumdar and H. S. Ramaswamy. 2003. Handbook of postharvest technology: cereals, fruits, vegetables, tea, and spices, 93. CRC press, UK.
- Chandra, R. and S. Govind. 1999. Genetic variability and performance of ginger genotypes under mid-hills of Meghalaya. *Indian Journal of Horticulture*, 56(3): 274-278.

- Chen, L.; Y. Liang and K. Wang. 2010. Inspection of rail surface defect based on machine vision system. 2nd International Conference on Information Science and Engineering, Hangzhou, China, 3793–3796, IEEE.
- Chopra, S.; B. Baboo; K. S. Alesksha and H. S. Oberoi. 2003. An effective on farm storage structure for tomatoes. Proceedings of the International Seminar on Downsizing Technology for Rural Development held at RRL, Bhubaneswar, Orissa, India, 7-9.
- Choudhury, B. A.; M. S. Islam; F. Begum and A. M. Parvez. 2005. Design and performance analysis of a cooling tower in sulfuric acid plant. Journal of Chemical Engineering, Bangladesh, Vol. ChE 23, 1995-2005.
- Christoudias, C.; B. Georgescu and P. Meer. 2002. Synergism in low-level vision, Proceedings of the 16th International Conference on Pattern Recognition, Vol. IV, Quebec City, Canada, August, 150–155.
- Cielo, P. 1988. Optical techniques for industrial inspection. Academic, San Diego, Boston, USA, 234–235.
- Clement, V.; J. Thompson; W. u. Stefanie; K. P. Catherine Hui and D. LeBlanc. 2009. Transportation of fresh horticultural produce. Postharvest Technologies for Horticultural Crops, 2(1): 1-24.
- Coster, M.; X. Arnould; J. L. Chermant; L. Chermant and T. Chartier. 2005. The use of image analysis for sintering investigations: the example of CeO₂ doped with TiO₂. Journal of the European Ceramic Society, 25(15): 3427– 3435.
- Cyganek, B. 2008. Color image segmentation with support vector machines: applications to road signs detection, International Journal of Neural Systems, 18(4): 339–345.

- Dadhich, S. M.; H. Dadhich and R. C. Verma. 2008. Comparative study on storage of fruits and vegetables in evaporative cool chamber and in ambient. *International Journal of Food Engineering*, 4(1): 1–11.
- Darwish, W.; W. Li; S.Tang and W. Chen. 2017. Coarse to fine global RGB-D frames registration for precise indoor 3D model reconstruction. *Proceedings of the International Conference on Localization and GNSS (ICL-GNSS)*, Nottingham, UK, 1-5.
- Das, S. K. and P. Chandra. 2001. Economic analysis of evaporatively cooled storage of horticultural produce. *Agricultural Engineering*, 25(3–4):1–9.
- Daut, D. G. and D. Zhao. 1989. Mathematical morphology and its application in machine vision. *Visual Communications and Image Processing IV*, 1199: 181–191.
- Dilip, J. and N. T. Gopal. 2002. Modeling and optimal design of evaporative cooling system in controlled environment greenhouse. *Energy Conversion and Management*, 43: 2235–2250.
- Dzivama, A. U.; F. O. Aboaba and U. B. Bindir. 1999. Evaluation of pad materials in construction of active evaporative cooler for storage of fruits and vegetables in arid environments. *JAMA*, 30(3): 51-55.
- Erdenee, B.; T. Ryutaro and G. Tana. 2010. Particular agricultural land cover classification: case study of Tsagaannuur, Mongolia. In: *IEEE International Geoscience & Remote Sensing Symposium*, 3194-3197.
- Esturk, O.; Y. Yakar and Z. Ayhan. 2014. Pesticide residue analysis in parsley, lettuce and spinach by LC-MS/MS. *Journal of Food Science and Technology*, 51: 458–466.

- Fan, T.; G. Medioni and R. Nevatia. 1987. Segmented descriptions of 3-D surface. *IEEE International Journal of Robot Automation*, 3(6): 527–538.
- FAO. 1995. Food and Agriculture Organization of the United Nations. Yearbook. Statistics Series No. 132. Rome, Italy.
- FAO. 2006. Food and Agriculture Organization of the United Nations. Postharvest Management of Fruit and Vegetables in the Asia-Pacific region. Retrieved from the website [http://www. Apo-Tokyo.org/ ooe-books/ AG-18_postharvest.pdf](http://www.Apo-Tokyo.org/ooe-books/AG-18_postharvest.pdf) on 25 May 2021.
- FAO. 2018. Food and Agriculture Organization of the United Nations, Rome. Retrieved from the website <http://www.fao.org/faostat/en/#data/QL>, on 11 September 2021.
- Flores, R.; M. L. Looper; M. G. Tomas and D. M. Hallford. 2004. Influence of bovin somatotropin on characteristics of estrus and reproduction of Holstein cows during summer months. *Professional Animal Scientist*, 20(2): 191-197.
- Ganesan, M.; K. Balasubramanian and R. V. Bhavani. 2004. Studies on the application of different levels of water on zero energy cool chamber with reference to the shelflife of brinjal. *Journal of the Indian Institute of Science*. 84: 107–111.
- George, M. 2015. Multiple fruit and vegetable sorting system using machine vision. *International Journal of Advanced Technology*, 6(1): 142-146.
- Ghamisi, P.; M. S. Couceiro; F. M. Martins and J.A. Benediktsson. 2014. Multilevel image segmentation based on fractional-order Darwinian particle swarm optimization. *IEEE Transactions on Geoscience and Remote Sensing*, 52(5): 2382-2394.

- Ghassem, H.; B. Mojtaba; D. Shahram and E. Jafar. 2009. Experimental investigation of two-stage indirect/direct evaporative cooling system in various climatic conditions. *Building and Environment*, 44: 2073–2079.
- Goncalves, J. F. D. C.; U. M. D. Santos Junior and E. A. D. Silva. 2008. Evaluation of a portable chlorophyll meter to estimate chlorophyll concentrations in leaves of tropical wood species from Amazonian forest. *Hoehnea*, 35: 185-188.
- Hager, G. 1997. A modular system for robust positioning using feedback from stereo vision. *Transactions on Robotics and Automation*, 13, 582–595.
- Haralick, R. M. 1987. Image analysis using mathematical morphology. *IEEE Transactions on Pattern Analysis and Machine Intelligence*, 9(4): 532–550.
- Haralick, R. M. 1997. Statistical and structural approaches to texture. *Proceedings of the IEEE*, 67(5): 768–804.
- Heijmans, H. J. A. M. 1991. Theoretical aspects of grey-scale morphology. *IEEE Transactions on Pattern Analysis and Machine Intelligence*, 13(6): 568–582.
- Hellickson, M. A.; J. N. Walker. 1983. Ventilation of agricultural structures. *American Society of agricultural engineers*, 6: 372.
- Horsfall, J. G. and R. W. Barratt. 1945. An improved grading system for measuring plant disease, *Phytopathology*, 35: 655.
- Hussain, S.; F. Khan; W. Cao; L. Wu and M. Geng. 2016. Seed priming alters the production and detoxification of reactive oxygen intermediates in rice seedlings grown under sub-optimal temperature and nutrient supply. *Frontiers in Plant Science*, 7: 439.

- Jain, D. 2007. Development and testing of two-stage evaporative cooler. *Building and Environment*, 42(7): 2549-2554.
- Jeong, M.; D. S. An; G. H. Ahn and D. S. Lee. 2013. Master packaging system for sweet persimmon applicable to produce supply chains. *Postharvest biology and technology*, 86: 141-146.
- Jha, S. N. 2008. Development of a pilot scale evaporative cooled storage structure for fruits and vegetables for hot and dry region. *Journal of Food Science and Technology*, 45(2): 148-151 .
- Jha, S. N. and S. K. Kudos. 2006. Determination of physical properties of pads for maximizing cooling in evaporative cooled store. *Journal of Agricultural Engineering*, 43(4): 92–97.
- Jhawar, J. 2016. Orange sorting by applying pattern recognition on color image, *Procedia Computer Science*, 78: 691–697.
- Jifon, J.; J. P. Syvertsen and E. Whaley. 2005. Growth Environment and Leaf Anatomy Affect Nondestructive Estimates of Chlorophyll and Nitrogen in Citrus sp. Leaves. *Journal of the American Society for Horticultural Science*, 130(2):152–158.
- Kader, A. A. and P. K. Lee. 1992. Preharvest and postharvest factors influencing vitamin C content of horticultural crops. *Postharvest Biology and Technology*, 20(3): 207-220.
- Kassem, A. W. S. 1994. Energy and water management in evaporative cooling systems in Saudi-Arabia. *Conservation and Recycling*, 12(3-4): 135-146.
- Khan, A. U. R. and Thakur, K. 2012. An efficient fuzzy logic based edge detection algorithm for gray scale image. *International Journal of Emerging Technology and Advanced Engineering*, 2 (8). Retrieved from the website

<http://citeseerx.ist.psu.edu/viewdoc/summary?doi=10.1.1.366.3454>

on 25 May 2021.

- Khodabakhshian, R.; B. Emadi; M. Khojastehpour and M.R. Golzarian. 2017. Determining quality and maturity of pomegranates using multispectral imaging, *Journal of the Saudi Society of Agricultural Sciences*, 16(4): 322–331.
- Kleinemeier, B. 1985. Real-time restoration of image sensor photoresponse nonuniformity. *Optical Engineering*, 24(1): 160–170.
- Kondo, N. 2010. Automation on fruit and vegetable grading system and food traceability. *Trends in food science and technology*, 21(3): 145–152.
- Krinidis, M. and I. Pitas. 2009. Color Texture segmentation based on the modal energy of deformable surfaces, *IEEE Transactions on Image Processing*, 18(7): 1613-1622.
- Li, L.; Q. Zhang and D. F. Huang. 2014. A review of imaging techniques for plant phenotyping. *Sensors*, 14(11): 20078-20111.
- Liao, C. M. and K. H. Chiu. 2002. Wind tunnel modeling the system performance of alternative evaporative cooling pads in Taiwan region. *Building and Environment*, 37: 177-187.
- Lin, C. M.; C.Y. Tsai; Y. C. Lai; S.A. Li. and C. C. Wong. 2018. Visual object recognition and pose estimation based on a deep semantic segmentation network. *IEEE Sensors Journal*, 18, 9370–9381.
- Liu, S.; P. Martre; S. Buis; M. Abichou; B. Andrieu and F. Baret. 2019. Estimation of plant and canopy architectural traits using the digital plant phenotyping platform. *Plant Physiology*, 181(3): 881-890.

- Lorente, D.; N. Aleixos; J. Gomez-Sanchis; S. Cubero; O.L. Garcia-Navarrete and J. Blasco. 2012. Recent advances and applications of hyperspectral imaging for fruit and vegetable quality assessment. *Food Bioprocess Technology*, 5(4): 1121-1142
- Lowe, A.; N. Harrison and A. P. French. 2017. Hyperspectral image analysis techniques for the detection and classification of the early onset of plant disease and stress. *Plant Methods*, 13(1): 1-12.
- Maini, S. B. and J. C. Anand. 1992. Evaporative cooling system for postharvest management of horticultural crops. *Agricultural Marketing*, 35(3): 34– 39.
- Malik, A. U.; M. U. Hasan; W. U. Hassan; A. S. Khan; M. S. Shah; I. A. Rajwana; M. Latif and R. Anwar. 2021. Postharvest quarantine vapour heat treatment attenuates disease incidence, maintains eating quality and improves bioactive compounds of ‘Gola’ and ‘Surahi’ guava fruits. *Journal of Food Measurement and Characterization*, 15: 1666–1679.
- Mampholo, B. M.; D. Sivakumar; M. Beukes and W. J. van Rensburg. 2013. Effect of modified atmosphere packaging on the quality and bioactive compounds of Chinese cabbage (*Brassica rapa* L. ssp. *chinensis*). *Journal of the Science of Food and Agriculture*, 93(8): 2008-2015.
- Marmol, U. and S. Mikrut. 2012. Attempts at automatic detection of railway head edges from images and laser data. *Image Processing Communication*, 17: 151–160.
- Medina, M. S.; A. Juan.; T. Alicia; M. A. Allende and M. I. Gil. 2012. Short postharvest storage under low relative humidity improves quality and shelflife of minimally processed baby spinach (*Spinacia oleracea* L.). *Postharvest Biology and Technology*, 67:1-9.

- Mehta, A. and H. N. Kaul. 1997. Physiological mass loss in potatoes under non refrigerated storage: contribution of respiration and transpiration. *Journal of the Indian Potato Association*, 24: 106–113.
- Mishra, P.; G. Polder and N. Vilsuction impeller fan. 2020b. Close range spectral imaging for disease detection in plants using autonomous platforms: a review on recent studies. *Current Robotics Reports*, 1(2): 43-48.
- Mishra, P.; G. Polder, A. Gowen, D. N. Rutledge and J. M. Roger. 2020a. Utilizing variable sorting for normalisation to correct illumination effects in close-range spectral images of potato plants. *Biosystems Engineering*, 197: 318–323.
- Mishra, P.; M. S. M. Asaari, A. Herrero-Langreo, S. Lohumi, B. Diezma, and P. Scheunders. 2017. Close range hyperspectral imaging of plants: A review. *Biosystem Engineering*, 164: 49–67.
- Mogaji, T. S. and O. P. Fapetu. 2011. Development of an evaporative cooling system for the preservation of fresh vegetables. *African Journal of Food Science*, 5(4): 255–266.
- Mordi, J. I and A. O. Olorunda. 2003. Effect of evaporative cooler environment on the visual qualities and storage life of fresh tomatoes. *Journal of Food Science*, 40(6): 587–591.
- Mudau, A. R.; M. M. Nkomo; P. Soundy; H. T. Araya; W. Ngezimana , and F. N. Mudau. 2015. Influence of postharvest storage temperature and duration on quality of baby spinach. *American Society for Horticultural Science*, 25(5): 665–670.
- Ndukwu, M. C.; S. I. Manuwa; O. J. Olukunle and I. B. Oluwalana. 2013. Development of an active evaporative cooling system for short-

- term storage of fruits and vegetable in a tropical climate. *Agricultural Engineering International: CIGR Journal*, 15(4): 307–313.
- Neil, N. 2008. Evaporative coolers. Retrieved from the website www.practicalaction.org. on 25 May 2021.
- Nyadanu, D.; R. Amoah; A. Adu; O. Kwarteng; R. Akromah; L. M. Aboagye; H. Adu- Dapaah; A. Dansi; F. Lotsu and A. Tsama. 2017. Domestication of jute mallow (*Corchorus olitorius* L.): ethnobotany, production constraints and phenomics of local cultivars in Ghana, *Genetic Resources and Crop Evolution*, 64: 1313- 1329.
- Nyman, G.; J. Häkkinen; E. M. Koivisto; T. Leisti; P. Lindroos; O. Orenius and T. Vuori. 2010. Evaluation of the visual performance of image processing pipes: information value of subjective image attributes. In *Image Quality and System Performance*. International Society for Optics and Photonics, 7529: 752905.
- Odesola, I.; F. and O. Onyebuchi. 2009. A review of porous evaporative cooling for the preservation of fruits and vegetables. *Pacific Journal of Science and Technology*, 10(2): 935–941.
- Otterbein, R. 1996. Installing and maintaining evaporative coolers. *Home Energy, U S*, 13(3), Retrieved from the website <https://www.osti.gov/biblio/456942> on 14 September 2021.
- Pabitra, M.; B.U. Shankar and K. P. Sankar. 2004. Segmentation of multispectral remote sensing images using active support vector machines, *Pattern Recognition Letters*, 25(9): 1067–1074.
- Pal, N. R. and S. K. Pal. 1993. A review on image segmentation techniques, *Pattern Recognition*, 26(9): 1277 – 1294.

- Papa, A. A. and D. A. El- Galabi. 1997. Constructed palm fibers pads of evaporative cooling as a ceiling of a dairy cows. Agriculture and developing in Arabic world, (1): 39-49.
- Peregrina, B. H.; V. R. Terol; M. J. Rangel; N. A. M. Herrera; H. L. A. Morales and G. F. Manríquez. 2013. Automatic grain size determination in microstructures using image processing. Measurement, 46(1): 249– 258.
- Pessu, P. O.; S. Agoda, I. U. Isong and I. Ikotun. 2011. The concepts and problems of postharvest food losses in perishable crops. African Journal of Food Science, 5(11): 603-613.
- Peterson, J. L. 1993. An effectiveness model for indirect evaporative coolers. ASHRAE Transactions, 99(2): 392–399.
- Raja, S. M.; N. Rajinikanth, and K. Latha. 2014. Otsu based optimal multilevel image thresholding using firefly algorithm. Modelling and Simulation in Engineering, (37): 37, Retrieved from the website <https://dl.acm.org/doi/abs/10.1155/2014/794574> on 22nd September 2021.
- Rashwan, M. A. 2016. effect of air speed and size vent area on the precooling cycle for cantaloupe fruits. Misr Journal of Agricultural Engineering, 33(1): 243-256.
- Richardson, S.; I. Tuna and M. Wu. 2002. Predicting earnings management: The case of earnings restatements. Social Science Research Network Working Paper Series. Retrieved from the website <https://citeseerx.ist.psu.edu/viewdoc/download?doi=10.1.1.194.8273&rep=rep1&type=pdf>.

- Roura, S. I.; L. A. Davidovich and, C. E. Del Valle. 2000. Postharvest changes in fresh Swiss chard (*Beta vulgaris*, type *cycla*) under different storage conditions. *Journal of Food Quality*, 23(2): 137-147.
- Roy, S. K. and R. K. Pal. 1994. A low-cost cool chamber: an innovative technology for developing countries [tropical fruits storage]. *Proceedings-Australian Centre for International Agricultural Research*, Australia, 393-395.
- Saltveit, M. E and L. L. Morris. 1990. Overview on chilling injury of horticultural crops. *Chilling Injury of Horticultural Crops*, 1: 3-15.
- Saltveit, M. E. 2016. Water Loss from harvested horticultural commodities. *Postharvest Ripening Physiology of Crops*, 139-156, Davis, California, US.
- Serra, J. 1982. *Image Analysis and Mathematical Morphology*. Academic Press. New york, London.
- Shaik, K. B.; P. Ganesan; V. Kalist; B. S. Sathish and J. M. M. Jenitha. 2015. Comparative study of skin color detection and segmentation in HSV and YCbCr color space. *Procedia Computer Science*, 57: 41-48.
- Sharma, S. K. and R. P. Kachru. 1990. Influence of storage period and storages on keeping qualities of potatoes. in processing of the XXVI annual convention of ISAE, Hissar, 84–90.
- Singh, R. K. P and K. K. Satapathy. 2006. Performance evaluation of zero energy cool chamber in hilly region. *Agricultural Engineering Today*, 30(5and6): 47-56.
- St- Pierre, N. R.; B. Cobanov and G. Schmitkey. 2003. Economic losses from heat stress by us livestock industries. *Journal of Dairy Science*, 86: 52-77.

- Sternberg, S. R. 1978. Parallel architectures for image processing. Proceedings of IEEE conference international computer software and applications, Chicago, 712–717.
- Taher, F.; N. Werghi; H. Al-Ahmad and C. Donner. 2013. Extraction and segmentation of sputum cells for lung cancer early diagnosis. Algorithms, 6: 512-531.
- Tang, H.; D. Li.; J. Wan; M. Imran and M. Shoaib. 2019. A reconfigurable method for intelligent manufacturing based on industrial cloud and edge intelligence. IEEE Internet of Things Journal, 7(5): 4248-4259.
- Tastimur, C.; E. Akin and M. Karakose. 2015. Detection of rail faults using morphological feature extraction based image processing. 23rd Signal Processing and Communications Applications Conference, Malatya, Turkey, 1244–1247.
- Tastimur, C.; H. Yetis and M. Karaköse. 2016. Rail defect detection and classification with real time image processing technique. International Journal of Computer Science and Software Engineering, 5: 283–290.
- Troncoso, R.; C. Espinoza; A. Sanchez-Estrada; M. E. Tiznado and S. G. Hugo. 2005. Analysis of the isothiocyanates present in cabbage leaves extract and their potential application to control Alternaria rot in bell peppers. Food Research International, 38: 701-708.
- Tudelaa, J. A.; A. Marína, Y. Garridoa, M. Cantwell, S. María, M. Martínez and M. I. Gil. 2013. Off-odour development in modified atmosphere packaged baby spinach is an unresolved problem. Postharvest Biology and Technology, 75: 75–85.

- Wang, W.; B. Vinocur and A. Altman. 2003. Plant responses to drought, salinity and extreme temperatures: towards genetic engineering for stress tolerance. *Planta*, 218: 1–14.
- Wang, X.; Y. Tang and P. Cheng. 2008. Machine vision detection for rail steel's surface flaws based on quantum neural network. 7th World Congress on Intelligent Control and Automation, Chongqing, China, 5050: 5.
- Wasker, D. P.; P. B. Khedkar and V. K. Garande. 1999. "Effect of postharvest treatments on storage behaviour of pomegranate fruits under room temperature and cool storage. *Indian Food Packer*, 53: 11-15.
- Wassner, D. F. and D. A. Ravetta. 2005. Temperature effects on leaf properties, resin content, and composition in *Grindelia chiloensis* (Asteraceae). *Industrial Crops and Products*, 21(2): 155-163.
- Watt, J. R. 1986. Theory of direct evaporative cooling. *Evaporative air conditioning handbook*, Springer, Boston, 12-25.
- Wescor, 2011. *Evaporative Cooling Basics*. Retrieved from the website <http://www.wescorhvac.com/Evaporative%20cooling%20white%20paper.htm> on 26th May 2021.
- Williams, W. B.; M. E. Cuvelier and C. Berset. 1995. Use of a free radical method to evaluate antioxidant activity. *Food Science and Technology*, 28(1): 25-30.
- Xu, J. L.; A. Gobrecht, D. Heran, N. Gorretta, M. Coque, A. A. Gowen, R. Bendoula and D. W. Sun. 2019 b. A polarized hyperspectral imaging system for in vivo detection: Multiple applications in sunflower leaf analysis. *Computers and Electronics in Agriculture*, 158: 258–270.

- Xu, J. L.; A. Gobrecht, N. Gorretta, D. Heran, A. A. Gowen and R. Bendoula. 2019 a. Development of a polarized hyperspectral imaging system for investigation of absorption and scattering properties. *Journal of Near Infrared Spectroscopy*, 27(4): 314–329.
- Xuan, Y. M.; F. Xiao; X. F. Niu; X. Huang and S. W. Wang. 2012. Research and application of evaporative cooling in China. *Renewable and Sustainable Energy Reviews*, 16(5): 3535–3546.
- Zhao, D. 2012. Imaging and range image processing. *Machine Vision Handbook*. Springer, London, 625-663.
- Zhao, X.; L. Shuli and S. B. Riffat. 2008. Comparative study of heat and mass exchanging materials for indirect evaporative cooling systems. *Building and Environment*, 43(11): 1902–1911.
- Zou, X. B.; J. W. Zhao; M. Holmes; H. P. Mao and J. Y. Shi. 2010. Independent component analysis in information extraction from visible/near-infrared hyperspectral imaging data of cucumber leaves. *Chemometrics and Intelligent Laboratory Systems*, 104: 265–270.



Appendices

7. APPENDICES

Table A-1. Variations of the air relative humidity with the evaporative cooling time at pad thickness of 10cm

Watering rate, ℓ/h	Time of evaporative cooling process, h	Inside air relative humidity,%			Ambient air relative humidity,%
		0.21m/s	0.17m/s	0.13m/s	
4 ℓ/h	9	98.7	96.5	96.7	68.8
	10	98.6	97.8	92.9	68.9
	11	97.2	93.1	90.1	69.3
	12	96.1	89.9	88.4	70.4
	13	94.3	85.1	84.9	67.5
	14	89.4	88.4	83.7	58.4
	15	87.7	90.7	85.9	49.8
	16	90.1	90.9	87.3	51.9
	17	91.2	89.4	88.8	52.1
2 ℓ/h	9	95.2	94.8	93.2	64.1
	10	93.8	92.4	93.9	67.9
	11	94.1	92.3	91.2	71.2
	12	89.2	89.5	88.4	72.1
	13	86.1	88.3	86.5	64.3
	14	84.4	83.9	82.1	59.1
	15	88.9	83.2	84.8	51.8
	16	89.2	85.9	86.7	48.3
	17	90.4	87.9	89.4	55.6
1 ℓ/h	9	94.3	92.9	91.4	65.7
	10	95.9	92.1	91.5	69.4
	11	93.8	93.4	89.5	69.5
	12	89.9	89.5	84.8	70.8
	13	85.8	86.2	82.9	65.8
	14	82.6	83.1	80.4	58.9
	15	87.4	81.4	83.8	51.2
	16	87.9	84.5	85.9	53.9
	17	89.2	87.8	86.4	54.8

Table A-2. Variations of the air relative humidity with the evaporative cooling time at pad thickness of 7cm

Watering rate, ℓ/h	Time of evaporative cooling process, h	Inside air relative humidity, %			Ambient air relative humidity, %
		0.21m/s	0.17m/s	0.13m/s	
4ℓ/h	9	87.4	85.1	84.2	66.4
	10	86.6	84.3	83.7	61.8
	11	84.2	83.1	83.1	58.1
	12	82.5	81.7	81.2	50.5
	13	79.8	78.9	77	42.1
	14	80.2	79.2	78.7	44.8
	15	80.9	80.3	80.2	46.2
	16	82.2	82.1	80.9	46.9
	17	84.9	83.4	81.3	49.3
2ℓ/h	9	83.5	81.4	80.6	67.8
	10	82.8	80.5	79.2	62.9
	11	80.3	80	78.4	55.4
	12	79.2	78.3	77.1	51.1
	13	78.3	76	76.6	42.5
	14	77.6	76.2	77.5	44.6
	15	78.1	77.7	79.1	46.9
	16	79.2	78.4	79.8	47.8
	17	79.8	79	80.1	50.2
1ℓ/h	9	81.3	80	79.7	66.8
	10	80.4	79.3	79.4	63.1
	11	79.3	78.1	78.3	52.3
	12	77.9	78	76.9	48.1
	13	76.7	75.2	76.1	41.2
	14	77	76	77.8	45.8
	15	77.5	76.8	79.2	48.3
	16	78.3	77	79.6	49.2
	17	78.8	77.5	79.8	51.1

Table A-3. Variations of the air temperature with the evaporative cooling time at pad thickness of 10cm

Watering rate, ℓ/h	Time of evaporative cooling process, h	Inside air temperature, °C			Ambient air temperature, °C
		0.21m/s	0.17m/s	0.13m/s	
4ℓ/h	9	20.2	20.8	21.7	29.3
	10	20.9	21.2	21.9	29.8
	11	22.5	22.4	22.6	30.4
	12	22.8	23.5	23.5	31.1
	13	23.6	24.3	24.8	33.2
	14	24.9	25.2	25.2	34.8
	15	23.8	25.4	25.5	32.7
	16	22.5	23.8	23.7	30.8
	17	21.7	22.1	23.2	30.1
2ℓ/h	9	20.7	21.2	21.4	30.8
	10	21.4	22.8	21.6	31.4
	11	22.3	22.8	22.4	33.6
	12	24.5	23.4	23.5	33.5
	13	24.6	24.5	24.8	34.7
	14	25.1	25.6	25.7	34.8
	15	23.8	25.1	25.2	33.1
	16	22.1	23.2	23.4	31.6
	17	21.9	22.3	22.7	29.8
1ℓ/h	9	21.4	22.1	22.5	29.7
	10	21.9	22.9	22.9	31.4
	11	22.5	23.7	23.4	32.8
	12	23.8	24.1	24.2	32.7
	13	23.5	24.8	24.6	33.4
	14	25.4	25.6	25.8	35.7
	15	25.1	24.3	23.8	34.6
	16	23.8	23.4	23.2	32.4
	17	22.9	22.6	22.9	31.5

Table A-4. Variations of the air temperature with the evaporative cooling time at pad thickness of 7cm

Watering rate, ℓ/h	Time of evaporative cooling process, h	Inside air temperature, °c			Ambient air temperature, °c
		0.21m/s	0.17m/s	0.13m/s	
4ℓ/h	9	22.1	23.3	23.9	31.2
	10	22.8	23.7	24.7	32.5
	11	23.8	24.8	25.6	33.8
	12	24.6	25.9	26.1	34.4
	13	25.9	26.4	27	35.7
	14	25.1	26	26.2	34.8
	15	24.7	25.1	25.8	33.1
	16	23.9	24.3	25.4	32.4
	17	23.5	24	25	31.8
2ℓ/h	9	23.2	23.9	24.1	32.1
	10	23.7	24.5	24.2	32.7
	11	24.5	25	24.8	33.5
	12	25	25.7	25.3	34.2
	13	26.4	26.8	26.3	35.9
	14	25.9	26.4	27.2	34.1
	15	25.3	25.5	26.3	32.9
	16	24.8	25	25.8	32.1
	17	24.1	24.8	25.5	31.5
1ℓ/h	9	24.2	24.8	24.4	31.6
	10	24.7	25.1	24.7	32.4
	11	25.1	25.8	25.7	33.7
	12	25.9	26.5	26.9	35.2
	13	26.7	27.1	27.5	36.3
	14	26.1	26.5	26.3	34.8
	15	25.4	25.7	25.9	32.8
	16	24.8	25.1	25.7	31.5
	17	24.5	25	25.6	30.8

Table A-5. Variations of the Jew’s Mallow instantaneous mass with the evaporative cooling time at superficial Air Velocities of AV1 (0.21m/s) and pad thickness of 7cm

Processing day	Daytime, h	Jew’s Mallow instantaneous mass inside evaporative cooler, g			Control Jew’s Mallow instantaneous mass, g
		4ℓ/h	2ℓ/h	1ℓ/h	
1st day	9	700	700	700	700
	11	697	694	693	680
	13	692	686	685	665
	15	690	683	677	633
	17	687	678	670	615
2nd day	9	684	675	665	597
	11	681	670	662	574
	13	677	668	660	562
	15	672	663	657	532
	17	670	661	642	510
3rd day	9	665	657	639	502
	11	662	653	635	496
	13	660	649	631	467
	15	659	644	627	439
	17	656	641	623	422

Table A-6. Variations of the Jew’s Mallow instantaneous mass with the evaporative cooling time at superficial Air Velocities of AV2 (0.17m/s) and pad thickness of 7cm

Processing day	Daytime, h	Jew’s Mallow instantaneous mass inside evaporative cooler, g			Control Jew’s Mallow instantaneous mass, g
		4ℓ/h	2ℓ/h	1ℓ/h	
1st day	9	700	700	700	700
	11	693	691	690	682
	13	690	688	687	668
	15	686	684	684	633
	17	684	679	680	618
2nd day	9	677	672	670	602
	11	672	668	667	580
	13	668	665	665	566
	15	664	661	660	537
	17	663	657	656	515
3rd day	9	655	648	646	506
	11	652	643	640	497
	13	649	641	638	471
	15	645	638	635	444
	17	641	635	631	425

Table A-7. Variations of the Jew’s Mallow instantaneous mass with the evaporative cooling time at superficial Air Velocities of AV3 (0.13 m/s) and pad thickness of 7cm

Processing day	Daytime, h	Jew’s Mallow instantaneous mass inside evaporative cooler, g			Control Jew’s Mallow instantaneous mass, g
		4ℓ/h	2ℓ/h	1ℓ/h	
1st day	9	700	700	700	700
	11	689	686	685	680
	13	688	684	682	662
	15	685	681	677	635
	17	682	677	673	623
2nd day	9	675	670	665	610
	11	671	665	662	592
	13	666	664	657	578
	15	662	662	655	540
	17	660	658	651	520
3rd day	9	653	650	644	510
	11	649	645	640	495
	13	645	639	637	473
	15	640	635	632	446
	17	635	632	625	426

Table A-8. Variations of the Jew’s Mallow instantaneous mass with the evaporative cooling time at superficial Air Velocities of AV1 (0.21 m/s) and pad thickness of 10cm

processing day	Daytime,h	Jew’s Mallow instantaneous mass inside evaporative cooler, g			Control Jew’s Mallow instantaneous mass, g
		4ℓ/h	2ℓ/h	1ℓ/h	
1st day	9	700	700	700	700
	11	699	698	697	685
	13	698	697	695	675
	15	695	696	692	650
	17	694	693	690	620
2nd day	9	689	687	687	598
	11	687	685	684	578
	13	685	682	680	565
	15	683	680	677	541
	17	680	678	675	518
3rd day	9	676	674	670	510
	11	673	672	669	502
	13	672	670	667	488
	15	670	668	664	443
	17	669	665	663	430

Table A-9. Variations of the Jew’s Mallow instantaneous mass with the evaporative cooling time at superficial Air Velocities of AV2 (0.17 m/s) and pad thickness of 10cm

processing day	Daytime, h	Jew’s Mallow instantaneous mass inside evaporative cooler, g			Control Jew’s Mallow instantaneous mass, g
		4ℓ/h	2ℓ/h	1ℓ/h	
1st day	9	700	700	700	700
	11	698	697	696	682
	13	695	694	695	664
	15	692	688	691	642
	17	689	686	687	628
2nd day	9	687	682	780	605
	11	685	680	677	582
	13	681	678	674	559
	15	679	675	669	539
	17	676	671	667	523
3rd day	9	672	668	663	506
	11	669	665	661	487
	13	665	660	657	453
	15	664	658	654	446
	17	662	657	651	432

Table A-10. Variations of the Jew’s Mallow instantaneous mass with the evaporative cooling time at superficial Air Velocities of AV2 (0.13 m/s) and pad thickness of 10cm

processing day	Daytime, h	Jew’s Mallow instantaneous mass inside evaporative cooler, g			Control Jew’s Mallow instantaneous mass, g
		4ℓ/h	2ℓ/h	1ℓ/h	
1st day	9	700	700	700	700
	11	695	694	692	680
	13	692	691	690	665
	15	690	689	686	639
	17	686	684	681	622
2nd day	9	684	680	677	615
	11	680	679	674	596
	13	678	675	671	572
	15	675	673	667	544
	17	672	668	665	528
3rd day	9	668	665	660	510
	11	665	663	658	490
	13	663	658	654	455
	15	660	655	653	430
	17	657	654	649	419



Arabic Summary

الملخص العربي

"هندسة حفظ الإنتاج الزراعي"

تصنيع مبرد تبخيري مناسب لإطالة العمر التخزيني للملوخية

يعتبر محصول الملوخية من أهم المحاصيل الزراعية في مصر لما له من أهمية غذائية كبيرة فهو أحد أكثر محاصيل الخضر في محتوى الحديد والكالسيوم والماغنسيوم والمنجنيز والبروتين والثيامين والريبوفلافين وحامض الفوليك والألياف والقيتامينات مثل فيتامين "أ" و"ب". حيث تبلغ المساحة المنزرعة من محصول الملوخية حوالي 2112964 فدان بانتاجية 0.472 طن /فدان، بانتاجية 9126 طن/سنة.

تعد عملية حفظ محصول الملوخية بواسطة التبريد التبخيري عملية مهمة للحفاظ عليها وتقليل التلف وإطالة العمر التخزيني، فالتداول غير السليم للمحصول يؤثر مباشرة على الصفات التسويقية له مما يقلل من جاذبيته أثناء التسويق كذلك الجروح تساعد على دخول الكائنات الحية الدقيقة والمسببة لتعفنها. ان عدم التداول الصحيح يقلل من اسعار البيع والأرباح الممكن تحقيقها. ويعد نظام التبريد التبخيري طريقة فعالة وأمنة من حيث سلامة البيئة لتخفيض درجات الحرارة حيث يتم استخدام المياه كسائل ترطيب فمثل هذه الأنظمة يعتبر حل جيد وفعال للمزارعين في المناطق ذو الطقس الحار والتي يستمر فيها الموسم الحار طويلا كما هو الحال في مصر حيث يطول فصل الصيف ذو الطقس الحار جدا والذي يحول دون المحافظة على المنتج الزراعي بحالة جيدة والتي على اثرها يتم فقد كميات كبيرة من المحصول والذي بدوره يؤثر على الدخل القومي من ناحية الغذاء.

نظام التبريد التبخيري الذي يتم فيه استخدام الوسادة والمروحة يعتبر من أنظمة التبريد المرنة والتي يمكننا اجراء العديد من التعديلات الممكنة عليها وذلك لجعل النظام المستخدم أكثر ملائمة في ظل الظروف المحلية. حيث يتم استخدام مواد تبخير محلية ومتداولة وغير مكلفة أيضا كبديل لمواد التبريد الصناعية والتي تكون مكلفة مقارنة بتلك وصعبة التصنيع وليست متوفرة بشكل مستمر. لذلك تم استخدام وسادة تبريد محلية وهي مادة الخيش لجعل النظام أسهل استخداما. أيضا أدى التطور في عالم الكمبيوتر إلى حل العديد من المشكلات في المجال الزراعي حيث يعتبر تصنيف وفرز الخضروات من المجالات المعقدة التي تتطلب خبرة بشرية كبيرة حيث يمكن أن يساهم ظهور تقنيات جديدة في حل المشكلات مثل الرؤية الآلية. نظراً لأن الملوخية هي من الخضروات الحساسة جداً للظروف البيئية وتندهر بسرعة بعد الحصاد ، لذلك من الضروري تكوين دليل مناسب لمفهوم التصنيف المرئي في مصانع تصنيع الأغذية المجمدة.

أهداف الدراسة:

الهدف العام:

يعد الهدف الرئيسي من البحث الحالي هو إمكانية تقليل أثر الاجهاد الحراري على الملوخية بعد الحصاد مباشرة من خلال تعديل المبرد التبخيري ليلائم الظروف الحقلية لحين نقله الى أماكن التسويق المختلفة وكذلك انشاء نماذج تصنيفية لأوراق الملوخية على أساس بصري لاستخدامها لاحقا في الآلات البصرية المستخدمة في تصنيف أوراق الملوخية.

الأهداف الفرعية:

- 1- دراسة الأداء الحراري للمبرد التبخيري وذلك تحت ظروف تشغيل مختلفة من معدلات الترطيب وسمك الوسادة.
- 2- دراسة أداء نظام التبريد التبخيري عند استخدام سرعات مختلفة من الهواء (0.13، 0.17، 0.21 م/ث).
- 3- تطوير معادلة تجريبية لمعدل التبريد التبخيري أثناء تخزين الملوخية.

4- إنشاء نماذج تصنيفية لاوراق الملوخية على أساس بصري لاستخدامها لاحقا فى الآلات البصرية المستخدمة فى تصنيف أوراق الملوخية.

تم تطوير نظام التبريد التبخيري لتخزين الملوخية بعد الحصاد فى مركز ميكنة الأرز (RMC) فى قرية ميت الدبية ، محافظة كفر الشيخ ، خلال فصل الصيف لعام 2017م. فى هذه الدراسة تم جمع المحاصيل من مزرعة خاصة بمحافظة كفر الشيخ. تم تنظيف الأوراق لإزالة جميع المواد الغريبة مثل الغبار والأوساخ والأجزاء غير الناضجة والتالفة.

لذا يتناول هذا البحث دراسة بعض المتغيرات البحثية مثل سرعة هواء وجه الوسادة ومعدل ترطيب الوسادة وسماكة الوسادة على كفاءة وأداء المبرد التبخيري. وقد تم تحديد ثلاث مستويات مختلفة من سرعات مواجهة للهواء 0,13 ، 0,17 و 0,21 متر/ثانية، ومعدل سريان للماء 1 و 2 و 4 لتر/ساعة وسمك طبقة الخيش 7 و 10 سنتيمتر. تم اتخاذ الرطوبة النسبية و درجة الحرارة والنقص فى وزن المحصول كمؤشرات جودة لأداء المبرد التبخيري، وللحصول على عوامل تطوير الجهاز والخروج بتصميم مناسب واقتصادي للظروف المحلية مع التوصيات لأفضل عوامل التشغيل لحفظ الملوخية (صنف الاسكندرانى). كما يتناول أيضا دراسة متغيرات تصنيف مرثيات أوراق الملوخية وفقا لقواعد المظهر العام وقياس الألوان الأولية ونسبة اللون الأسود إلى اللون الأبيض لنسب ذبول مختلفة لأوراق الملوخية. تم اختيار مجموعة كبيرة من الأوراق قيد الدراسة من حيث شدة الإخضرار والتي تختلف باختلاف الظروف البيئية لها. تم استخدام مقياس بصري CCM-200 لقياس مؤشر محتوى الكلوروفيل لكل ورقة. تم اجراء هذه الدراسة فى شهر نوفمبر من العام 2019م بمعمل قسم البساتين بكلية الزراعة جامعة كفر الشيخ.

وكانت مؤشرات الكفاءة كالتالى:

1. الانخفاض فى درجة الحرارة.
2. الرطوبة النسبية.
3. وزن المادة المخزنة (الملوخية).
4. ظهور فروق تحليلية مرئية بين مجموعات التصنيف المختلفة لأوراق الملوخية.

أهم النتائج:

1- بعد الاجراءات التجريبية تم الحصول على أقل فقد للوزن للملوخية 0,85% عند معدل سريان للماء 4 لتر/ساعة وسمك طبقة للخيش 10سم وسرعة مواجهة هواء 0,21 متر/ثانية.

2- وصلت الرطوبة النسبية ودرجة الحرارة للمبرد التبخيري 98,7% ، 20,2م على التوالي ليصبح الفرق بين درجات الحرارة داخل وخارج المبرد 9,1م حيث كانت درجة الحرارة خارج المبرد 29,3 مئوية ورطوبة نسبية 68,8%. بينما كان الفقد فى الوزن خارج المبرد التبخيري 11,4%.

3- امكانية استخدام الخيش كوسادة فعالة فى نظام التبريد التبخيري.

4- يمكن التنبؤ بدرجات الحرارة والرطوبة النسبية للمبرد التبخيري باستخدام النموذج الرياضي التجريبي لأداء المبرد التبخيري المعدل باستخدام المعادلتين التاليتين:

$$RH = -135.4AV^2 - 0.261WR^2 + 0.25PT^2 \quad R^2 = 0.987$$
$$+ 82.67AV + 3.248WR + 1.38AV \cdot WR$$
$$- 1.11AV \cdot PT - 0.066WR \cdot PT + 56.7$$

$$T_c = -88.54AV^2 + 0.225WR^2 - 0.03489PT^2 \quad R^2 = 0.971$$

$$+ 41.04AV - 0.74856WR$$

$$- 5.2223AV.WR - 1.25AV.PT$$

$$+ 0.0151WR.PT + 24.51$$

5- يتم استخدام المعادلتين السابقتين تحت الظروف الآتية

م	بند	الظروف
1	الظروف المناخية	درجات حرارة من 29-37 درجة مئوية ورطوبة نسبية من 40-74%
2	سرعة مواجهة للهواء	0.13-0.21 متر/ثانية
3	معدل سريان الماء المستخدم في تبليل الوسادة	1-4 لتر/دقيقة
4	سمك وسادة طبقة الخيش	7-10 سنتيمتر

6- تم وضع مقياس لصور الأوراق من النضارة إلى الذبول وفقاً لقواعد المظهر العام (GA) ونسبة الذبول.

1- تم انشاء خريطة تعريفه لونه على أساس مقياس الألوان الأوليه (أحمر و أخضر و أزرق) للتصنيف على أساسها أوراق الملوخية من الأخضر الداكن والفتح والأصفر وأخيرا الأسود

2- التحليل المورفولوجي لأوراق الملوخية أظهر فروقاً كبيرة بين الفئات المختلفة بناء على نسبة مساحة اللون الأسود الى اللون الأبيض.

3- تم الحصول على معادلة انحدار غير خطية متعددة الحدود يمكن من خلالها التنبؤ بنسبة الذبول في أوراق الملوخية بناء على التحليل الاحصائي لتوزيع شدة البيكسل Pixel intensity distribution لصورة ورقة الملوخية:

$$P, \% = 18281.77E^2 + 0.018M^2 + 1.75D^2 - 281789E$$

$$+ 382.28M - 664.39D - 52.01EM + 68.39ED \quad R^2 = 0.99$$

$$- 0.53MD + 1091100$$

حيث أن

$P, \%$	نسبة الذبول للورقة
E	انثروبيا شدة البيكسل للمنطقة تحت الدراسة
M	متوسط شدة البيكسلات في الصورة
D	الانحراف القياسي لشدة البيكسل

التوصيات التطبيقية:

بصفة عامة توضح النتائج السابقة أن أفضل سرعة تؤدي لأعلى وأكفاً أداء للمبرد التبخيري هي 21, متر/ثانية. وكان معدل الترطيب 4 لتر/ساعة وكذلك استخدام سمك الوسادة 10 سنتيمتر هما الأنسب لاعطاء أعلى كفاءة للمبرد التبخيري المعدل في هذه الدراسة واستخدام التقنيات الحديثة في تحليل الصور لفرز المحصول.

"هندسة حفظ الإنتاج الزراعي" تصنيع مبرد تبخيري مناسب لإطالة العمر التخزيني للملوخية

رسالة مقدمة من

ريهام محمد أحمد المسيري
بكالوريوس الهندسة الزراعية- كلية الزراعة- جامعة كفر الشيخ، 2012
كجزء من المتطلبات للحصول على درجة
الماجستير
فى العلوم الزراعية (الهندسة الزراعية)

لجنة الاشراف

الأستاذ الدكتور

سعيد الشحات عبدالله
أستاذ هندسة التصنيع الزراعي
قسم الهندسة الزراعية- كلية الزراعة
جامعة كفر الشيخ

الدكتور

محمد طه عبيد
رئيس بحوث بمعهد بحوث الهندسة
الزراعية- الدقى- الجيزة

الدكتور

وائل محمد المسيري
أستاذ مساعد الهندسة الزراعية
قسم الهندسة الزراعية- كلية الزراعة
جامعة كفر الشيخ

2022